Journal of Catalysis 439 (2024) 115761

Contents lists available at ScienceDirect

Journal of Catalysis

journal homepage: www.elsevier.com/locate/jcat

Research article

New ruthenium(II) isocyanide catalysts for the transfer hydrogenation of ethyl levulinate to γ-valerolactone in C_2-C_6 alcohols

Lorenzo Biancalana [a,b], Nicola Di Fidio [a,b], Domenico Licursi [a,b], Stefano Zacchini [c], Alessia Cinci [a], Anna Maria Raspolli Galletti [a,b], Fabio Marchetti [a,b], Claudia Antonetti [a,b,*]

[a] Università di Pisa, Dipartimento di Chimica e Chimica Industriale, Via Giuseppe Moruzzi 13, I-56124 Pisa, Italy
[b] Consorzio Interuniversitario Reattività Chimica e Catalisi (CIRCC), Via Celso Ulpiani 27, 70126, Bari, Italy
[c] Università di Bologna, Dipartimento di Chimica Industriale "Toso Montanari", Via Piero Gobetti 85, 40129 Bologna, Italy

ARTICLE INFO

Keywords:
Ruthenium complexes
Isocyanide ligands
Transfer hydrogenation
Ethyl levulinate
γ-valerolactone
C_2-C_6 alcohols
Biomass valorization

ABSTRACT

Transfer hydrogenation (TH) processes are receiving great attention for biomass valorization and ruthenium(II) complexes are renowned TH catalysts both on laboratory and industrial scale. Only a few homogeneous catalytic precursors are available in the literature for the TH of ethyl levulinate (EL) to γ-valerolactone (GVL). Herein, starting from simple, commercially available isocyanides, two classes of air-stable ruthenium(II) complexes were synthesized and tested as catalytic precursors. First, an optimized preparation of Ru(II) *p*-cymene isocyanide complexes was developed. Then, the thermally induced *p*-cymene/DMSO substitution gave access to unprecedented ruthenium isocyanide-DMSO complexes. All the complexes were characterized and tested in TH of EL to GVL showing promising performances, adopting 2-propanol as hydrogen donor, a low catalyst (Ru) and co-catalyst (KOH) amount, working under microwave heating for 1 h at 150 °C. The most selective systems were also successfully tested with different biomass-derived alcohols, including 2-butanol. Finally, the recycling of the best catalyst was also investigated, thus improving the efficiency of the entire process.

1. Introduction

Isocyanides (CNR) are versatile ligands for transition metal complexes which offer several advantages with respect to other commonly-used classes of ligands. Their effective and tunable σ-donor and π-acceptor character provides a robust metal – carbon bond adapting to diverse metal centers [1] and the multi-site reactivity of coordinated isocyanides gives access to other organometallic fragments [2]. Several alkyl and aryl isocyanides are available either commercially or through documented synthetic procedures [3]. Generally, they can be manipulated in the presence of air/moisture and they require a simple ligand exchange step for their coordination. Their bonding with metal centers can be regulated by the varying substituent (R) and can be easily detected by FT-IR spectroscopy, based on the fact that the CN stretching vibration provides an intense absorption in a clean spectral region. Despite these useful features and their cost-effectiveness, isocyanides have been overlooked with respect to more popular monodentate ligands, such as carbonyl, phosphanes and NHC carbenes, especially in catalyst development [4], a topic, up to now, not thoroughly investigated in the literature [5]. Ruthenium represents a privileged choice, due to the superior catalytic performances of Ru-based catalysts with respect to other noble metals [6,7], thus resulting one of the most active metals for several industrially important reactions [8]. Specifically, half-sandwich ruthenium complexes with η^6-arene ligands have been extensively investigated as catalysts for a variety of reactions, including (de)hydrogenation/hydrogen borrowing processes [9–11], hydration of nitriles [12], arylation of C(sp^2)-H bonds [13] and alkene metathesis [14]. The {Ru(η^6-arene)}$^{2+}$ moiety is capable of coordinating a wide range of ligands starting from the halido-bridged dimers [RuX(μ-X)(η^6-arene)]$_2$ (X=halide) [15], which can be prepared in gram-scale and almost quantitative yield from $RuCl_3$ hydrate [16,17]. However, among thousands of these derivatives, only few have been reported with isocyanides (L=CNR) [18,19]. Despite the η^6-arene ligand in piano-stool ruthenium(II) complexes is often considered a spectator ligand in catalytic cycles, its thermally-induced displacement has been sometimes invoked as the key step to generate the active species [10b,11,13c,14,20]. In this respect, it is known that the ruthenium – arene bond is labilized by competing π-acceptor ligand(s) [16,21]:

* Corresponding author.
E-mail address: claudia.antonetti@unipi.it (C. Antonetti).

https://doi.org/10.1016/j.jcat.2024.115761
Received 28 June 2024; Received in revised form 11 September 2024; Accepted 12 September 2024
Available online 15 September 2024

therefore, the coordination of an isocyanide to the $Ru^{II}(\eta^6$-arene) scaffold should facilitate this reactivity, which has never been investigated up to now and bears foreseeable (positive) implications for the catalytic activity.

In the 1990's, ruthenium(II) η^6-arene complexes rose to prominence for catalytic transfer hydrogenation (CTH) reactions [6b,22], which still today represent a valid alternative to hydrogenation reactions with molecular hydrogen [23]. The main advantages of CTH over hydrogenation with molecular hydrogen include the reduction of risks and safety restrictions, the added value of exploiting molecular diversity in the reducing agent. Other advantages of adopting hydrogen donor(s) over other traditional methodologies involve the requirement of cheaper reagents, resulting less hazardous than, for example, boron, aluminum and silicon hydrides, generally employed as reducing agents. Moreover, avoiding the use of molecular hydrogen would allow the employment of milder reaction conditions, mainly in term of the reaction pressure, resulting both in a lower environmental impact and in easier downstream operations, if the selectivity parameter is rightly addressed [23b,23c]. In particular, Noyori-Ikariya catalysts (Fig. 1, **E**) and subsequent generations, are commercially available and have found widespread use for CTH reactions [24], including the conversion of biomass-derived molecules, such as furfural and other furanic derivatives, levulinic acid/levulinate esters [25]. Specifically, these latter compounds represent emerging building blocks in the biomass conversion field, as demonstrated by the several applications developed up to now, such as the synthesis of oxygenated bio-fuels, fragrances, plasticizers, intermediates for chemical and pharmaceutical industry, food additives and bio-solvents [26]. Among them, levulinate esters can be advantageously upgraded into more valuable bio-products, such as ketals [27], alkoxypentanoates [28] and γ-valerolactone (GVL) [11,29], due to the greater stability of the esters with respect to the corresponding acids, thus generally reducing the formation of by-products [30]. GVL is a key compound due to its widespread application, highlighting its use as green additive for lubricants, plasticizers, fuels and green solvents in organic synthesis and biomass refinery [31]. Regarding the CTH of levulinate esters, ethyl levulinate (EL) is an intriguing molecule derived directly from biomass and its conversion to GVL through CTH approach has been extensively studied particularly employing heterogeneous catalysts. Anyway, some unsolved drawbacks still remain, including the use of high amount of catalyst and harsh reaction conditions, both hampering the sustainability of the process [32]. Research into EL conversion using homogeneous catalysts has been comparatively limited [33], despite these systems are usually characterized by higher catalytic efficiency and turnover numbers than the heterogeneous ones, at the same time requiring milder reaction conditions. To date, the most promising results obtained in the CTH of EL to GVL in the presence of homogeneous catalytic precursors (Fig. 1) are summarized in Table 1.

The main drawbacks of the catalytic systems developed in the studies reported in Table 1 are related to the instability of the catalysts under air [33a,33b,33c,33g], the high amount of the catalyst [33a,33d,33f], the long reaction time [33a,33b,33f], the use of fossil-based solvents [33a], and/or the high amount of base [33b,33e,33f,33g]. The air- and moisture-stable Ru(II) complex [RuCl{κ^2*N*-((4-C_6H_{10}OH)N=CH)$_2$}(η^6-*p*-cymene)]BPh_4, previously studied by us, was found to be the best catalytic precursor for the CTH of EL to GVL among a series of related α-diimine complexes, affording the maximum GVL yield of 62 mol% under mild reaction conditions (1 h at 160 °C) [11]. Considering the sustainability issues, low amounts of both Ru catalyst (0.56 mol%, respect to EL) and of the base potassium hydroxide (1 mol% respect to EL) were used. Moreover, this reaction was performed in the presence of 2-propanol as hydrogen-source and solvent, employing microwave (MW) as efficient heating system, aimed at improving the process efficiency, exploiting fast temperature increase, short reaction times and energy saving [31a,34] (Entry 8, Table 1). On the basis of these positive outcomes, the MW heating was proposed for the CTH of EL to GVL with the ruthenium(II) isocyanide complexes investigated in this paper and never proposed for any catalytic application. Moreover, the CTH of EL to GVL was studied in the presence of a wide range of biomass-derived alcohols, including isopropanol, ethanol, butanol, pentanol and hexanol [35], with the aim of optimizing the sustainability degree of the entire process. Finally, in this perspective, some insights on the spent catalyst were provided, being of paramount importance for the recycle issue, an aspect barely considered in the literature. In summary, the adoption of *i)* very low amount of a new air-stable and easily synthesizable Ru(II)-based catalysts, *ii)* a biobased solvent, *iii)* mild reaction conditions, also exploiting the efficient microwave heating, represent the main strengths for improving the sustainability of the EL conversion to GVL over the state of the art.

2. Results and discussion

2.1. Synthesis and characterization of η^6-arene isocyanide complexes

Given the paucity of studies about isocyanide ligands in catalysis and the absence of prior works on the catalytic activity of the target compounds of this work (see the Introduction Section), we employed a

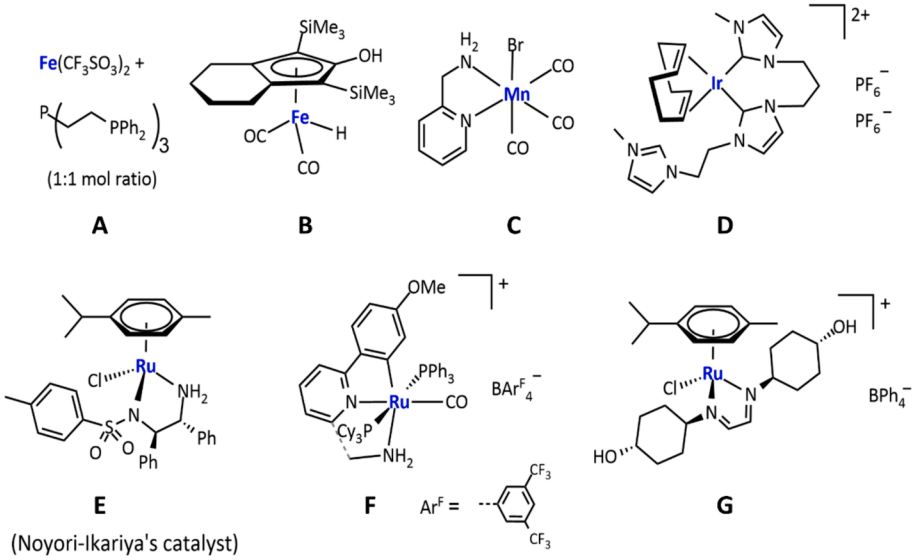

Fig. 1. Structure of the pre-catalysts reported in Table 1.

Table 1
Best catalytic performances for the TH of EL to GVL using **A-G** as homogeneous pre-catalysts.

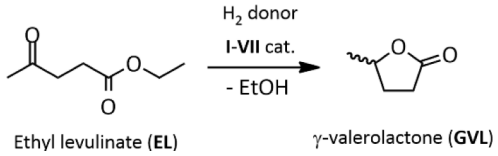

Entry	Temperature, reaction time [a]	Base (mol% vs EL)	Metal, Catalyst (mol% vs EL)	Hydrogen donor, solvent	EL Conversion (mol%)	GVL Yield (mol%)	Ref.
1	140 °C, 24 h	–	**Fe**, **A** [b] (5 %)	HCO_2H, 1,4-dioxane	> 99	98	[33a]
2	100 °C, 19 h	$NaHCO_3$ (5 %)	**Fe**, **B** [b] (1 %)	^{i}PrOH (H-donor and solvent)	96	95	[33b]
3	80 °C, 20 min	^{t}BuOK (1 %)	**Mn**, **C** [b] (0.5 %)	^{i}PrOH (H-donor and solvent)	98	82	[33c]
4	140 °C, 3 h MW heating	–	**Sc**$(OTf)_3$ (5 %)	^{i}PrOH (H-donor and solvent)	98	92	[33d]
5	150 °C, 3 h	$Ba(OH)_2$ (100 %)	**Ir**, **D** ($1.34\bullet10^{-4}$ %) [c]	Glycerol, H_2O	–	68	[33e]
6	30 °C, 18 h	*N*-methyl piperidine[d]	**Ru**, **E** (1 %)	HCO_2H (excess) [d], MeOH	94	[e]	[33f]
7	82 °C, 30 min	K_2CO_3 (5 %)	**Ru**, **F** [b] (0.01 %)	^{i}PrOH (H-donor and solvent)	98	94	[33g]
8	160 °C, 1 h MW heating	KOH (1 %)	**Ru**, **G** (0.56 %)	^{i}PrOH (H-donor and solvent)	81	62	[11]

[a] Conventional heating, unless otherwise specified.
[b] Under inert atmosphere and anhydrous conditions.
[c] Blank test (without catalyst) is not reported.
[d] Formic acid/N-methyl piperidine 1:1 mol ratio; in large excess with respect to EL.
[e] Enantiomeric excess of (*R*)-GVL is 82 %.

selection of commercially-available and inexpensive isocyanides with different alkyl or aryl substituents. The starting materials $[RuX_2(\eta^6\text{-}p\text{-cymene})]_2$ (X=Cl, I) were prepared in 95–99 mol% yield from commercial $RuCl_3$ hydrate, according to published procedures [10b,16]. Next, $[RuCl_2(\eta^6\text{-}p\text{-cymene})]_2$ (up to 500 mg, 1.6 mmol) was allowed to react with the selected isocyanides (CNR) to afford the corresponding $[RuCl_2(CNR)(\eta^6\text{-}p\text{-cymene})]$ derivatives (R: xylyl, Xyl, **1a**; 2-naphthyl, **1b**; benzyl, Bn, **1c**; cyclohexyl, Cy, **1d**; *tert*-butyl, **1e**; Scheme 1a), according to an optimized procedure. The reactions were carried out in stoichiometric conditions at room temperature in CH_2Cl_2. Instead, $[RuI_2(CN^{t}Bu)(\eta^6\text{-}p\text{-cymene})]$, **1f**, was prepared from the iodide dimer $[RuI_2(\eta^6\text{-}p\text{-cymene})]_2$ in refluxing CH_2Cl_2 (Scheme 1b). The conversion of the isocyanide can be easily evaluated by FT-IR spectroscopy and was typically complete within 1 h. Therefore, excess of ligand and/or longer reaction times are unnecessary [19b,19 g,19i,19j]. Previously-reported $[RuX_2(CNR)(\eta^6\text{-arene})]$ complexes (X=Cl, I) were purified by (re)crystallization and/or silica gel chromatography [19]. Instead, **1a-f** were herein purified by a simple filtration of the reaction mixture over celite, which is nevertheless fundamental to remove a brown solid by-product (see Experimental Section for details), followed by a final washing with diethyl ether or hexane. Thus, orange (**1a-e**) or violet-red (**1f**) air-stable powders were isolated in 89–97 mol% yields. Remarkably, the preparation of **1a-e** was alternatively carried out using the less-hazardous acetonitrile, with no significant difference in yield and purity of the final compound [36].

To the best of our knowledge, **1a** [19j], **1d** [19b,19e] and **1e** [19b,19e,19 g,19i] were previously reported in the literature, whereas **1b-c** are unprecedented. Compounds **1a-f** were characterized by elemental (CHN) analyses, FT-IR and NMR spectroscopy (Figures S1-S24). CH_2Cl_2 and $CDCl_3$ were used as standard solvents for IR and NMR

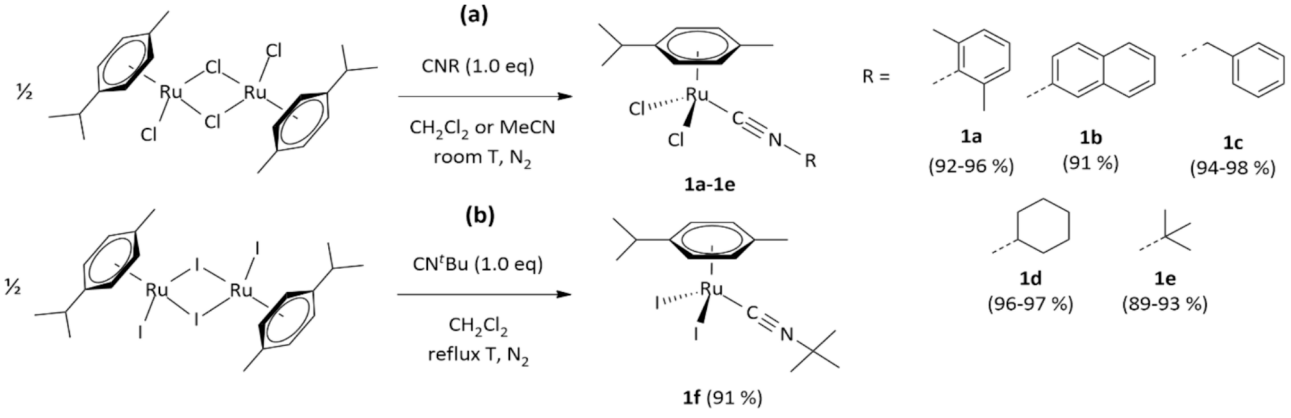

Scheme 1. Synthesis of ruthenium complexes **1a-f** from commercially available isocyanides and the corresponding $[RuX_2(\eta^6\text{-}p\text{-cymene})]_2$ (X=Cl, I) dimer. Isolated yields (mol%) in parentheses.

measurements, respectively. The isocyanide ligand is characterized by a strong IR absorption in the 2150–2160 or 2185–2200 cm^{-1} range (aromatic/aliphatic group) and by a relatively broad ^{13}C NMR signal around 150 or 140 ppm (aromatic/aliphatic group). The shift of the C≡N stretching band (in CH_2Cl_2) with respect to the free isocyanide indicates a scarce π-backdonation from the {Ru(η^6-*p*-cymene)}$^{2+}$ moiety [19b,19 g,19j] and reflects the relative donor/acceptor properties of the isocyanide substituent and the halide co-ligand (Table S1). The molecular structures of **1d** and **1e** were elucidated by single-crystal X-Ray diffraction (Figs. 2 and 3, Table 2). These complexes display a three-legged piano-stool geometry, as found in the few related compounds where Ru is bonded to a η^6-*p*-cymene, two halides and one isocyanide ligand [19f,19j,19 h]. The C(1)-N(1) contact [1.148(2) Å and 1.147(8) Å in **1d** and **1e**] and the Ru-C(1)-N(1) angle [173.74°(13) and 179.5°(7) in **1d** and **1e**, respectively] is in agreement with a σ-bonded isocyanide with little π-backdonation from the metal center [1]. The bonding parameters of the coordinated CN^{t}Bu ligand are comparable with those previously reported for analogous complexes [37]. Remarkably, only few crystal structures of ruthenium cyclohexyl isocyanide complexes have been reported so far in the literature and none of them with an arene co-ligand [38].

2.2. Synthesis and characterization of DMSO/isocyanide complexes

The addition of a π-acceptor ligand (such as a monodentate phosphane, saturated NHC, allenylidene or a bidentate *N*-heterocycle) to the Ru^{II}(η^6-arene) scaffold results in the labilization of the ruthenium-arene bond [14–21]. Coordinating solvents (such as MeCN, DMSO, H_2O) may facilitate the dissociation of the arene by binding to the vacant coordination sites on the metal [39]. As a matter of fact, several well-established synthetic procedures are based on the thermal or photochemical cleavage of the arene ligand from Ru(II) complexes in MeCN solution [40]. In the case of DMSO, the undesired release of *p*-cymene in DMSO or DMSO/water solution has been often reported while assessing the suitability of the respective Ru(II) complexes for biological applications [41,42]. However, the isolation of Ru(DMSO)$_x$ (x = 1–3) complexes, taking advantage of the DMSO/arene exchange as a useful synthetic step, has been rarely accomplished [43,44]. Even fewer studies

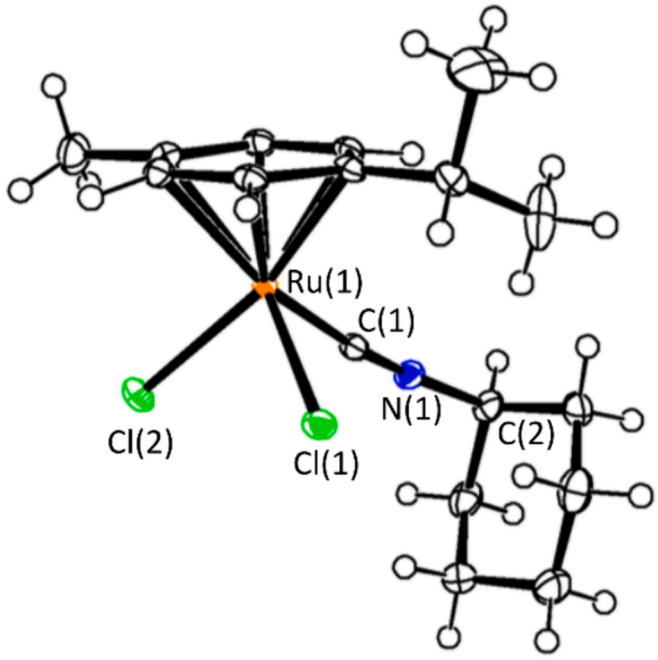

Fig. 2. Molecular structure of **1d.** Displacement ellipsoids are at the 50 % probability level.

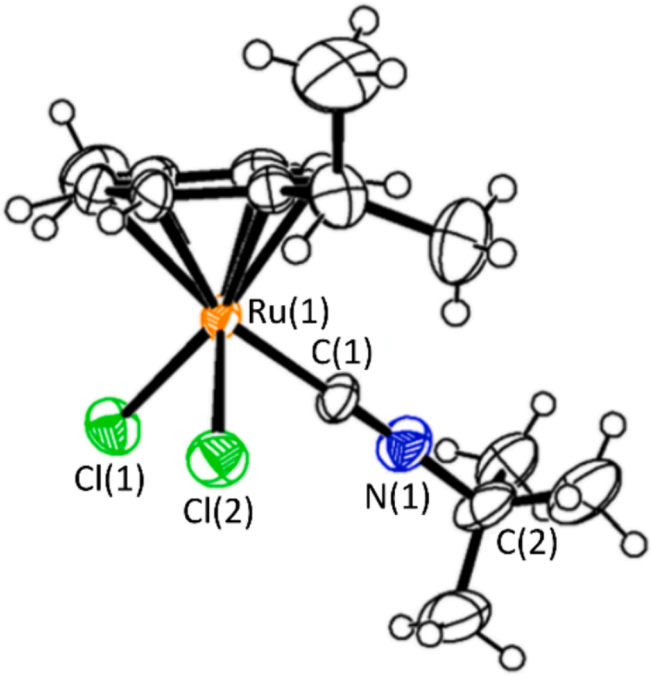

Fig. 3. Molecular structure of **1e**. Displacement ellipsoids are at the 50 % probability level. Only the main image of the disordered ^{t}Bu group is represented.

Table 2
Main bond distances (Å) and angles (°) of **1d** and **1e**.

	1d	1e
Ru(1)-C(*p*-cymene)$_{av}$	2.210(4)	2.200(14)
Ru(1)-Cl(1)	2.4143(4)	2.4018(18)
Ru(1)-Cl(2)	2.4110(4)	2.4113(17)
Ru(1)-C(1)	1.9759(15)	1.975(6)
C(1)-N(1)	1.148(2)	1.147(8)
N(1)-C(2)	1.4510(19)	1.461(9)
Cl(1)-Ru(1)-Cl(2)	88.226(13)	88.29(7)
Cl(1)-Ru(1)-C(1)	85.47(4)	85.1(2)
Cl(2)-Ru(1)-C(1)	87.90(4)	85.2(2)
Ru(1)-C(1)-N(1)	173.74(13)	179.5(7)
C(1)-N(1)-C(2)	170.05(16)	175.9(7)

provide a complete spectroscopic and/or crystallographic characterization, including the assessment of the stereochemistry and binding mode of DMSO ligands [45,46].

With this background in mind, the *p*-cymene/DMSO exchange process for **1a-e** was investigated in two different conditions. First, a one-pot procedure in toluene solution was developed. Thus, a suspension of **1a-e**, freshly prepared from [$RuCl_2$(η^6-cymene)]$_2$ and the respective isocyanide, was treated with DMSO (5–10 eq. respect to Ru; Scheme 2a). The reactions proceeded at 55–110 °C for 2–6 h, accompanied by a progressive color change from orange to yellow. The formation of a by-product (**3**, see Experimental Section) in a variable amount was ascertained, depending on temperature/excess of DMSO and the type of isocyanide ligand (especially for **1c,e**). Optimization of the reaction conditions and workup allowed us to isolate **2a,b,d** in 56–79 mol% yields, whereas **2c,e** could not be separated from the by-product **3c,e**. Next, the *p*-cymene/DMSO exchange on **1a-d** was investigated in DMSO as less-hazardous solvent (Scheme 2b) [36]. In comparison with the previous approach, the reactions proceeded at higher temperature (100–130 °C), but required shorter times (for instance, less than 30 min for **1a**). Subsequent removal of excess DMSO was carried out by water (NaCl)/$CHCl_3$ extraction followed by trituration in Et_2O. Hence, compounds **2a-d** were isolated as colorless or pale-yellow solids in 56–82

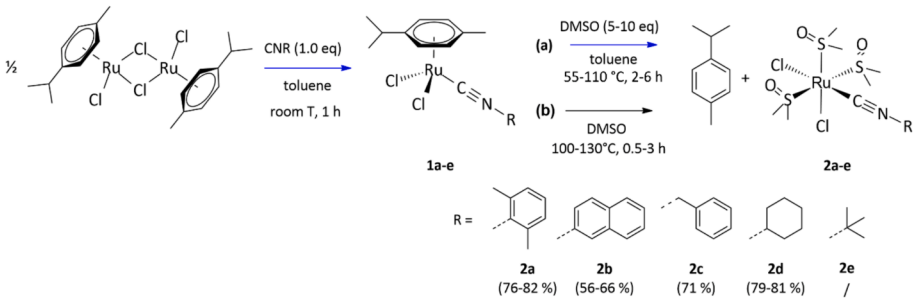

Scheme 2. Preparation of ruthenium complexes **2a-e** by DMSO-assisted *p*-cymene cleavage from **1a-e** in toluene (**a**) or DMSO (**b**) as solvents. Blue arrows indicate the one-pot procedure in toluene starting from $[RuCl_2(\eta^6\text{-}p\text{-cymene})]_2$. Isolated yields in parentheses (for **2c** the yield obtained in DMSO is reported; **2e** was not isolated as a pure compound – see Experimental Section for details).

mol% yields.

In summary, complexes containing aryl isocyanides (**1a-b**) required a lower temperature/time for the complete conversion and offered a more straightforward procedure than those featuring aliphatic isocyanides (**1c-e**). Compounds **2a,b,d** were thus obtained in comparable yield and purity by both procedures, while **2c** is best prepared in DMSO as solvent.

Compounds **2a-e** were characterized by CHNS analyses, FT-IR (solid-state or CH_2Cl_2) and NMR (acetone-d_6 and $CDCl_3$) techniques. FT-IR and NMR spectra are displayed in Figures S25-S47; selected data are reported in Table S1. Overall, the data are consistent with a *cis*,*mer*-$[RuCl_2(CNR)(\kappa S\text{-DMSO})_3]$ formulation for all the compounds.

The isocyanide ligand (CNR) shows a relatively broadened ^{13}C NMR resonance in the 145–160 ppm range and a strong IR absorption around 2130 or 2165 cm^{-1} for aromatic and aliphatic substituents, respectively. The isocyanide stretching band in **2a-e** is shifted to lower wavenumbers (≈ -30 cm^{-1}) with respect to **1a-e** and closer to that of the free isocyanide, suggesting an increased π-backdonation from the Ru(II) center. Intense absorptions within 1085–1115 cm^{-1} are present in the solid-state FT-IR spectra, accounting for S=O stretching vibrations [47]. In the ^1H and ^{13}C NMR spectra, the methyl groups belonging to the DMSO ligands give rise to three resonances of equal intensity around 3.30–3.50 and 43–48 ppm, respectively. Both FT-IR and NMR features are indicative of κ*S*-coordinated DMSO [47–49]. Results of ^1H NOESY, ^1H–^{13}C HMBC and HSQC NMR experiments combined with the symmetry of the three possible isomers (*fac*, *trans-mer*, *cis-mer*; Chart S1) allowed us to establish the stereochemistry in solution. Moreover, the crystal structure of *mer*,*cis*-**2a** was elucidated by X-ray diffraction (Fig. 4). It displays a slightly distorted octahedral geometry around the metal center. All the DMSO ligands are *S*-bonded, according to the NMR data. The Ru(1)-S(2) distance [2.2725(4) Å] *trans* to Cl(2) is shorter than Ru(1)-S(1) [2.3274 (5) Å] and Ru(1)-S(3) [2.3739(5) Å] which are in mutual *trans* position, in view of the different *trans* influence of Cl^- and DMSO. Conversely, Ru (1)-Cl(1) [2.4209(4) Å] and Ru(1)-Cl(2) [2.4454(4) Å] distances are very similar. The C(1)-N(1)-C(2) [167.63(19)°] angle significantly departs from linearity, even more than in the precursor **1a** [171.9(2)°], and also the C(1)-N(1) distance of **2a** [1.165(2) Å] is slightly longer than in **1a** [1.159(3) Å] [19j], in accordance with an increased π-backdonation.

To the best of our knowledge, a poorly-characterized coordination polymer obtained from 1,4-diisocyanobenzene and $[RuCl_2(DMSO)_4]$ represents the only example reported in the literature of a ruthenium compound containing isocyanide and sulfoxide ligands [50]. Structurally-characterized compounds that are somehow related to **2** are *cis*,*mer*-$[RuCl_2(CO)(\kappa S\text{-TMSO})_3]$ (TMSO=tetramethylene sulfoxide / tetrahydrothiophene *S*-oxide) [51] and $[RuCl_2(CO)(\kappa S\text{-DMSO})_2(\kappa O\text{-DMSO})]$ (*cis*,*cis*,*trans*, *all-trans, all-cis* isomers) [52].

The *cis*,*mer* stereochemistry adopted by compounds **2** is presumably more stable than the *trans*,*mer* stereochemistry on electronic grounds, by placing an electron-donating ligand (Cl^-) instead of a moderately π-acceptor ligand (κ*S*-DMSO) [48] *trans* to the strong π-acceptor

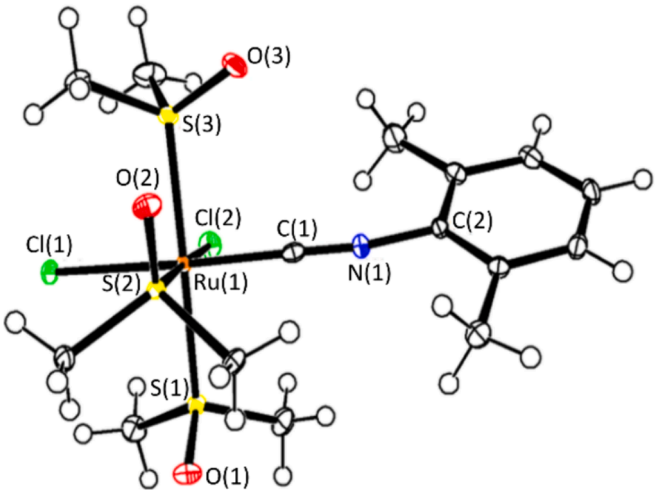

Fig. 4. Molecular structure of *cis*,*mer*-$[RuCl_2(CNXyl)(\kappa S\text{-DMSO})_3]$, **2a**. Displacement ellipsoids are at the 50 % probability level. Main bond distances (Å) and angles (°): Ru(1)-C(1) 1.9256(19), Ru(1)-Cl(1) 2.4209(4), Ru(1)-Cl(2) 2.4454(4), Ru(1)-S(1) 2.3274(5), Ru(1)-S(2) 2.2725(4), Ru(1)-S(3) 2.3739(5), C(1)-N(1) 1.165(2), N(1)-C(2) 1.405(2), S(1)-O(1) 1.4832(14), S(2)-O(2) 1.4825(13), S(3)-O(3) 1.4827(14), Cl(1)-Ru(1)-C(1) 175.95(5), Cl(1)-Ru(1)-S (2) 178.408(17), S(1)-Ru(1)-S(3) 175.310(17), Ru(1)-C(1)-N(1) 177.22(16), C (1)-N(1)-C(2) 167.63(19).

isocyanide ligand. Accordingly, the stability (assessed by DFT calculations) of $[RuCl_2(CO)(DMSO)_3]$ complexes is higher for those isomers featuring a chloride *trans* to the carbonyl ligand instead of a κ*S* or κ*O*-coordinated DMSO [53]. Competition for π-backdonation, as well as increased steric hindrance, are likely responsible for the lower stability of the *fac* isomer of **2**, as assessed for $[RuCl(C,C)(\kappa S\text{-DMSO})_3]$ (C, C=bidentate monoanionic ligand; DFT) [45].

Compounds **2a-d** are labile in solution at room temperature, due to the (partial) release of DMSO. The timing and outcome of the process are markedly dependent on the type of solvent, temperature and isocyanide substituent. In this respect, freshly-prepared solutions of **2a-d** in acetone-d_6 show only a minimal amount of DMSO, which slightly increases in the following 24 h. Conversely, dissolution of **2a-d** in $CDCl_3$ causes an immediate and significant release of DMSO (up to 20–25 mol%). New ^1H NMR resonances appear in the typical ranges of κ*S*- (3.0–3.5 ppm) and μ-κ*S*,κ*O*-DMSO (3.7–3.9 ppm; Figures S48-S49) [54]. Therefore, acetone-d_6 is recommended for NMR analyses of **2**. A solution of **2a** in DMSO-d_6 rapidly exchanged all the sulfoxide ligands within a few hours.

Compounds **3**, namely by-products in the preparation of complexes **2** in toluene as solvent, are characterized (see Experimental Section) by an IR absorption at 2166–2190 cm^{-1} for the isocyanide ligand, about 25–35 cm^{-1} higher than in **2**, and a 1:1 isocyanide/DMSO ratio (^1H NMR). In this regard, compounds **3** could result from the displacement

of DMSO from **2**, a process which is inhibited by working in DMSO as solvent.

The NMR monitoring of the reaction between **1a** or **1d** and DMSO (4 eq.) in toluene-d_6 provided useful insights into the arene/DMSO exchange process (Tables S2-S3, Figures S50-S51). After about 20 h at room temperature, the partial formation of **2a,d** together with another, major [$RuCl_2$(CNR)(κ*S*-DMSO)$_3$] species (**2a,d^X**) was observed. Heating to 60–65 °C for 1–3 h resulted in a significant increase in the relative amount of **2a,d** (50–70 %), a decrease in **1a,d** and related Ru(η^6-*p*-cymene) species (about 13–15 %), together with a marked decrease or disappearance of **2a,d^X**. These results indicate a comparatively low barrier for *p*-cymene dissociation, in accordance with the hypothesized labilization effect operated by the isocyanide ligand in [$RuCl_2$(CNR)(*p*-cymene)] complexes (**1**). Furthermore, the kinetic product **2a,d^X** could correspond to *fac*-[$RuCl_2$(CNR)(κ*S*-DMSO)$_3$], arising from the pseudo-facial arrangement of the *p*-cymene ligand in **1a,d**. In each case, *p*-cymene was identified in solution in stoichiometric amount (1:1 mol ratio) with respect to **2a,d** (or **2a,d** + **2a,d^X**). Further heating (60–65 °C) for 15–18 h resulted in the formation of **2a** and **2d** with overall 82 and 52 mol% NMR yield, respectively, accompanied by **3a,d** as major by-products. These data confirm that a lower amount of DMSO in the reaction mixture results in an increased formation of the by-product **3**, particularly with aliphatic isocyanides (**1d**: cyclohexyl isocyanide).

Prolonged heating of a solution of **2a** in toluene under reflux produced a new compound (**4a**) as a pale-yellow precipitate, which was collected by filtration. The strong absorption at 1030 cm^{-1} in the solid state FT-IR-spectrum, in the mid-region between that of *S*-DMSO and *O*-DMSO, and two downfield-shifted ^{1}H NMR resonances of the SCH_3 groups (*ca.* 3.8 ppm, $CDCl_3$) are indicative [47] of the presence of the rare [55] bridging DMSO ligand (μ-κ^1*O*,κ^1*S*) (Figures S52-S53). The xylyl isocyanide ligand in **4a** gives rise to a sharp FT-IR band at 2138 cm^{-1} (CH_2Cl_2 solution). The ^{1}H NMR set of signals indicates an overall isocyanide/κ*S*-DMSO/bridging-DMSO 1:1:1 ratio, leading to the proposal of the [$RuCl_2$(κ*S*-DMSO)(μ-DMSO)(CNXyl)]$_2$ formulation for **4a**.

3. Catalytic transfer hydrogenation

The isocyanide Ru-based complexes were tested in the CTH reaction of EL to GVL, working in different alcohols as hydrogen donor/solvents, and exploiting MW irradiation. The generalized mechanism for explaining the CTH of ketones in the presence of Ru-based complexes was proposed by Chowdhury and Bäckvall [56]. According to Scheme 3, it involves the preliminary deprotonation of the alcohol (R_1R_2CHOH) with a base (MOH), leading to chloride dissociation (MCl) and enabling the coordination of the alkoxide (step a), which undergoes in turn β-hydrogen elimination to give the corresponding carbonyl compound (the oxidized compound from alcohol) (step b) and the ruthenium hydride complex (step c). Then, the position of the formed carbonyl compound is replaced by the ketone of the substrate (O=CR_3R_4), namely the EL (step d), and the subsequent migration of the hydride results in the formation of a new alkoxide complex (step e), which is protonated by the alcohol (step f), thus closing the catalytic cycle with the coordination of the alkoxide anion of the alcohol (step b).

In the above general mechanism, the preliminary deprotonation of the alcohol by a strong Brønsted base promotes the catalytic cycle, shortening the time required to attain the equilibrium between the ketonic substrate and the alcoholic product.

In order to evaluate the catalytic behavior of the two classes of compounds, preliminary reactions were carried out with the xylyl isocyanide derivatives **1a** and **2a** as representative examples, working either in the presence of 1 mol% KOH and under base-free conditions, for 60 min at 160 °C, under MW heating (Table 3). These reaction conditions, including the choice of KOH as the best promotor, were selected starting from our previous study [11].

Results in Table 3 highlight the key role of KOH as the promotor towards the CTH reaction, significantly enhancing EL conversion. At the same time, it is interesting to note the high GVL selectivity in these tests (entries 1 and 3, Table 3). Maximum GVL yields of 53 and 58 mol% were ascertained working in the presence of **1a** and **2a**, respectively. Moreover, propyl levulinate (PL) could be formed as a consequence of the *trans*-esterification reaction occurring between EL and 2-propanol, but it was never detected (with or without KOH), thus not affecting the GVL selectivity (Table 3). In the presence of KOH, **1a** and **2a** showed comparable catalytic performances. Compound **2a** enabled us to reach the highest GVL yield and was further employed for investigating the effect of the reaction temperature. In the perspective of improving the sustainability of our approach, this parameter was progressively lowered, trying to improve the GVL selectivity, at the same time keeping high EL conversion. Fig. 5 shows the results achieved by working at 150, 140 and 130 °C (including the already tested 160 °C), keeping constant the other reaction parameters.

The temperature decrease from 160 to 150 °C significantly improved the GVL selectivity from 60.6 to 78.0 mol%, respectively, leading only to a slight decrease of the EL conversion (about 10 mol%). At 150 °C, the maximum GVL yield of 67.7 mol% was achieved. Further reduction of the reaction temperature to 140 and 130 °C worsened the GVL yield (57.2 and 51.3 mol%, respectively). Based on these promising results, the temperature of 150 °C was selected for investigating the catalytic performances of all the different Ru-based complexes synthesized in this work. Moreover, the commercially-available [$RuCl_2$(η^6-*p*-cymene)]$_2$ and $RuCl_3$·nH_2O, herein employed as starting materials for the synthesis of complexes **1**–**2**, and sometimes used as pre-catalysts for TH reactions [57], were included in the panel of the tested compounds. The results of the corresponding catalytic tests carried out under the previously identified best reaction conditions are reported in Table 4.

All the synthetized complexes **1** and **2** show good catalytic activities towards this reaction, achieving EL conversion from 75 to 93 mol% and GVL selectivities in the range 57–86 mol% after 1 h of reaction time. For compounds **1**, the GVL yield is markedly influenced by the different isocyanide substituent, reaching the highest value for the xylyl (**1a**) and

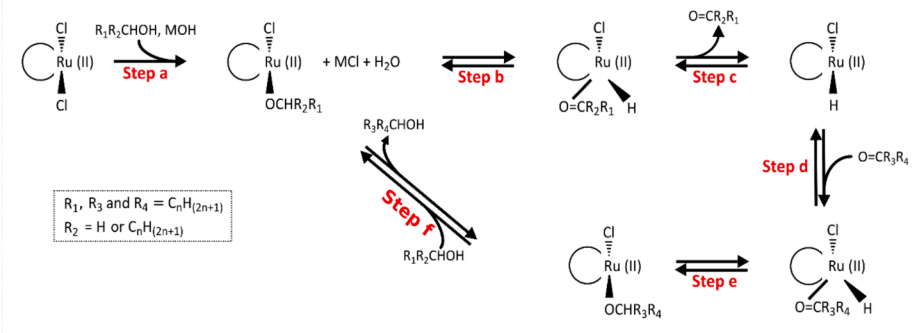

Scheme 3. General catalytic cycle for the TH of ketones with alcohol and a ruthenium-chloride catalytic precursor.

Table 3
Effect of KOH (1 mol% respect to EL) on CTH of EL (5 mmol) to GVL in 2-propanol (10 mL), using **1a** or **2a** (0.56 mol% with respect to EL) as the catalyst precursors. Reaction conditions: MW heating, T=160 °C, t = 60 min.

Entry	Catalytic precursor	Base	EL conversion (mol %)	GVL selectivity (mol %)	GVL yield (mol %)	Propyl levulinate yield (mol %)	Other products yield (mol %)
1	**1a**	KOH	92.1 (1.8)	57.5 (1.2)	53.0 (1.1)	–	39.2 (0.8)
2	**1a**	–	68.0 (1.5)	19.9 (0.4)	13.5 (0.3)	–	54.5 (1.2)
3	**2a**	KOH	95.5 (1.4)	60.6 (0.9)	57.9 (0.9)	–	37.6 (0.6)
4	**2a**	–	20.1 (0.4)	18.6 (0.4)	3.7 (0.1)	–	16.3 (0.3)

Standard deviation values are reported in parenthesis.

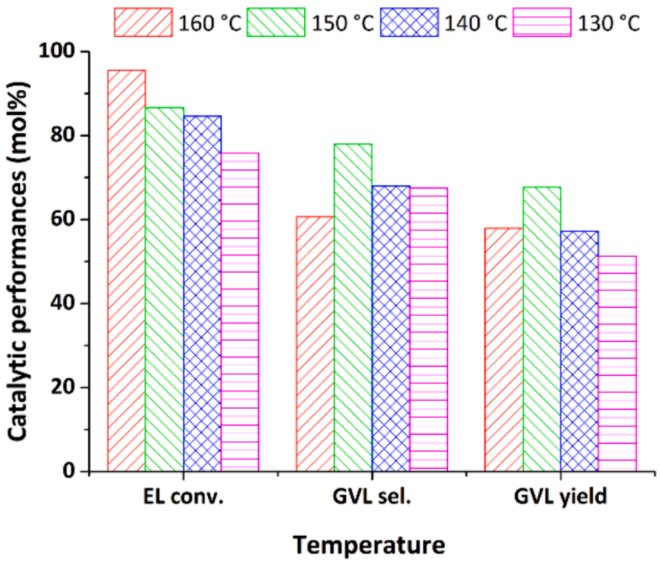

Fig. 5. Effect of the reaction temperature on CTH of EL (5 mmol) to GVL, working in 2-propanol (10 mL) as hydrogen donor, in the presence of KOH (1 mol% with respect to EL), using **2a** (0.56 mol% with respect to EL) as the catalytic precursor. Reaction conditions: MW heating, t = 60 min.

t-butyl (**1e**) derivatives (about 73 mol% in both cases). Comparatively minor differences were observed for compounds **2**, except for the xylyl derivative **2a** offering a significantly better GVL yield (68 mol%). Moreover, for complexes **1a-d** and **2a-c** the production of PL was negligible, while the yield of other by-products was quite considerable, whereas for **2d**, also traces of PL were detected.

Taking into account complexes **1e** and **1f**, the presence of chloride or iodide ligand can significantly affect the selectivity of the reaction: in fact, at comparable EL conversion, the GVL selectivity was about 86 mol % with **1e** (Ru-Cl) and 63 mol% with **1f** (Ru-I). This result suggests that the dissociation of the halide plays a key role on the catalytic mechanism. For both these two complexes, the PL yields were almost negligible, as well as the yield of other by-products for **1e**. Furthermore, by comparing each couple of catalysts characterized by the same isocyanide ligand, but belonging to the two different structures, namely **1a** and **2a**, **1b** and **2b**, **1c** and **2c**, **1d** and **2d**, in most cases, the η^6-arene isocyanide complexes (complexes **1**) showed comparable conversion with the corresponding DMSO/isocyanide ones (complexes **2**), but a much better selectivity (than complexes **2**). The lower GVL selectivity offered by **2a-d** could be related to their thermally-induced (partial) conversion into less-active species, due to the lability of sulfoxide ligands (Section 2.2). Accordingly, **4a**, derived from **2a** by thermal rearrangement of the DMSO ligands, provided a significantly lower GVL selectivity (63 mol%) at comparable EL conversion, and higher yields in PL and other by-products than the values achieved for **1a** and **2a**.

Remarkably, $[RuCl_2(\eta^6\text{-}p\text{-cymene})]_2$ and $RuCl_3{\cdot}nH_2O$ were characterized by worse catalytic performances, achieving GVL yields of 34.4 and 14.9 mol% respectively (entries 16 and 17, Table 4), thus demonstrating that the synthetic precursors of **1**–**2** are not suitable to catalyze the reaction of interest.

In order to deepen the catalytic performances of the most performing catalysts **1a** and **2a**, these complexes were further tested for the same reaction, but in the presence of different solvents as hydrogen donors, such as ethanol, 1-propanol, 1-butanol, 2-butanol, 1-pentanol, 2-pentanol, 1-hexanol and 2-hexanol. All these solvents can be obtained from renewable sources, guaranteeing the sustainability of the proposed process [58]. Regarding the chain length of the employed solvent/hydrogen donor, its effect towards the CTH of EL strongly relies on the corresponding standard enthalpy change of dehydrogenation reaction from alcohol to ketone/aldehyde [59], the latter defining the reducing tendency of ketone/aldehyde (corresponding oxidized species) to alcohol (reduced species). From this perspective, a higher standard enthalpy dehydrogenation change is associated to a greater stability of the corresponding alcohol, which exhibits increasingly weak reducing performances, unfavorably acting towards the CTH process. Correspondingly, lower standard enthalpy dehydrogenation change of alcohols is desirable for the CTH, indicating better hydrogen donor performances [60]. The standard enthalpy dehydrogenation change generally decreases with the increase of the chain length of the alcohol and this is true moving from methanol up to butanol, whereas an increase of the standard enthalpy dehydrogenation change occurs moving from butanol to pentanol (Table S4), suggesting a weakening of the hydrogen donor performances of the latter alcohol [60,61]. As expected, among isomeric alcohols, the secondary ones generally show the lowest standard enthalpy dehydrogenation change, thus providing increased hydrogen donor activities than the corresponding primary ones [60,62]. Moreover, alcohol isomerism is mainly related to the electron-releasing inductive effect of the alkyl group(s). In particular, primary alcohols are generally less active than secondary ones, due to a lower electron-releasing inductive effect, arising from only one alkyl group rather than two [61]. For such purpose, 2-butanol, 2-pentanol and 2-hexanol, together with the corresponding primary alcohols (1-butanol, 1-pentanol and 1-hexanol), were tested for the same reaction, in order to systematically evaluate the effect of the chain length, position of the hydroxyl moiety and steric hindrance. For this goal, also ethanol was tested as hydrogen donor. It is noteworthy that only a few studies have systematically investigated the use of different alcohols as hydrogen donors in TH reactions and the obtained results are reported in Table 5, together with those previously obtained with 2-propanol.

For all the investigated alcohols, the catalytic performances of **1a** were better than those of **2a**, especially in terms of selectivity to GVL after 1 h of reaction, as previously ascertained with 2-propanol, confirming the key contribution of the catalyst structure on the mechanism. EL conversion values were generally comparable between the two catalytic precursors employed in the same solvent/hydrogen donor. All the secondary alcohols showed better results than the primary ones, with

Table 4
Catalytic performances of **1a-f**, **2a-d**, **4a**, $[RuCl_2(\eta^6\text{-}p\text{-cymene})]_2$ and $RuCl_3$ hydrate (0.56 mol%, with respect to EL) on CTH of EL (5 mmol) to GVL, working in 2-propanol (10 mL) and in the presence of KOH (1 mol% with respect to EL). Reaction conditions: MW heating, T=150 °C, t = 60 min.

Entry	Catalytic precursor	EL conversion (mol %)	GVL selectivity (mol %)	GVL yield (mol %)	Propyl levulinate yield (mol %)	Other products yield (mol %)
5	**1a**	84.6 (1.4)	86.1 (1.5)	72.9 (1.2)	–	11.7 (0.2)
6	**2a**	86.7 (0.9)	78.0 (0.8)	67.7 (0.7)	–	19.0 (0.2)
7	**1b**	75.3 (0.8)	78.0 (0.8)	58.7 (0.6)	–	16.6 (0.2)
8	**2b**	79.9 (2.0)	67.6 (1.7)	54.0 (1.4)	–	25.9 (0.6)
9	**1c**	89.0 (1.4)	76.0 (1.2)	67.6 (1.1)	–	21.4 (0.3)
10	**2c**	91.6 (1.8)	60.4 (1.2)	55.3 (1.1)	–	36.3 (0.7)
11	**1d**	88.3 (1.1)	57.2 (0.7)	50.5 (0.7)	–	37.8 (0.5)
12	**2d**	92.8 (1.9)	61.8 (1.3)	57.4 (1.2)	3.5 (0.1)	31.9 (0.7)
13	**1e**	85.0 (1.7)	85.8 (1.8)	73.0 (1.5)	3.8 (0.1)	8.3 (0.2)
14	**1f**	84.9 (1.3)	62.6 (0.9)	53.1 (0.8)	4.6 (0.1)	27.2 (0.4)
15[a]	**4a**	83.4 (1.3)	62.5 (0.9)	52.1 (0.8)	7.6 (0.1)	23.7 (0.4)
16[a]	$[RuCl_2(\eta^6\text{-}p\text{-cymene})]_2$	81.4 (1.5)	42.3 (0.8)	34.4 (0.7)	–	46.9 (0.9)
17	$RuCl_3{\cdot}nH_2O$	34.6 (0.7)	43.0 (0.8)	14.9 (0.3)	–	19.7 (0.4)

Standard deviation values are reported in parenthesis.
[a] The % catalyst amount was calculated as (mol Ru/mol EL)•100.

both **1a** and **2a**, as the former selectively favored the TH mechanism of EL to GVL, rather than the *trans*-esterification of EL to the corresponding levulinate ester, a typical reaction of primary alcohols [60,62]. As shown in Table 5, in the presence of secondary alcohols, the yield of the corresponding levulinate ester was negligible (<3 mol%), whilst in the presence of primary alcohols, it was always higher than that of GVL, for both **1a** and **2a**. For example, by comparing entries 5–6 with 20–21, namely 2-propanol with 1-propanol, the EL conversion was high in all cases (>80 mol%), whereas the GVL selectivity significantly decreased moving from 2-propanol (80 mol%) to 1-propanol (25 mol%). The same trend can be observed by comparing 2-butanol (entries 24–25) with 1-butanol (entries 22–23), whereas the GVL selectivity decreased from approximately 75–80 to 15–20 mol%. Similar trends of the GVL selectivity have been ascertained by comparing 2-pentanol (entries 28–29) with 1-pentanol (entries 26–27) even if in this case lower EL conversions were achieved in 1-pentanol than in 2-pentanol (about 55 mol% in 1-pentanol and about 74 mol% in 2-pentanol). In addition, in all these tests (entries 26–29), GVL conversions are lower than those previously obtained with C_3 and C_4 alcohols. This outcome agrees with the highest standard enthalpy dehydrogenation change of 1-pentanol and 2-pentanol compared to the C_4 isomers (1-butanol and 2-butanol, in the case of 2-pentanol/2-butanol the value is comparable), and with the increased steric hindrance, which is less significant for C_3 isomers. Remarkably, the influence of steric factors in the catalytic mechanism is even more pronounced within the 1-hexanol/2-hexanol couple (entries 30–33), showing the worst catalytic outcomes. In fact, with the increase of the chain length, the higher steric hindrance leads to a worsening of the catalytic performances: both for primary and secondary alcohol, GVL yields decrease moving from butanol to pentanol and this detrimental effect is more marked in the presence of hexanol. These last outcomes are similar to those obtained with ethanol, which is a weak hydrogen donor. On the other hand, 2-butanol, a secondary alcohol characterized by one of the lowest standard enthalpy dehydrogenation changes (see Table S4), but at the same time featured by mild steric hindrance, revealed to be the best hydrogen donor. Comparing the data obtained from 2-propanol (the most commonly used alcohol in CTH studies) with those from 2-butanol, 2-pentanol and 2-hexanol, it is noteworthy that 2-butanol shows the best synergy among the effects of the chain length, isomerism and steric hindrance. At the same time, the negative effect of the steric hindrance was not considerable for 2-butanol, whereas it became more impactful for longer-chain alcohols (1-pentanol/2-pentanol and 1-hexanol/2-hexanol). This synergy highlighted for 2-butanol has a significant effect on its corresponding catalytic performances. A comparative evaluation between 2-propanol and 2-butanol reveals a slightly higher GVL yield with the latter (76 versus 73 mol%, respectively) in the presence of **1a** (the most performing pre-catalyst identified in this study). Regarding the comparison with longer-chain secondary alcohols, 2-pentanol and 2-hexanol, in the presence of the same pre-catalysts **1a**, for the last ones the steric hindrance became predominant and GVL yield significantly decreased as a function of the increase in the chain length. In particular, for 2-pentanol and 2-hexanol the GVL yields were 51 and 24 mol%, respectively.

To demonstrate the scalability of the proposed approach, the CTH reaction of EL to GVL with **1a** in the presence of 2-butanol as hydrogen donor was carried out in a pressure tube, adopting the traditional heating with an oil bath. For this purpose, the reaction time was changed, using 120 min instead of 60 min employed in the MW reaction, considering the well-known high efficiency of the latter approach [34b,34c,63]. A comparison between the catalytic results obtained with the two heating systems is reported in Fig. 6.

The comparison between microwave and traditional heating did not highlight any specific effects of microwaves, underlining the absence of any remarkable differences in the catalytic performances, in terms of both selectivity and yield parameters, achieved at comparable EL conversion. The translatability of the reaction using **1a** as catalytic precursor and 2-butanol as hydrogen donor has been fully demonstrated, which is a highly desirable aspect for taking into account the possible scale-up of the reaction. In particular, for the entries reported in Fig. 6, adopting both MW and traditional heating systems, promising GVL productivities (calculated as molGVL/(molRu × h)) were ascertained for

Table 5
Effect of the hydrogen donors (10 mL) on CTH of EL (5 mmol) to GVL working in the presence of KOH (1 mol% with respect to EL) and **1a** or **2a** as the catalytic precursor. Reaction conditions: MW heating, T=150 °C, t = 60 min.

Entry	Catalytic precursor (mol%)	Hydrogen donor	EL conversion (mol%)	GVL selectivity (mol%)	GVL yield (mol%)	Levulinate ester yield (mol%)	Other products yield (mol%)
18	**1a**	ethanol	38.4	52.1	20.0	–	18.4
	(0.56 mol%)		(0.4)	(0.5)	(0.2)		(0.2)
19	**2a**	ethanol	39.3	36.8	14.5	–	24.9
	(0.56 mol%)		(0.8)	(0.8)	(0.3)		(0.5)
20	**1a**	1-propanol	80.2	27.0	21.6	35.2	23.3
	(0.56 mol%)		(1.6)	(0.5)	(0.4)	(0.7)	(0.5)
21	**2a**	1-propanol	90.0	22.7	20.5	66.1	3.4
	(0.56 mol%)		(2.3)	(0.6)	(0.5)	(1.7)	(0.1)
5[a]	**1a**	2-propanol	84.6	86.1	72.9	0.0	11.7
	(0.56 mol%)		(1.4)	(1.5)	(1.2)		(0.2)
6[a]	**2a**	2-propanol	86.7	78.0	67.7	0.0	19.0
	(0.56 mol%)		(0.9)	(0.8)	(0.7)		(0.2)
22	**1a**	1-butanol	83.9	22.9	19.3	62.5	2.2
	(0.56 mol%)		(1.9)	(0.5)	(0.4)	(1.4)	(0.1)
23	**2a**	1-butanol	84.2	16.3	13.8	57.8	12.7
	(0.56 mol%)		(1.2)	(0.2)	(0.2)	(0.8)	(0.2)
24	**1a**	2-butanol	95.7	79.8	76.4	2.0	17.3
	(0.56 mol%)		(2.7)	(2.2)	(2.1)	(0.1)	(0.5)
25	**2a**	2-butanol	87.0	77.4	67.3	2.1	17.6
	(0.56 mol%)		(2.6)	(2.3)	(2.0)	(0.1)	(0.5)
26	**1a**	1-pentanol	57.7	21.1	12.2	41.0	4.5
	(0.56 mol%)		(1.5)	(0.4)	(0.3)	(0.9)	(0.1)
27	**2a**	1-pentanol	54.8	20.5	11.2	41.9	1.7
	(0.56 mol%)		(1.6)	(0.6)	(0.3)	(1.3)	(0.1)
28	**1a**	2-pentanol	73.8	68.7	50.7	1.9	21.2
	(0.56 mol%)		(2.2)	(2.1)	(1.5)	(0.1)	(0.6)
29	**2a**	2-pentanol	75.4	69.1	52.1	1.8	21.5
	(0.56 mol%)		(2.3)	(2.1)	(1.6)	(0.1)	(0.6)
30	**1a**	1-hexanol	36.3	18.8	6.8	20.5	9.0
	(0.56 mol%)		(0.7)	(0.4)	(0.1)	(0.4)	(0.2)
31	**2a**	1-hexanol	35.8	20.7	7.4	20.7	7.7
	(0.56 mol%)		(0.5)	(0.3)	(0.1)	(0.3)	(0.1)
32	**1a**	2-hexanol	41.0	59.7	24.5	1.9	14.7
	(0.56 mol%)		(1.2)	(1.8)	(0.7)	(0.1)	(0.4)
33	**2a**	2-hexanol	43.3	55.9	24.2	1.7	17.4
	(0.56 mol%)		(1.3)	(1.7)	(0.7)	(0.1)	(0.5)
34	**1a**	2-butanol	87.8	85.0	74.6	0.0	13.2
	(0.11 mol%)		(2.2)	(2.1)	(1.9)		(0.3)

Standard deviation values are reported in parenthesis.
[a] Taken from Table 4.

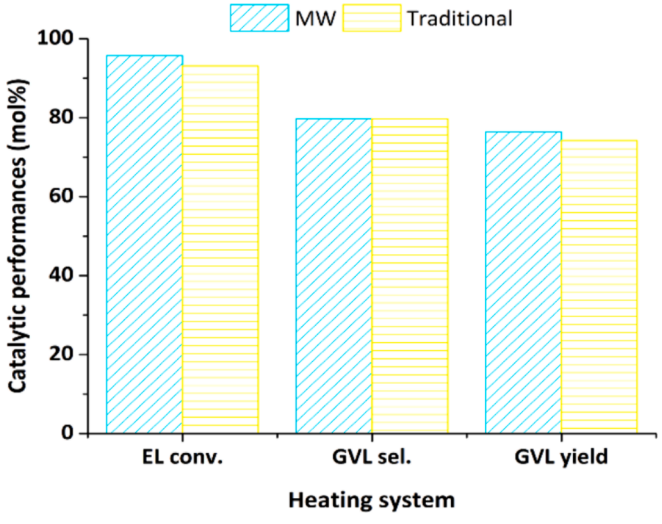

Fig. 6. Comparison of MW and traditional heating systems for CTH reaction of EL (5 mmol) to give GVL in 2-butanol (10 mL), using the complex **1a** (0.56 mol % with respect to EL). Reaction conditions: T=150 °C, KOH=1 mol% respect to EL, reaction time = 60 min for MW heating or 120 min for traditional heating.

MW and traditional best entries, amounting to 136.4 h^{-1} and 66.3 h^{-1}, respectively. These productivities are significantly higher than those claimed in most of the available literature studies (Table 1, Fig. 1). In particular, Dai *et al.* claimed a productivity of 5 h^{-1}, working with iron (II) hydroxycyclopentadienyl hydride (**B**, Fig. 1) as the catalyst [33b]. Besides, Fu *et al.* obtained 1.2 h^{-1}, employing an iron-based homogeneous catalyst (**A**, Fig. 1) [33a]. Shende *et al.* achieved the productivity of 4.6 h^{-1}, using the Noyori-Ikariya's catalyst (**E**, Fig. 1) [33f]. Remarkably, the MW-related productivity of 136.4 h^{-1} of the present work is even higher than that achieved under the optimized conditions of our previous study equal to 110 h^{-1}, obtained using a ruthenium *p*-cymene complex with α-diimine ligand (**G**, Fig. 1) as catalytic precursor (KOH as base, 2-propanol as hydrogen donor, T=160 °C and MW as the heating system) [11].

The reaction mixture obtained under the optimized MW reaction conditions, namely that obtained with **1a** as catalytic precursor and 2-butanol as hydrogen donor, was qualitatively analyzed by GC–MS, to better characterize the involved reaction products and obtain useful information on the reaction mechanism. Based on the identified molecules (Figures S54-S58), and starting from our previous work [11], the following reaction pathways have been proposed (Scheme 4).

The main pathway (pathway 1) involves the traditional TH mechanism of EL to GVL, whose formation is favored by the efficiency of EtOH as leaving group [64]. In this context, ethyl-4-hydroxypentanoate intermediate of pathway 1 was not identified by GC–MS, in agreement with its high instability [11,65]. On the other hand, in pathway 2, EL

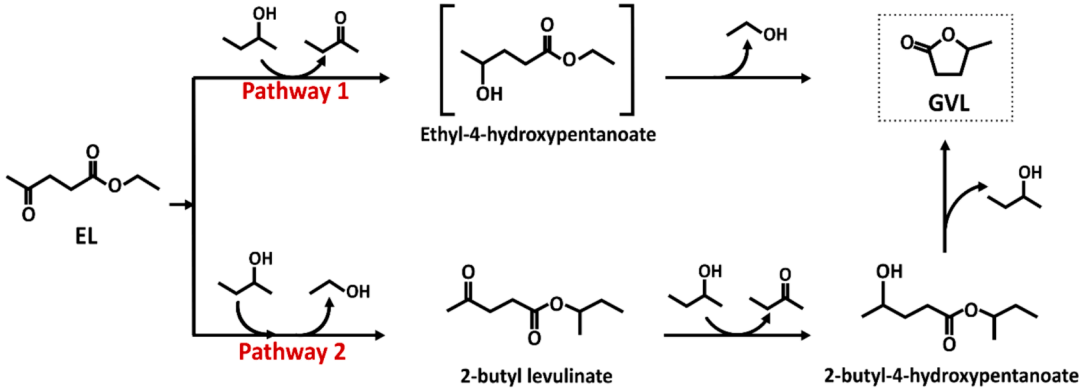

Scheme 4. General reaction pathways proposed for the CTH of EL to GVL, working in the presence of 1a as the catalytic precursor and 2-butanol as hydrogen donor.

first undergoes a *trans*-esterification reaction with 2-butanol, giving 2-butyl levulinate, the latter reacting with 2-butanol to give the 2-butyl-4-hydroxypentanoate, which is converted in turn to GVL, through a ring-closing reaction. Despite the occurrence of the *trans*-esterification reaction, pathway 2 does not prevail over pathway 1, as already demonstrated by Tabanelli *et al.* [64] for TH of EL with 2-propanol. In our case, the even greater steric hindrance of 2-BuOH probably stabilizes both intermediates of pathway 2, namely 2-butyl levulinate and 2-butyl-4-hydroxypentanoate, which have been experimentally identified by the GC–MS analysis of the reaction mixture (Figures S57-S58). The proposed mechanism is consistent with that already reported in our previous work [11], also considering the results reported in Table 5. Indeed, besides the *trans*-esterified levulinate ester, another by-product could be represented by the other intermediate from pathway 2, namely the corresponding reduced species of the levulinate ester, that is 2-propyl-4-hydroxypentanoate, 2-butyl-4-hydroxypentanoate, 2-pentyl-4-hydroxypentanoate and 2-hexyl-4-hydroxypentanoate.

Moreover, a preliminary characterization of the spent catalyst was carried out. For this purpose, at the end of the reaction carried out under the optimized conditions (2-butanol as hydrogen donor, **1a** = 0.56 mol% with respect to EL, KOH=1 mol% with respect to EL, 150 °C, 1 h, under MW heating), the formation of a black precipitate was observed. The suspension was filtered and ICP-OES analysis of the liquid phase was performed for the Ru quantification. The concentration of soluble Ru species in the final reaction mixture amounted to 59 % of the initial value. The FT-IR spectrum of the black solid showed no diagnostic absorption (such as isocyanide stretching) and the elemental analyses indicated a low organic content (see Experimental Section). SEM-EDS analyses (Figure S59) indicated the presence of Ru(0) particles, whose unwanted formation agrees with the prevailing reducing environment of the TH reaction medium [66]. In addition, KCl was also identified, whose formation indicates the catalytic cycle advancement, taking into account that this salt results from the release of the chloride ligand originally present in **1a** and the employment of KOH as the co-catalyst. It should be noted that, up to now, literature dealing with Ru-based catalysts has not specifically considered the characterization of the spent catalyst and its possible recycle. In principle, in our case, the precipitation of 41 % of Ru metal has occurred under the best reaction conditions, but its potential next recovery/reuse after oxidation to $RuCl_3$ is reasonable [67]. Even better, in order to minimize *a priori* the precipitation of the Ru^0, the CTH of EL to GVL was carried out in the presence of **1a** in 2-butanol, employing a much milder reaction temperature (110 °C). After 2 h, the promising GVL selectivity of 65.7 mol% was achieved, although the corresponding EL conversion was 26.8 mol%. Besides the confirmation of the desirable absence of any Ru metal precipitate after this reaction, the ^1H NMR spectrum of the final reaction mixture (see ESI for details) showed signals in the aromatic region due to the xylyl group and small, characteristic resonances due to ruthenium hydride species (δ_H/ppm = -21.1, –23.5 ppm) which are possibly related to the homogeneous, catalytically active species. Under these new reaction conditions, a recycling test was carried out in 2-butanol by replenishing the consumed EL (up to 5 mmol), confirming the previous catalytic results (EL conversion = 25.3 mol%, GVL selectivity = 62.8 mol%), again highlighting the absence of Ru metal in the reaction medium, which is a highly desirable aspect for improving the catalyst reuse.

Lastly, in order to increase the productivity of the proposed catalytic approach, a single reaction (entry 34, Table 5) was carried out with a 5-fold lower amount of catalyst **1a** (0.11 mol%, respect to EL) under the previously optimized reaction conditions (2-butanol as hydrogen donor, KOH=1 mol% respect to EL, 150 °C, 1 h, under MW heating). The EL conversion was 87.8 mol%, slightly lower than that obtained in entry 24 (95.7 mol%), but the GVL selectivity (at comparable EL conversion) was improved (85.0 versus 79.8 mol%), allowing the similar GVL yield of 74.6 mol% to that achieved in entry 24 (76.4 mol). Based on these outstanding results, the maximum GVL productivity was increased up to 666 h^{-1}, a noteworthy achievement, especially if compared with the results already available for homogeneous and heterogeneous (0.63–3.86 h^{-1}) systems [60,64,67]. Such a very high productivity, together with the use of efficient MW irradiation and a simple and high-yielding preparation of the Ru complexes (95 % and 78 % overall yield for **1a** and **2a**, respectively, from commercial $RuCl_3$ hydrate) improve the techno-economic assessment of the CTH conversion of EL to GVL, in agreement with the life cycle assessment (LCA) given by Van Slagmaat *et al.* [68]. In conclusion, the main strengths of our new Ru(II)-based catalyst are (i) the stability of our catalysts under air environment, (ii) the easy and high-yield synthesis of the catalysts, (iii) the high turnover number and turnover efficiency, (iv) the very high GVL productivity and (v) the feasible recycle under milder reaction conditions. In fact, one of the main bottlenecks of the available homogeneous Ru-based catalysts is their degradation during the reaction, due to the precipitation of Ru metal, thus hindering at the moment the complete catalyst reuse [65]. This issue was specifically considered in this work, and the drawback of the Ru metal precipitation was overcome by operating at a lower temperature (110 °C), which resulted in lower EL conversion and GVL yield, but in a satisfactory GVL selectivity (66 mol% of the first recycle versus 80 mol% of the direct run), which is a highly desirable aspect for next industrial purposes. However, the precipitation of ruthenium as solid phase could result also in a potentiality, thanks to its possible recovery/reuse after oxidation to $RuCl_3$.

4. Conclusions

Six ruthenium(II) η^6-*p*-cymene complexes with different aryl/alkyl isocyanide and halide ligands were prepared in 89–97 mol% yield, starting from commercially available $RuCl_3$ hydrate and isocyanides. Two synthetic procedures were developed, which allowed us to isolate four *cis,mer*-$[RuCl_2(CNR)(\kappa S\text{-}DMSO)_3]$ compounds in 56–82 mol% yield, representing the first ruthenium complexes with DMSO and isocyanide

as ligands. All these air- and moisture-stable isocyanide complexes are effective catalytic precursors for the transfer hydrogenation of ethyl levulinate to γ-valerolactone. The reaction conditions involve a low catalyst loading (0.56 mol%), short reaction time (1 h) and the energy-saving microwave heating (150 °C), thus pointing to an improvement in the sustainability of the process with respect to the literature, where anhydrous systems and inert atmosphere are often needed. The selectivity for γ-valerolactone is generally higher for the *p*-cymene derivatives with respect to the corresponding DMSO complexes, possibly due to the lability of sulfoxide ligands in solution, and this feature is affected by the isocyanide group in each series. The best catalytic performances are offered by the xylyl isocyanide derivatives **1a** and **2a** (γ-valerolactone yields equal to 72.9 and 67.7 mol%, respectively). Remarkably, **1a** and **2a** are also effective catalytic precursors in 2-butanol, a more sustainable solvent and hydrogen donor with respect to isopropanol, providing 76.4 and 67.3 mol% of γ-valerolactone yield, respectively, under the optimized conditions, together with the promising γ-valerolactone productivity of 136.4 h^{-1} for **1a**. Moreover, the catalytic performances of **1a** in 2-butanol with traditional heating are consistent with those obtained using MW heating, a desirable feature for the process scale-up. In order to demonstrate the possible catalyst recycle, the temperature was decreased up to 110 °C, avoiding the thermal degradation of **1a**, and fresh EL was added and converted to GVL. Finally, to further increase the catalyst productivity, the catalyst amount was reduced to 0.11 mol%, obtaining the EL conversion of 87.8 mol% and the GVL selectivity and yield of 85.0 and 74.6 mol%, respectively, thus increasing the GVL productivity up to the highest value of 666 h^{-1}. In summary, we demonstrated that isocyanide coordination to ruthenium(II) scaffolds provides catalytic activity for the transfer hydrogenation. This represents the basis for the development of new compounds with improved catalytic activity, particularly concerning the catalyst stability in the employed reaction conditions. This goal could be reached by keeping a simple synthetic design of the catalytic precursors, as we did in this work, which is a fundamental aspect in the perspective of catalyst development beyond the academic level.

5. Experimental section

5.1. General experimental details

All reagents and solvents were obtained from Alfa Aesar, Merck, Carlo Erba or TCI Europe and were used without further purifications. 1-pentyl levulinate and 1-hexyl hexanoate were purchased by Biosynth and Chemspace, respectively, and used as received. Isocyanides were stored at 4 °C or – 20 °C; contaminated labware was treated with methanolic HCl. Compounds $[RuX_2(\eta^6\text{-}p\text{-cymene})]_2$ (X=Cl, I) were prepared according to the literature [10b,16,17]. The preparation of **1a-e** was carried out under N_2 using standard Schlenk techniques. Anhydrous CH_2Cl_2 was obtained from SPS 5 solvent purifier (MBraun) and stored over 4 Å MS. All the other operations, including work-up procedures, were carried out in air with non-anhydrous solvents. Filtrations were carried out on G3 sintered-glass filters, unless otherwise specified (G4); celite Standard Supercel® (Alfa Aesar) was used when indicated. All the isolated complexes are free-flowing powders relatively inert to air and moisture which were kept under N_2 for long time storage as a precaution. Percent reaction yields are calculated on molar basis with respect to $[RuX_2(\eta^6\text{-}p\text{-cymene})]_2$ and are referred to the isolated, powdered material. Carbon, hydrogen, nitrogen and sulfur (CHNS) analyses were performed on a Vario MICRO cube instrument (Elementar). Infrared spectra of solid samples (650–4000 cm^{-1} range) were recorded on a Perkin Elmer Spectrum Two spectrometer equipped with a diamond-ATR sampling accessory. FT-IR spectra of solutions were recorded using a CaF_2 liquid transmission cell (1500–2300 cm^{-1}) on a Perkin Elmer Spectrum 100 FT-IR spectrometer. FT-IR spectra were processed with Spectragryph [69]. NMR spectra were recorded on YH JNM-ECZ400S or JNM-ECZ500R instruments (JEOL) equipped with Royal HFX Broadband probes. $CDCl_3$ stored in the dark over Na_2CO_3 was used for NMR analysis. $^{13}C\{^1H\}$ NMR spectra were recorded with 6 s relaxation time. Chemical shifts are referenced to the residual solvent peaks (^1H, ^{13}C) [70]. NMR resonances were assigned with the support of ^1H-NOESY (mix time 750 ms, relaxation time 1 sec, linewidth 15 Hz), $^1H–^{13}C$ *gs*-HSQC and *gs*-HMBC correlation experiments.

5.2. Synthesis and characterization of arene-isocyanide complexes

*Procedure **a** (Scheme 1).* In a 25 mL Schlenk tube under N_2, a solution of $[RuX_2(\eta^6\text{-}p\text{-cymene})]_2$ (100–300 mg; X =Cl, I) in anhydrous CH_2Cl_2 (8–10 mL) was treated with a stoichiometric amount of the selected isocyanide. The orange (X=Cl) or violet-red (X=I) mixture was stirred for 1–3 h at room or reflux temperature, respectively. The conversion was checked by FT-IR analysis (CH_2Cl_2), then the resulting orange-red (X=Cl) or violet-red (X=I) suspension was filtered in air over celite. The filtrate was taken to dryness under vacuum and the residue was triturated with Et_2O/hexane 1:1 *V/V* mixture and stirred at room temperature for some hours. Next, the suspension was filtered (G3 sintered glass filter) and the resulting orange (X=Cl) or red-violet (X=I) solid was washed with Et_2O/hexane 1:1 *V/V*, hexane and then dried under vacuum (40 °C). The filtration is fundamental to remove a dark brown solid (by-product). Samples isolated without the filtration step appear with a brownish shade and have a lower CHN content, while showing no impurities on the ^1H and ^{13}C NMR spectra.

*Procedure **b** (Scheme 1).* The reactions were carried out as described above using deaerated MeCN as solvent.

$[RuCl_2(CNXyl)(\eta^6\text{-}p\text{-cymene})]$, 1a (Chart 1).

Prepared according to procedure ***a*** using $[RuCl_2(\eta^6\text{-}p\text{-cymene})]_2$ (300 mg, 0.980 mmol Ru) and XylNC (131 mg, 1.00 mmol); reaction time: 3 h; yield: 412 mg, 96 mol%. Alternatively prepared from $[RuCl_2(\eta^6\text{-}p\text{-cymene})]_2$ (251 mg, 0.818 mmol Ru) in MeCN (10 mL) according to procedure ***b***; reaction time: 45 min; yield: 344 mg, 96 mol %. The previous literature preparation in lower scale (60 mg of $[RuCl_2(\eta^6\text{-}p\text{-cymene})]_2$) and similar reaction conditions resulted in an 86 mol% yield of **1a** after recrystallization [19j]. Soluble in CH_2Cl_2, MeCN, poorly soluble in toluene, insoluble in hexane. Anal. Calcd. for $C_{19}H_{23}Cl_2NRu$: C, 52.18; H, 5.30; N, 3.20. Found: C, 52.48; H, 5.23; N, 3.16. IR (solid state): $\tilde{\nu}/cm^{-1}$ = 3048w, 2968w, 2922w, 2872w, 2148 s (C≡N), 1591w, 1541w, 1498w, 1468 m, 1441w-sh, 1377 m, 1324w, 1318w, 1280w, 1262w, 1203w, 1183w, 1169w, 1117w, 1091w, 1059w, 1032 m, 1002w, 923w, 894-886w, 859w, 815w, 768 s, 718w, 692w, 665 m. IR (CH_2Cl_2): $\tilde{\nu}/cm^{-1}$ = 2162 s (C≡N). IR (MeCN): $\tilde{\nu}/cm^{-1}$ = 2159 (CN). IR (toluene): $\tilde{\nu}/cm^{-1}$ = 2156 (C≡N). ^1H NMR ($CDCl_3$): δ/ppm = 7.19–7.15 (m, 1H, $C^{13}H$), 7.09 (d, $^3J_{HH}$=7.6 Hz, 2H, $C^{12}H$), 5.70 (d, $^3J_{HH}$=6.1 Hz, 2H, C^4H), 5.53 (d, $^3J_{HH}$=6.1 Hz, 2H, C^3H), 2.93 (hept, $^3J_{HH}$=6.9 Hz, 1H, C^6H), 2.47 (s, 6H, $C^{11}H$), 2.35 (s, 3H, C^1H), 1.33 (d, $^3J_{HH}$=6.9 Hz, 6H, C^7H). $^{13}C\{^1H\}$ NMR ($CDCl_3$): δ/ppm = 151.7 (br, C^8), 135.8 (C^{10}), 129.3 (C^{13}), 128.0 (C^{12}), 127.3 (br, C^9), 108.5 (C^5), 107.9 (C^2); 88.8, 88.3 (C^3 + C^4); 31.6 (C^6), 22.7 (C^7); 19.2, 19.1 (C^1 + C^{11}). ^1H NMR (CD_3OD): δ/ppm = 7.31–7.18 (m, 3H, $C^{12}H$+$C^{13}H$); 5.92 (d, $^3J_{HH}$=6.1 Hz, 2H, C^4H), 5.70 (d, $^3J_{HH}$=6.1 Hz, 2H, C^3H), 2.89 (hept,

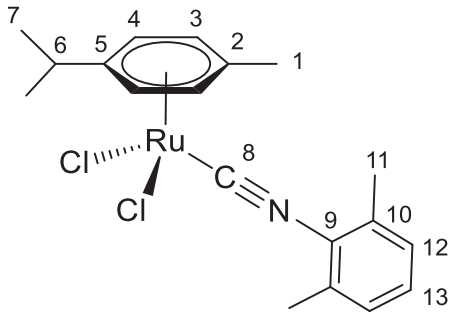

Chart 1. Structure of **1a** (numbering refers to carbon atoms).

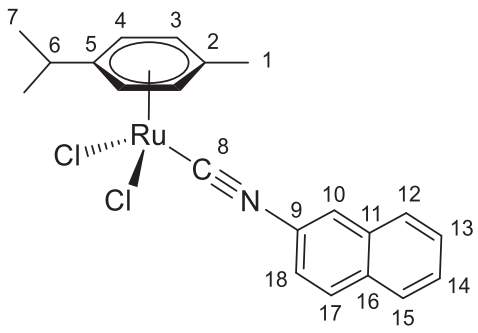

Chart 2. Structure of **1b** (numbering refers to carbon atoms).

$^3J_{HH}$=6.9 Hz, 1H, C^6H), 2.49 (s, 6H, $C^{11}H$), 2.28 (s, 3H, C^1H), 1.33 (d, $^3J_{HH}$=6.9 Hz, 6H, C^7H).

[$RuCl_2${CN(2-naphthyl)}(η^6-*p*-cymene)] , 1b (Chart 2).

Prepared according to procedure ***a*** using [$RuCl_2(\eta^6$-*p*-cymene)]$_2$ (106 mg, 0.346 mmol Ru) and 2-naphthyl isocyanide (59 mg, 0.35 mmol); reaction time: 1 h; yield: 145 mg, 91 mol%. Soluble in CH_2Cl_2, poorly soluble in toluene, insoluble in ^{i}PrOH, hexane. Anal. Calcd. For $C_{21}H_{21}Cl_2NRu$: C, 54.91; H, 4.61; N, 3.05. Found: C, 54.51; H, 4.41; N, 3.10. IR (solid state): ũ/cm^{-1} = 3053w, 2968w, 2933w, 2874w; 2152 s, 2107 m-sh (C≡N); 1623w, 1594w, 1501w, 1470w, 1381w, 1358w, 1358w-sh, 1326w, 1283w, 1267w, 1245w, 1207w, 1163w, 1121w, 1094w, 1064w, 1039w, 954w, 930w, 898w, 881w, 861 s, 833w, 754 m, 708w, 665w. IR (CH_2Cl_2 or toluene): ũ/cm^{-1} = 2171 m-sh, 2160 s (C≡N), 2141 m-sh, 2120w-sh; shoulder absorptions are present also in the FT-IR spectrum of 2-naphthyl isocyanide and are probably related to interactions of the 2-naphthyl groups in solution. ^{1}H NMR ($CDCl_3$): δ/ppm = 7.95 (s, 1H, $C^{10}H$); 7.86 (d, $^3J_{HH}$=8.7 Hz, $C^{17}H$) + 7.89–7.80 (m, $C^{13}H$+$C^{14}H$) (3H); 7.60–7.53 (m, 2H, $C^{12}H$+$C^{15}H$); 7.47 (dd, $^3J_{HH}$=8.7 Hz, $^4J_{HH}$=1.2 Hz, 1H, $C^{18}H$), 5.74 (d, $^3J_{HH}$=5.8 Hz, 2H, C^4H); 5.57 (d, $^3J_{HH}$=5.8 Hz, 2H, C^3H); 2.94 (hept, $^3J_{HH}$=6.9 Hz, 1H, C^6H), 2.37 (s, 3H, C^1H), 1.36 (d, $^3J_{HH}$=6.9 Hz, 6H, C^7H). $^{13}C\{^1H\}$ NMR ($CDCl_3$): δ/ppm = 149.5 (br., C^8), 133.0 (C^{16}), 132.6 (C^{11}), 129.8 (C^{17}); 128.*13*, 128.*07*, 128.*01*, 127.7 (C^{12} + C^{13} + C^{14} + C^{15}); 126.4 (C^{10}); 124.6 (C^9); 123.4 (C^{18}); 108.9, 108.3 (C^2 + C^5); 88.9 (C^3 + C^4); 31.5 (C^6); 22.7 (C^7); 19.1 (C^1).

[$RuCl_2$(CNCH_2Ph)(η^6-*p*-cymene)] , 1c (Chart 3).

Prepared according to the procedure ***a*** using [$RuCl_2(\eta^6$-*p*-cymene)]$_2$ (110 mg, 0.359 mmol Ru) and benzyl isocyanide (47 µL, 0.39 mmol); reaction time: 1.5 h; yield: 147 mg, 97 mol%. Alternatively prepared from [$RuCl_2(\eta^6$-*p*-cymene)]$_2$ (80 mg, 0.26 mmol Ru) in MeCN (5 mL) according to procedure ***b***; reaction time: 2 h; yield: 104 mg, 94 mol%. Soluble in CH_2Cl_2, MeCN, poorly soluble in ^{i}PrOH, insoluble in Et_2O. Anal. Calcd. for $C_{18}H_{21}Cl_2NRu$: C, 51.07; H, 5.00; N, 3.31. Found: C, 51.2; H, 4.99; N, 3.37. IR (solid state): ũ/cm^{-1} = 3084w, 2977w, 2960w, 2929w, 2913w, 2872w-sh, 2214 s (C≡N), 2170w-sh, 1605w, 1534w, 1498w, 1454w, 1429w, 1389w, 1355 m, 1277w, 1197w, 1158w, 1107w, 1076w, 1052w, 1027w, 875w, 798w, 740 s, 695 m, 678w, 602 m, 524w, 483w. IR (CH_2Cl_2): ũ/cm^{-1} = 2200 s (C≡N). IR (MeCN): ũ/cm^{-1} = 2201 s (C≡N). ^{1}H NMR ($CDCl_3$): δ/ppm = 7.42–7.33 (m, 5H, Ph), 5.57 (d, $^3J_{HH}$=5.7 Hz, 2H, C^4H), 5.42 (d, $^3J_{HH}$=5.7 Hz, 2H, C^3H), 5.03 (s, 2H, C^9H), 2.74 (hept, $^3J_{HH}$=6.8 Hz, 1H, C^6H), 2.24 (s, 3H, C^1H), 1.20 (d, $^3J_{HH}$=6.9 Hz, 6H, C^7H). $^{13}C\{^1H\}$ NMR ($CDCl_3$): δ/ppm = 141.3 (br. C^8), 132.0 (C^{10}), 129.2 (C^{11}), 128.9 (C^{13}), 127.1 (C^{12}); 107.*48*, 107.*45* (C^2 + C^5); 87.*94*, 87.*86* (C^3 + C^4); 48.8 (C^9), 31.3 (C^6), 22.5 (C^7), 18.9 (C^1).

[$RuCl_2$(CNCy)(η^6-*p*-cymene)] , 1d (Chart 4).

Prepared according to procedure ***a*** using [$RuCl_2(\eta^6$-*p*-cymene)]$_2$ (300 mg, 0.980 mmol Ru) and cyclohexyl isocyanide (125 µL, 1.00 mmol); reaction time: 2.5 h; yield: 396 mg, 97 mol%. Alternatively prepared from [$RuCl_2(\eta^6$-*p*-cymene)]$_2$ (499 mg, 1.63 mmol Ru) in MeCN (5 mL) according to procedure ***b***; reaction time: 1.5 h; yield: 656 mg, 96 mol%. The literature preparation involved the use of excess isocyanide, prolonged reaction time and purification via silica gel chromatography, as follows: 5.0 eq CyNC, CH_2Cl_2, 20 h, room T, 58 mol% yield [19b]. Soluble in CH_2Cl_2, acetone, toluene, MeCN; poorly soluble in ^{i}PrOH, Et_2O, insoluble in hexane. Crystals of **1d** suitable for X-ray diffraction were obtained from a CH_2Cl_2 solution layered with hexane and settled aside at – 20 °C. Anal. Calcd. For $C_{17}H_{25}Cl_2NRu$: C: 49.16; H: 6.07; N: 3.37. Found: C: 48.98; H: 5.91; N: 3.34. IR (solid state): ũ/cm^{-1} = 3060w, 3043w, 2959 m, 2937 m, 2919 m-sh, 2861 m, 2195 s (C≡N), 2157–2148 m-sh, 1538w, 1497w, 1469 m-sh, 1462 m-sh, 1446 m, 1386 m, 1378 m, 1362 m, 1352 m, 1325 m, 1276w, 1241w, 1203w, 1154w, 1143w, 1127wm 1115 m, 1092 m, 1055 m, 1033 m, 1022–1015 m-sh, 998w-sh, 933w, 916 m, 876 m, 863 m, 822w, 800w, 875w, 675w, 657 m. IR (CH_2Cl_2): ũ/cm^{-1} = 2194 s (C≡N). IR (MeCN): ũ/cm^{-1} = 2192 s (C≡N). IR (toluene): ũ/cm^{-1} = 2186 s (C≡N). ^{1}H NMR ($CDCl_3$): δ/ppm = 5.57 (d, $^3J_{HH}$=5.9 Hz, 2H, C^4H), 5.40 (d, $^3J_{HH}$=5.8 Hz, 2H, C^3H), 4.01 (s-br, 1H, C^9H), 2.85 (hept, $^3J_{HH}$=6.9 Hz, 1H, C^6H), 2.29 (s, 3H, C^1H); 2.02–1.92 (m, 2H), 1.87–1.75 (m, 4H), 1.51–1.37 (m, 4H) ($C^{10}H$+$C^{11}H$+$C^{12}H$); 1.30 (d, $^3J_{HH}$=6.9 Hz, 6H, C^7H). $^{13}C\{^1H\}$ NMR ($CDCl_3$): δ/ppm = 138.7 (br, C^8N), 107.2 (C^5), 106.9 (C^2); 87.7, 87.5 (C^3 + C^4), 55.4 (C^9), 32.8 (C^{10}), 31.5 (C^6), 24.9 (C^{12}), 22.9 (C^{11}), 22.7 (C^7), 19.0 (C^1). ^{1}H NMR (CD_3OD): δ/ppm = 5.76 (d, $^3J_{HH}$=6.1 Hz, 2H, C^4H), 5.54 (d, $^3J_{HH}$=6.0 Hz, 2H, C^3H), 4.26–4.12 (m, 1H, C^9H), 2.82 (hept, $^3J_{HH}$=6.9 Hz, 1H, C^6H), 2.23 (s, 3H, C^1H); 2.01–1.89 (m, 2H), 1.89–1.75 (m, 4H), 1.58–1.41 (m, 4H) ($C^{10}H$+$C^{11}H$+$C^{12}H$); 1.30 (d, *J*=6.9 Hz, 6H, C^7H).

[$RuCl_2$(CN^{t}Bu)(η^6-*p*-cymene)] , 1e (Chart 5).

Prepared according to procedure ***a*** using [$RuCl_2(\eta^6$-*p*-cymene)]$_2$ (200 mg, 0.653 mmol Ru) and *tert*-butyl isocyanide (75 µL, 0.66 mmol); reaction time: 3 h; yield: 237 mg, 93 mol%. Alternatively prepared from [$RuCl_2(\eta^6$-*p*-cymene)]$_2$ (76 mg, 0.25 mmol Ru) in MeCN (5 mL) according to procedure ***b***; reaction time: 2.5 h; yield: 87 mg, 89 mol%. Previous literature preparations involve the use of excess isocyanide, prolonged reaction time and/or higher temperature and purification via (re)crystallization, as follows: 5.0 eq ^{t}BuNC, CH_2Cl_2, room T, 20 h, 64 mol% yield [19b]; 3.5 eq ^{t}BuNC, hexane, reflux T, overnight, 61.5 mol% yield [19 g]; 1.5 eq ^{t}BuNC, toluene, room T, 6 h, ≥ 85 mol% yield [19i]. Soluble in CH_2Cl_2, MeCN, insoluble in petroleum ether. Crystals of **1e** suitable for X-ray diffraction were obtained from a CH_2Cl_2 solution

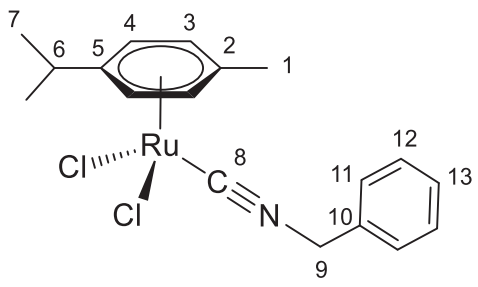

Chart 3. Structure of **1c** (numbering refers to carbon atoms).

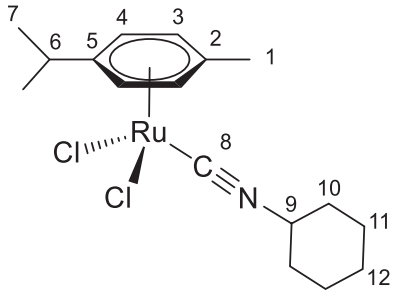

Chart 4. Structure of **1d** (numbering refers to carbon atoms).

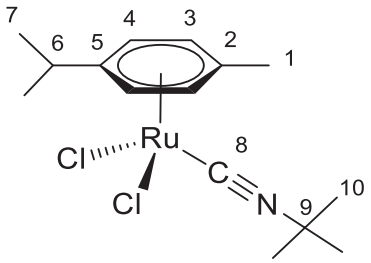

Chart 5. Structure of **1e** (numbering refers to carbon atoms).

layered with hexane and settled aside at – 20 °C. Anal. Calcd. For $C_{15}H_{23}Cl_2NRu$: C, 46.28; H, 5.95; N, 3.60. Found: C, 45.98; H, 5.86; N, 3.53. IR (solid state): ũ/cm^{-1} = 3056w, 3032w, 2981w, 2968w, 2962w, 2929w, 2873w, 2192 s (C≡N), 1617w, 1540w, 1466 m, 1442w-sh, 1404w, 1387w, 1372w, 1322w, 1279w, 1236w-sh, 1195 m, 1168w-sh, 1141w, 1117w, 1093w, 1057w, 1030w, 1003w, 975w, 957w, 920w, 877w, 859w-sh, 800w, 691w, 675w. IR (CH_2Cl_2): ũ/cm^{-1} = 2186 (C≡N). IR (MeCN): ũ/cm^{-1} = 2185 (C≡N). ^{1}H NMR ($CDCl_3$): δ/ppm = 5.55 (d, $^3J_{HH}$=6.0 Hz, 2H, C^{4}H), 5.39 (d, $^3J_{HH}$=6.0 Hz, 2H, C^{3}H), 2.83 (hept, $^3J_{HH}$=6.9, C^{6}H), 2.29 (s, 3H, C^{1}H), 1.54 (s, 9H, C^{10}H), 1.30 (d, $^3J_{HH}$=6.9 Hz, C^{7}H). ^{13}C{^{1}H} NMR ($CDCl_3$): δ/ppm = 137.9 (br., C^8); 107.8, 106.6 (C^2 + C^5); 87.6, 87.4 (C^3 + C^4); 58.7 (C^9); 31.5 (C^6); 30.8 (C^{10}); 22.7 (C^7); 18.9 (C^1).

[RuI$_2$(CN^{t}Bu)(η^6-*p*-cymene)] , 1f (Chart 6).

Prepared according to procedure ***a*** using [RuI$_2$(η^6-*p*-cymene)]$_2$ (127 mg, 0.26 mmol Ru) and *tert*-butyl isocyanide (30 µL, 0.27 mmol); reaction time: 2 h (reflux temperature); yield: 135 mg, 91 mol%. Soluble in CH_2Cl_2, poorly soluble in Et_2O, insoluble in hexane. Anal. Calcd. for: C, 31.48; H, 4.05; N, 2.45. Found: C, 31.42; H, 3.99; N, 2.48. IR (solid state): ũ/cm^{-1} = 3063w, 3035w, 2980w, 2953w, 2924w, 2898w, 2862w, 2166 s (C≡N), 2051w-sh, 1541w, 1506w, 1465w, 1443 m, 1349w, 1366 m, 1326w, 1304w, 1282w, 1230 m-sh, 1200 m, 1156w-sh, 1109w, 1089w, 1053w, 1016w, 1012w, 932w, 885w, 854 m, 803w, 735w, 677w, 631w, 517 m. IR (CH_2Cl_2): ũ/cm^{-1} = 2169 s (C≡N). ^{1}H NMR ($CDCl_3$): δ/ppm = 5.60 (d, $^3J_{HH}$=6.0 Hz, 2H, C^{4}H), 5.49 (d, $^3J_{HH}$=6.0 Hz, 2H, C^{3}H), 2.94 (hept, $^3J_{HH}$=6.9 Hz, 1H, C^{6}H), 2.56 (s, 3H, C^{1}H), 1.49 (s, 9H, C^{10}H), 1.31 (d, $^3J_{HH}$=6.9 Hz, 6H, C^{7}H). ^{13}C{^{1}H} NMR ($CDCl_3$): δ/ppm = 135.8 (br., C^8), 109.8 (C^5), 106.1 (C^2), 89.2 (C^4), 87.6 (C^3), 58.4 (C^9), 32.1 (C^6), 30.8 (C^{10}), 23.1 (C^7), 20.5 (C^1).

5.3. Synthesis and characterization of DMSO-isocyanide complexes

*Procedure **a*** (Scheme 2). In a 50 mL round-bottom flask, a brick-red suspension of [RuCl$_2$(η^6-*p*-cymene)]$_2$ (about 100 mg), the selected isocyanide (CNR, 1.0 eq) in toluene (5 mL) was stirred at room temperature for 1.0–1.5 h. The quantitative conversion of the isocyanide and the formation of **1a-e** was assessed by FT-IR (CH_2Cl_2) analyses on an aliquot of the resulting mixture (R=Xyl, ^{t}Bu: red–orange solution + solid; R=2-naphthyl or Bn: abundant orange precipitate; R=Cy: dark red–orange opalescent solution). Increased concentration of the initial reaction mixture should be avoided. A reaction performed with xylyl isocyanide and 35 mg [RuCl$_2$(η^6-*p*-cymene)]$_2$ per mL of toluene led to the formation of a dark green oil and a lower purity of the final product. Next, DMSO (5–10 eq.) was introduced and the mixture was stirred at 55–110 °C for 2–6 h, as specified below. A yellow solution was obtained and the formation of **2a-e** was monitored by FT-IR (toluene). The mixture was cooled to room temperature and filtered over celite (with the assistance of CH_2Cl_2) to remove a small amount of dark brown solid. The filtrate was taken to dryness under vacuum. The resulting yellow sticky solid was stirred with Et_2O (**2a-c**) or Et_2O/hexane 1:1 *V/V* (**2d-e**) (about 15 mL) until a suspension is obtained. Otherwise, after 1–2 h the pale-yellow solution was removed and the residue was triturated with fresh solvent. The suspension was filtered (yellow filtrate), affording a pale yellow/colorless solid which was washed with Et_2O/hexane 1:1 *V/V*, hexane and then dried under vacuum (40 °C).

*Procedure **b*** (Scheme 2). In a 10 mL test tube, **1a-d** (0.33–0.35 mmol) and DMSO (1.5 mL) were introduced. The red solution was heated at 100 °C for 35 min (**1a**), 2 h (**1b-c**) or 130 °C for 3 h (**1d**), affording a yellow solution. The mixture was diluted with an aqueous NaCl solution (250 g/L) and extracted three times with $CHCl_3$. The pale-yellow aqueous phase was discarded. The combined organic solutions were extracted with water and taken to dryness under vacuum. The yellow-orange oily residue was dissolved in CH_2Cl_2 and filtered over celite. The filtrate was thoroughly dried under vacuum to remove residual DMSO and the resulting yellow/orange oily residue which was treated as described above.

***Cis,mer*-[RuCl$_2$(CNXyl)(κ*S*-DMSO)$_3$] , 2a** (Chart 7).

Prepared from [RuCl$_2$(η^6-*p*-cymene)]$_2$ (98 mg, 0.32 mmol Ru), XylNC (42 mg, 0.32 mmol) and DMSO (0.12 mL, 1.7 mmol, 5.3 eq) according to procedure ***a*** (2nd step: 55 °C, 4 h or 90 °C, 20 min); yield: 130 mg, 76 mol%. Alternatively prepared from **1a** (151 mg, 0.346 mmol) according to procedure ***b***; yield: 153 mg, 82 mol%. The yield of both procedures over a 60–150 mg scale range is reproducible (Procedure ***a***: yield = 77 ± 3 mol% for 6 preparations. Procedure ***b***: yield = 79.7 ± 2.5 mol% for 3 preparations.) and the purity of the final product is identical. Colorless solid. Soluble in CH_2Cl_2, $CHCl_3$, THF, acetone, MeCN, sparingly soluble in toluene, Et_2O, insoluble in hexane. X-ray quality crystals of **2a** were obtained from a CH_2Cl_2 solution layered with hexane and settled aside at – 20 °C. Anal. Calcd. For $C_{15}H_{27}Cl_2NO_3RuS_3$: C, 33.52; H, 5.06; N, 2.61; S, 17.89. Found: C, 33.74; H, 5.05; N, 2.59; S, 17.09. IR (solid state): ũ/cm^{-1} = 3018w, 3004w, 2981w, 2918w, 2122 s (C≡N), 2051w, 1466w, 1444w, 1418w, 1404w, 1386w, 1372w, 1307w, 1286w; 1110 s, 1093 s (S=O); 1029 m-sh, 1011 m, 972 m, 936w, 918w, 909w, 786 m, 728–721 m, 684 m-sh, 674 m, 518 m, 515 m. IR (CH_2Cl_2): ũ/cm^{-1} = 2131 s (C≡N). ^{1}H NMR (acetone-d_6): δ/ppm = 7.26–7.17 (m, 3H, C_6H_3), 3.52 (s, 6H, C^a-H), 3.41 (s, 6H, C^b-H), 3.40 (s, 6H, C^c-H), 2.58 (s, 6H, C$^5H_3$). ^{13}C{^{1}H} NMR (acetone-d_6): δ/ppm = 159.0 (br., C≡N), 136.7 (C^2), 129.3 (C^4), 128.8 (C^3), 47.9 (C^a), 46.0 (C^c), 43.2 (C^b), 19.3 (C^5). ^{1}H NMR ($CDCl_3$): δ/ppm = 7.20–7.14 (m, 1H), 7.13–7.08 (m, 2H) (C_6H_3); 3.53 (s, 6H, C^{a}H); 3.45 (s, 6H, C^{b}H); 3.37 (s, 6H, C^{c}H); 2.56 (s, 6H, C^{5}H). ^{13}C{^{1}H} NMR ($CDCl_3$): δ/ppm = 156.5 (br., C≡N), 135.9 (C^2), 129.0 (C^4), 128.3 (C^3), 47.8 (C^a), 46.1 (C^c), 43.3 (C^b), 19.3 (C^5). ^{1}H NMR (DMSO-d_6): δ/ppm = 7.28–7.21 (m, 3H, C_6H_3), 3.44 (s, SCH_3), 2.49 (s, 6H, CCH_3); the signal at 3.44 ppm in the freshly-prepared solution accounts for the 17 % of the total DMSO expected, and it is absent after 24

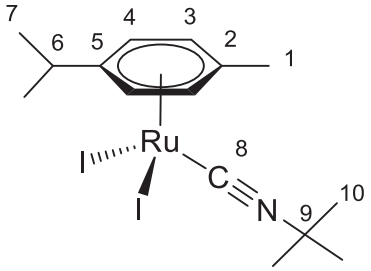

Chart 6. Structure of **1f** (numbering refers to carbon atoms).

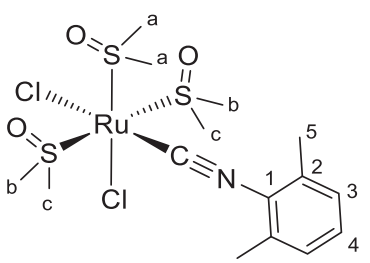

Chart 7. Structure of **2a** (numbering refers to carbon atoms).

h, due to ligand exchange with DMSO-d_6. The diethyl ether/petroleum solution used in the last stage of the workup (according to procedure a) was taken to dryness under vacuum. The residue was analyzed by FT-IR and ^{1}H NMR, showing the presence of comparable amounts of **2a** and an unidentified {Ru(DMSO)(CNXyl)} species, **3a**. IR (CH_2Cl_2): $\tilde{\upsilon}$/cm^{-1} = 2166 s (C≡N). ^{1}H NMR (acetone-d_6): δ/ppm = 3.39 (s, 6H, SCH_3), 2.50 (s, 6H, CCH_3).

***Cis,mer*-[RuCl$_2${CN(2-naphthyl)}(κ*S*-DMSO)$_3$], 2b** (Chart 8).

Prepared from [RuCl$_2$(η^6-*p*-cymene)]$_2$ (107 mg, 0.351 mmol Ru), 2-naphthyl isocyanide (54 mg, 0.36 mmol) and DMSO (0.15 mL, 2.1 mmol, 6.0 eq), according to procedure ***a*** (2nd step: 70 °C, 6 h); yield: 110 mg, 56 mol% (54 ± 2 mol% for 3 preparations over a 90–120 mg scale range). Alternatively prepared from **1b** (150 mg, 0.328 mmol) according to procedure ***b***; yield: 121 mg, 66 mol%. Procedure ***b*** provides **2b** in a slightly higher purity. Pale-yellow solid. Soluble in CH_2Cl_2, acetone, poorly soluble in Et_2O, insoluble in petroleum ether. Anal. Calcd. for $C_{17}H_{25}Cl_2NO_3RuS_3$: C, 36.49; H, 4.50; N, 2.50; S, 17.19. Found: C, 36.61; H, 4.57; N, 2.43; S, 16.87. IR (solid state): $\tilde{\upsilon}$/cm^{-1} = 3007w, 2919w, 2125 s-sh; 2111 s-br, 2057w-sh (C≡N); 1625w, 1594w, 1505w, 1410 m, 1361w, 1309w, 1291w; 1106 s, 1092 s (S=O); 1015 s, 972 m, 934 m, 922 nm 861 m, 815 m, 751 m, 720 m, 680 m, 533w, 497 m, 474 m. IR (CH_2Cl_2): $\tilde{\upsilon}$/cm^{-1} = 2145 m-sh, 2133 s, 2117 s-sh, 2104 m-sh (C≡N). ^{1}H NMR (acetone-d_6): δ/ppm = 8.21 (d, $^4J_{HH}$=1.4 Hz, 1H, C^{2}H), 8.05 (d, $^3J_{HH}$=8.6 Hz, 1H, C^{9}H), 8.01–7.97 (m, 2H, C^{4}H+C^{7}H), 7.72 (dd, $^3J_{HH}$=8.7 Hz, $^4J_{HH}$=2.0 Hz, 1H, C^{10}H), 7.65–7.60 (m, 2H, C^{5}H+C^{6}H), 3.50 (s, 6H, C^{a}H), 3.45 (s, 6H, C^{b}H), 3.43 (s, 6H, C^{c}H). ^{13}C{^{1}H} NMR (acetone-d_6): δ/ppm = 158.6 (C≡N), 133.8 (C^3), 133.6 (C^8), 130.7 (C^9); 128.*84*, 128.*79* (C^4 + C^7); 128.5, 128.4 (C^5 + C^6), 127.2 (C^1), 126.1 (C^2), 124.6 (C^{10}), 47.6 (C^a), 46.0 (C^b), 43.1 (C^c). ^{1}H NMR ($CDCl_3$): δ/ppm = 8.00–7.85 (m, 4H), 7.61–7.54 (m, 3H) ($C_{10}H_7$); 3.53 (s, 6H), 3.48 (s, 6H), 3.45 (s, 6H) (SCH_3).

***Cis,mer*-[RuCl$_2$(CNBn)(κ*S*-DMSO)$_3$], 2c** (Chart 9).

Prepared from **1c** (148 mg, 0.350 mmol) according to procedure ***b***; yield: 130 mg, 71 mol%. Colorless solid. Soluble in CH_2Cl_2, toluene, acetone, poorly soluble in Et_2O, insoluble in petroleum ether. Anal. Calcd. for $C_{14}H_{25}Cl_2NO_3RuS_3$: C, 32.12; H, 4.81; N, 2.68; S, 18.37. Found: C, 33.49; H, 4.93; N, 2.76; S, 17.56. IR (solid state): $\tilde{\upsilon}$/cm^{-1} = 3024w, 3007w, 2970w, 2922w, 2185 s (C≡N), 1499w, 1456w, 1430w, 1412w, 1369w, 1313w, 1292w; 1112 s-sh, 1098 s, 1087 s (S=O); 1020 s, 969 m, 836w, 917w, 739 m, 723 m, 699 m, 678 m, 608 m, 503w, 491w. IR (CH_2Cl_2): $\tilde{\upsilon}$/cm^{-1} = 2168 (C≡N). ^{1}H NMR (acetone-d_6): δ/ppm = 7.65 (d, $^3J_{HH}$=7.3 Hz, 2H, C^{3}H), 7.43 (t, $^3J_{HH}$=7.3 Hz, 2H, C^{4}H), 7.40–7.35 (m, 1H, C^{5}H), 5.33 (s, 2H, C^{1}H), 3.35 (s, 6H, C^a), 3.34 (s, 6H, C^b), 3.27 (s, 6H, C^c). ^{13}C{^{1}H} NMR (acetone-d_6): δ/ppm = 148.6 (br., C≡N), 134.6 (C^2), 129.7 (C^4), 129.1 (C^5), 128.2 (C^3), 49.3 (C^1), 47.5 (C^a), 45.8 (C^b), 43.1 (C^c). NMR ($CDCl_3$): δ/ppm = 7.52 − 7.34 (m, 5H, Ph), 5.08 (s, 2H, CH_2); 3.41 (s, 6H), 3.37 (s, 6H), 3.25 (s, 6H) (SCH_3). The reaction of [RuCl$_2$(η^6-*p*-cymene)]$_2$ (112 mg, 0.366 mmol Ru), benzyl isocyanide (45 mg, 0.37 mmol) and DMSO (0.13 mL, 0.83 mmol, 5.0 eq), according to procedure ***a*** (2nd step: reflux, 17 h) affords a beige solid, containing **2c** and an unidentified by-product (**3c**) in comparable amount [IR (CH_2Cl_2): $\tilde{\upsilon}$/cm^{-1} = 2199 (C≡N)].

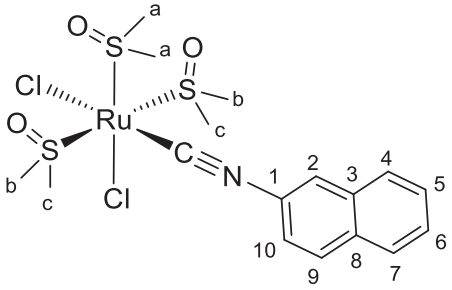

Chart 8. Structure of **2b** (numbering refers to carbon atoms).

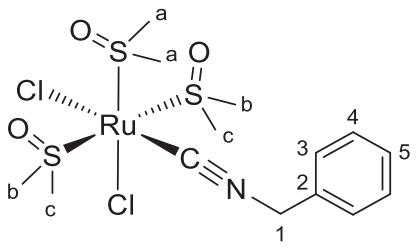

Chart 9. Structure of **2c** (numbering refers to carbon atoms).

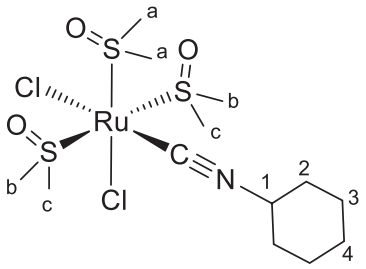

Chart 10. Structure of **2d** (numbering refers to carbon atoms).

***Cis,mer*-[RuCl$_2$(CNCy)(κ*S*-DMSO)$_3$], 2d** (Chart 10).

Prepared from [RuCl$_2$(η^6-*p*-cymene)]$_2$ (106 mg, 0.347 mmol Ru), cyclohexyl isocyanide (44 μL, 0.35 mmol) and DMSO (0.25 mL, 3.5 mmol, 10 eq), according to procedure ***a*** (2nd step: 90 °C, 2 h); yield: 142 mg, ≈ 79 mol%. Alternatively prepared from **1d** (140 mg, 0.336 mmol) according to procedure ***b***; yield: 140 mg, 81 mol%. Procedure ***b*** provides **2d** in a slightly higher purity. Colorless solid. Soluble in toluene, acetone, THF, CH_2Cl_2; poorly soluble in Et_2O and Et_2O/hexane mixtures, insoluble in hexane. Anal. Calcd. for: $C_{13}H_{29}Cl_2NO_3RuS_3$: C, 30.29; H, 5.67; N, 2.72; S, 18.66. Found: C, 30.45; H, 5.72; N, 2.74; S, 18.26. IR (solid state): $\tilde{\upsilon}$/cm^{-1} = 3011w, 2929w, 2858w, 2169 s (C≡N), 1617w, 1451w, 1411w, 1364w, 1311w, 1291w, 1105 s, 1090 s (S=O); 1018 s, 975 m, 939w, 923w, 893w, 719w, 678 m, 577w, 512w. IR (CH_2Cl_2): $\tilde{\upsilon}$/cm^{-1} = 2165 s (C≡N). ^{1}H NMR (acetone-d_6): δ/ppm = 4.29–4.23 (m, 1H, C^{1}H), 3.40 (s, 6H, C^{a}H), 3.34 (s, 6H, C^{b}H), 3.31 (s, 6H, C^{c}H), 2.03–1.96 (m, 2H, C^{2}H); 1.93–1.85 (m, 4H), 1.51–1.37 (m, 4H) (C^{2}H+C^{3}H+C^{4}H). ^{13}C{^{1}H} NMR (acetone-d_6): δ/ppm = 146.4 (br., C≡N), 56.0 (C^1), 47.6 (C^a), 45.8 (C^c), 43.1 (C^b), 33.2 (C^2); 25.7 (C^3), 23.3 (C^4). ^{1}H NMR ($CDCl_3$): δ/ppm = 4.09–4.01 (m, 1H, NCH^{Cy}); 3.46 (s, 6H), 3.42 (s, 6H), 3.34 (s, 6H) (SCH_3); 2.14–2.03 (m, 2H), 1.91–1.78 (m, 4H), 1.47–1.36 (m, 4H). Reactions performed according to procedure a with a lower amount of DMSO (5.0 eq at 90 °C for 4 h or 120 °C for 2 h) afforded a pale orange solid, containing **2d** and an unidentified {Ru(DMSO)(CNCy)} species, **3d**. IR (CH_2Cl_2): $\tilde{\upsilon}$/cm^{-1} = 2190 s (C≡N). ^{1}H NMR (acetone-d_6): δ/ppm = 4.13 (m, 1H, C^{1}H), 3.27 (s, 6H, SCH_3).

***Cis,mer*-[RuCl$_2$(CN^{t}Bu)(κ*S*-DMSO)$_3$], 2e** (Chart 11).

Prepared from [RuCl$_2$(η^6-*p*-cymene)]$_2$ (107 mg, 0.348 mmol Ru), *tert*-butyl isocyanide (42 μL, 0.37 mmol) and DMSO (80 μL, 1.1 mmol, 3.2 eq), according to procedure ***a*** (2nd step: 110 °C, 6 h). Pale yellow

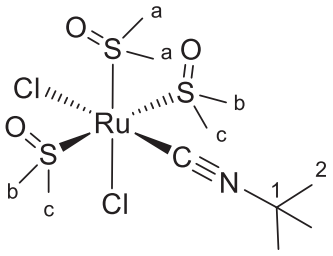

Chart 11. Structure of **2e** (numbering refers to carbon atoms).

solid; yield: 135 mg, in admixture with an unidentified {Ru(DMSO)(CN^{t}Bu)} species, **3e** (**2e**/**3e** ratio ≈ 1.6). IR (solid state): ũ/cm^{-1} = 3008w, 2983w, 2926w; 2164 s, 2141 s-sh (C≡N, **2e** + **3e**); 1468w, 1409w, 1371w, 1308w, 1288w, 1198 m; 1111 s, 1093 s (S=O); 1014 s, 968 m, 926 m, 723 m, 681 m, 550w, 528w. IR (CH_2Cl_2): ũ/cm^{-1} = 2180 m-sh (C≡N, **3e**), 2154 s (C≡N, **2e**). ^{1}H NMR (acetone-d_6): δ/ppm (**2e**) = 3.39 (s, 6H, C^{a}H), 3.34 (s, 6H, C^{b}H), 3.30 (s, 6H, C^{c}H), 1.61 (s, 9H, C^{2}H); δ/ppm (**3e**) = 3.25 (s, 6H, SCH_3), 1.54 (s, 9H, CCH_3). ^{13}C{^{1}H} NMR (acetone-d_6): δ/ppm (**2e**) = 59.8 (C^1), 47.7 (C^a); 45.9, 43.1 (C^b + C^c), 30.6 (C^2); δ/ppm (**3e**) = 59.2 ($\underline{C}CH_3$), 44.8 (SCH_3), 30.8 ($C\underline{C}H_3$); data from ^{1}H–^{13}C HMBC experiment.

5.4. Monitoring of the p-cymene/DMSO exchange in toluene-d_8

An orange suspension of **1a,d** (0.020 mmol) in toluene-d_8 (1.0 mL) was treated with DMSO (6 μL, 0.08 mmol, about 4 eq), stirred at room temperature overnight then heated at 60–65 °C for 15–21 h. The solution was analysed by ^{1}H and ^{1}H–^{13}C *gs*-HMBC NMR experiments at selected time intervals. In both cases, the formation of a transient complex, presumably *fac*-[$RuCl_2$(CNR)(κ*S*-DMSO)$_3$] (R=Xyl, **2a^X**; R=Cy, **2d^X**) was observed. NMR data, spectra and other experimental details are reported in the ESI.

[$RuCl_2$(CNXyl)(κ*S*-DMSO)(μ-DMSO)$_2$]$_2$, 4a (Chart 12).

A suspension of **2a** (260 mg, 0.483 mmol) in toluene (5 mL; corresponding to 52 mg **2a**/mL solvent) was stirred under reflux for 4 h, affording a pale-yellow solution and solid. The mixture was cooled to room temperature and filtered. The resulting pale-yellow solid was washed with toluene, Et_2O, hexane and dried under vacuum. Yield: 160 mg, 67 mol%. The formation of **4a** is presumably assisted by its precipitation in the rection mixture. Analogous reactions carried out in more dilute solutions (about 10–12 mg **1a**/mL toluene) led to the predominant formation of **3a** as assessed by FT-IR (CH_2Cl_2). Soluble in CH_2Cl_2, $CHCl_3$; poorly soluble in MeOH, MeCN, toluene, acetone, insoluble in diethyl ether, hexane. Anal calcd. for: $C_{26}H_{42}Cl_4N_2O_4Ru_2S_4$: C, 33.99; H, 4.61; N, 3.05; S, 13.96. Found: C, 32.87; H, 4.40; N, 2.94; S, 13.43. IR (solid state): ũ/cm^{-1} = 3009w, 2997w, 2921w, 2911w, 2137 s (C≡N), 1467w, 1443w, 1421w, 1410w, 1315wm 1297w; 1121 s, 1099 s (S=O); 1030 s (μ-S=O); 980w, 926w, 819w, 777 m, 733 m, 683 m, 673 m, 523 m. IR (CH_2Cl_2): ũ/cm^{-1} = 2138 cm^{-1}. ^{1}H NMR ($CDCl_3$): δ/ppm = 7.19–7.08 (m, 6H, C_6H_3); 3.84 (s, 6H), 3.83 (s, 6H) (μ-SO(CH_3)$_2$); 3.47 (s, 6H), 3.27 (s, 6H) (κ*S*-SO(CH_3)$_2$), 2.53 (s, 12H, CCH_3); referred to the major set of signals. Other, minor ^{1}H NMR resonances are ascribed to different isomers of **4a**.

5.5. X-ray crystallography

Crystal data and collection details for **1d**, **1e** and **2a** are reported in Table S3. Data were recorded on a Bruker APEX II diffractometer equipped with a PHOTON2 detector using Mo–Kα radiation. The structures were solved by direct methods and refined by full-matrix least-squares based on all data using F^2 [71]. Hydrogen atoms were fixed at calculated positions and refined using a riding model.

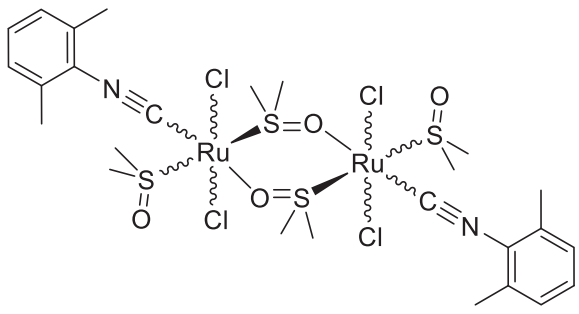

Chart 12. Proposed general structure of **4a** (wavy bonds represent different isomers).

5.6. Catalytic studies

All operations were carried out in air using non-anhydrous solvents. The catalytic conversion of EL into GVL was carried out in a monomodal CEM Discover S-class System microwave reactor. Regarding the experimental setup of the microwave reactor, in a standard procedure, a 35 mL reactor vessel was charged with EL (5 mmol), alcoholic solvent (10 mL) as hydrogen donor, KOH (0.05 mmol) and the selected ruthenium complex in the proper amount, evaluated with respect to EL. The reaction time was kept constant at 60 min, always working under magnetic stirring. The studied temperature range was within 110–160 °C. In the case of traditional heating, a 40 mL pressure tube immersed in an oil bath was employed, charged with the same amounts of reagents and heated at the set-point temperature. The reaction time was fixed at 120 min, always working under magnetic stirring. At the end of each reaction, the reactor was promptly cooled to room temperature with an external air flow, the reaction mixture was filtered and *n*-dodecane (0.64 mmol) was added as the internal standard for GC-FID analysis.

EL conversion (mol%), GVL yield (mol%), levulinate ester yield (mol %) and the yield of other unidentified products (mol%) were calculated according to the following equations:

$$\text{EL conversion} = [(\text{Imol}_{\text{EL}} - \text{Fmol}_{\text{EL}})/\text{Imol}_{\text{EL}}] \times 100 \quad (1)$$

$$\text{GVL yield} = (\text{mol}_{\text{GVL}}/\text{Imol}_{\text{EL}}) \times 100 \quad (2)$$

$$\text{Levulinate ester yield} = (\text{mol}_{\text{levulinate\_ester}}/\text{Imol}_{\text{EL}}) \times 100 \quad (3)$$

$$\text{Other products yield} = [(\text{Imol}_{\text{EL}} - \text{Fmol}_{\text{EL}} - \text{mol}_{\text{GVL}} - \text{mol}_{\text{levulinate\_ester}})/\text{Imol}_{\text{EL}}] \times 100 \quad (4)$$

where Imol_{EL} is the starting moles of EL added into the reactor, Fmol_{EL} is the final moles of EL after the reaction, mol_{GVL} represents the moles of synthesized GVL and $\text{mol}_{\text{levulinate\_ester}}$ represents the moles of *trans*-esterified levulinate ester.

The quantification of EL, GVL and EL esters was performed using a DANI GC1000 instrument equipped with an FID detector employing a 100 % dimethylpolysiloxane HP-PONA capillary column (50 m x 0.2 mm x 0.5 mm) for the separation. Nitrogen was adopted as carrier gas with the flow rate of 1 mL/min. The injector and detector temperatures were maintained at 250 °C and the following temperature program was used: 60 °C isothermal for 2 min; 10 °C/min up to 230 °C; 230 °C isothermal for 5 min. The average experimental error of the conversion, selectivity and yield data was within 3 %.

The qualitative identification of EL, GVL and reaction by-products was carried out adopting a GC–MS (Agilent 7890B-5977A) instrument using a (5 %-phenyl)-methylpolysiloxane HP-5MS capillary column (30 m x 0.25 mm x 0.25 mm) and a single-quadrupole MSD 5977 detector. Helium was the carrier gas with the flow rate of 1 mL/min. The injector and detector temperatures were set at 250 °C and 280 °C, respectively. Each analysis was carried out according to the following temperature program: 40 °C isothermal for 2 min; 10 °C/min up to 230 °C; 230 °C isothermal for 5 min, working under splitless mode.

CRediT authorship contribution statement

Lorenzo Biancalana: Writing – review & editing, Writing – original draft, Resources, Formal analysis, Data curation, Conceptualization. **Nicola Di Fidio:** Writing – original draft, Resources, Formal analysis, Data curation. **Domenico Licursi:** Writing – original draft, Resources, Formal analysis, Data curation. **Stefano Zacchini:** Formal analysis. **Alessia Cinci:** Formal analysis. **Anna Maria Raspolli Galletti:** Writing – review & editing, Resources. **Fabio Marchetti:** Writing – review & editing, Resources. **Claudia Antonetti:** Writing – review & editing,

Writing – original draft, Supervision, Resources, Data curation, Conceptualization.

Declaration of competing interest

The authors declare that they have no known competing financial interests or personal relationships that could have appeared to influence the work reported in this paper.

Data availability

Data will be made available on request.

Acknowledgements

LB, NDF, DL and CA thank the University of Pisa for financial support: this work is supported by the Università di Pisa under the "PRA 2022-2023 – Progetti di Ricerca di Ateneo" (Institutional Research Grants) - Project no. PRA_2022_12 "*New challenges of transition metal and lanthanide complexes in the perspective of green chemistry*". Moreover, the authors thank Dr. Beatrice Campanella (ICCOM – CNR, Pisa) for the ICP-OES analyses. NDF acknowledges the support of the RTD-A contract (no. 1112/2021, Prot. no. 0165823/2021) co-funded by the University of Pisa with respect to the PON "Ricerca e Innovazione" 2014–2020 (PON R&I FSE-REACT EU), Azione IV.6 "Contratti di ricerca su tematiche Green".

Appendix A. Supplementary material

Supplementary data to this article can be found online at https://doi.org/10.1016/j.jcat.2024.115761.

References

[1] a) E. Singleton, H.E. Oosthuizen, Adv. Organomet. Chem. 22 (1983) 209–310; b) W. Sattler, L.M. Henling, J.R. Winkler, H.B. Gray, J. Am. Chem. Soc. 137 (3) (2015) 1198–1205; c) S. Mukhopadhyay, A.G. Patro, R.S. Vadavi, S. Nembenna, Eur. J. Inorg. Chem. 2022 (31) (2022) e202200469.

[2] a) A.J.L. Pombeiro, M.F.C. Guedes Da Silva, R.A. Michelin, Coord. Chem. Rev. 218 (2001) 43–74; b) H.W. Frühauf, Coord. Chem. Rev. 230 (1–2) (2002) 79–96; c) L.G.M. Slaughter, ACS Catal. 2 (8) (2012) 1802–1816; d) V.P. Boyarskiy, N.A. Bokach, K.V. Luzyanin, V. Yu, Chem. Rev. 115 (7) (2015) 2698–2779; e) J.W. Collet, T.R. Roose, E. Ruijter, B.U.W. Maes, R.V.A. Orru, Angew. Chem. Int. Ed. 59 (2) (2020) 540–558.

[3] P. Patil, M. Ahmadian-Moghaddam, A. Dömling, Green Chem. 22 (20) (2020) 6902–6911.

[4] a) M. Knorn, E. Lutsker, O. Reiser, Chem. Soc. Rev. 49 (21) (2020) 7730–7752; b) K.T. Mahmudov, V.Y. Kukushkin, A.V. Gurbanov, M.A. Kinzhalov, V. P. Boyarskiy, M.F.C. Guedes da Silva, A.J.L. Pombeiro, Coord. Chem. Rev. 384 (2019) 65–89.

[5] a) A. Naik, T. Maji, O. Reiser, Chem. Commun. 46 (25) (2010) 4475–4477; b) D. Cahard, V. Bizet, X. Dai, S. Gaillard, J.L. Renaud, J. Fluor. Chem. 155 (7) (2013) 78–82; c) R. Bigler, R. Huber, A. Mezzetti, Angew. Chem. 54 (7) (2015) 5171–5174; d) J.B. Curley, N.E. Smith, W.H. Bernskoetter, N. Hazari, B.Q. Mercado, Organometallics 37 (21) (2018) 3846–3853; e) D.H. Nguyen, D. Merel, N. Merle, X. Trivelli, F. Capeta, R.M. Gauvin, Dalton Trans. 50 (29) (2021) 10067–10081.

[6] a) G.C. Vougioukalakis, R.H. Grubbs, Chem. Rev. 110 (3) (2010) 1746–1786; b) R. Noyori, S. Hashiguchi, Acc. Chem. Res. 30 (2) (1997) 97–102; c) A. Fürstner, J. Am. Chem. Soc. 141 (1) (2019) 11–24; d) T. Koike, M. Akita, Inorg. Chem. Front. 1 (8) (2014) 562–576; e) C. Gunanathan, D. Milstein, Chem. Rev. 114 (24) (2014) 12024–12087.

[7] a) P. Swain, C. Mallika, R. Srinivasan, U. Kamachi Mudali, R. Natarajan, J. Radioanal. Nucl. Chem. 298 (2) (2013) 781–796; b) T. Suoranta, O. Zugazua, M. Niemelä, P. Perämäki, Hydrometall. 154 (2016) 56–62.

[8] a) H.J. Yang, M. Redington, D.P. Miller, E. Zurek, M. Kim, C.S. Yoo, S.Y. Lim, H. Cheong, S.A. Chae, D. Ahn, N.H. Hur, Catal. Sci. Technol. 12 (21) (2022) 6556–6565; b) S. Doherty, J.G. Knight, T. Backhouse, T.S.T. Tran, R. Paterson, F. Stahl, H. Y. Alharbi, T.W. Chamberlain, R.A. Bourne, R. Stones, A. Griffiths, J.P. White, Z. Aslam, C. Hardare, H. Daly, J. Hart, R.H. Temperton, J.N. O'Shead, N.H. Rees, Catal. Sci. Technol. 12 (11) (2022) 3549–3567; c) T. Touge, M. Kuwana, Y. Komatsuki, S. Tanaka, H. Nara, K. Matsumura, N. Sayo, Y. Kashibuchi, T. Saito, Org. Process Res. Dev. 23 (4) (2019) 452–461; d) P.A. Dub, J.C. Gordon, Nat. Rev. Chem. 2 (2018) 396–408.

[9] a) A.S. Phearman, J.M. Moore, D.D. Bhagwandin, J.M. Goldberg, D.M. Heinekey, K.I. Goldberg, Green Chem. 23 (4) (2021) 1609–1615; b) Z. Wu, Z.Q. Wang, H. Cheng, Z.H. Zheng, Y. Yuan, C. Chen, F. Verpoort, Appl. Cat. A 630 (2022) 118443; c) P. Liu, N. Thanh Tung, X. Xu, J. Yang, F. Li, J. Org. Chem. 86 (3) (2021) 2621–2631; d) A. Verma, S. Hazra, P. Dolui, A.J. Elias, Asian J. Org. Chem. 10 (3) (2021) 626–633; e) Z. Wang, Z. Zhao, Y. Li, Y. Zhong, Q. Zhang, Q. Liu, G.A. Solan, Y. Ma, W. H. Sun, Chem. Sci. 11 (26) (2020) 6766–6774; f) M.N.A. Fetzer, G. Tavakoli, A. Klein, M.H.G. Prechtl, ChemCatChem 13 (5) (2021) 1317–1325.

[10] a) L. Biancalana, I. Abdalghani, F. Chiellini, S. Zacchini, G. Pampaloni, M. Crucianelli, F. Marchetti, Eur. J. Inorg. Chem. 2018 (26) (2018) 3041–3057; b) R. Colaiezzi, C. Saviozzi, N. di Nicola, S. Zacchini, G. Pampaloni, M. Crucianelli, F. Marchetti, A. Di Giuseppe, L. Biancalana, Catal. Sci. Technol. 13 (7) (2023) 2160–2183.

[11] L. Biancalana, S. Fulignati, C. Antonetti, S. Zacchini, G. Provinciali, G. Pampaloni, A.M. Raspolli Galletti, F. Marchetti, New J. Chem. 42 (21) (2018) 17574–17586.

[12] R. González-Fernández, P. Crochet, V. Cadierno, Inorg. Chim. Acta 517 (2020) 120180.

[13] a) P.B. Arockiam, C. Bruneau, P.H. Dixneuf, Chem. Rev. 112 (11) (2012) 5879–5918; b) C. Binnani, D. Tyagi, R.K. Rai, S.M. Mobin, S.K. Singh, Chem. Asian J. 11 (21) (2016) 3022–3031; c) T. Rogge, L. Ackermann, Angew. Chem. Int. Ed. 58 (44) (2019) 15640–15645.

[14] a) C.S. Day, D.E. Fogg, Organometallics 37 (24) (2018) 4551–4555; b) M. Bassetti, F. Centola, D. Sémeril, C. Bruneau, P.H. Dixneuf, Organometallics 22 (22) (2003) 4459–4466.

[15] a) P. Kumar, R.K. Gupta, D.S. Pandey, Chem. Soc. Rev. 43 (2) (2014) 707–733; b) G. Süss-Fink, J. Organomet. Chem. 751 (2014) 2–19.

[16] M.A. Bennett, A.K. Smith, J. Chem. Soc. Dalton Trans. 2 (1974) 233–241.

[17] M.A. Bennett, T.N. Huang, T.W. Matheson, A.K. Smith, S. Ittel, W. Nickerson, Inorg. Syntheses, Wiley, New York, 1982.

[18] Ca. 36 [RuX_2(CNR)(η^6-arene)] derivatives among ca. 3900 [RuX_2(L)(η^6-arene)] complexes (X = halide; L = generic monodentate ligand except halides). Sci-Finder (https://scifinder-n.cas.org), 19/02/2024.

[19] (a) F. Faraone, V. Marsala, Inorg. Chim. Acta 27 (1978) L109–L110; (b) R. Dussel, D. Pilette, P.H. Dixneuf, W.P. Fehlhammer, Organometallics 10 (9) (1991) 3287–3291; (c) Y. Yamamoto, R. Satoh, T. Tanase, J. Chem. Soc. Dalton Trans. 2 (1995) 307–311; (d) S. Krawielitzki, W. Beck, Chem. Ber. 130 (1997) 1659; (e) F. Simal, S. Sebille, L. Hallet, A. Demonceau, A.F. Noels, Macromol. Symp. 161 (1) (2000) 73–86; (f)Y. Yamamoto, H. Nakamura, J.F. Ma, J. Organomet. Chem. 640, pp. 1–2, 2001 10–20. (g) E. Hodson, S.J. Simpson, Polyhedron 23 (17) (2004) 2695–2707; (h) O. Kaufhold, A. Flores-Figueroa, T. Pape, F.E. Hahn, Organometallics 28 (3) (2009) 896–901; (i) G. Albertin, S. Antoniutti, J. Castro, S. Paganelli, J. Organomet. Chem. 695 (18) (2010) 2142–2152; (j) A.P. Walsh, W.W. Brennessel, J.D. Jones, Inorg. Chim. Acta 407 (2013) 131–138; (k) C. Hubbert, M.C. Dietl, D. Zahner, F. Rominger, M. Rudolph, A.S.K. Hashmi, Organometallics 42 (19) (2023) 2762–2770.

[20] K. Salzmann, C. Segarra, M. Albrecht, Angew. Chem. Int. Ed. 59 (23) (2020) 8932–8936.

[21] a) J. Popp, S. Hanf, E. Hey-Hawkins, ACS Omega 4 (27) (2019) 22540–22548; b) S.J. Dougan, M. Melchart, A. Habtemariam, S. Parsons, P.J. Sadler, Inorg. Chem. 45 (26) (2006) 10882–10894; c) D.A. Freedman, S. Kruger, C. Roosa, C. Wymer, Inorg. Chem. 45 (23) (2006) 9558–9568.

[22] T. Ikariya, A.J. Blacker, Acc. Chem. Res. 40 (12) (2007) 1300–1308.

[23] a) R. Ghosh, N.C. Jana, S. Panda, B. Bagh, A.C.S. Sustain, Chem. Eng. 9 (13) (2021) 4903–4914; b) S. Baldino, S. Facchetti, H. Günter Nedden, A. Zanotti-Gerosa, W. Baratta, ChemCatChem 8 (20) (2016) 3195–3198; c) R. Padilla, Z. Ni, D. Mihrin, R. Wugt Larsen, M. Nielsen, ChemCatChem 15 (2) (2023); d) R.A. Farrar-Tobar, Z. Wei, H. Jiao, S. Hinze, J.G. De Vries, Chem Eur J 24 (11) (2018) 2725–2734; e) N.K. Oklu, B.C.E. Makhubela, New J. Chem. 44 (22) (2020) 9382–9390, e202200819.

[24] a) A.M.R. Hall, D.B.G. Berry, J.N. Crossley, A. Codina, I. Clegg, J.P. Lowe, A. Buchard, U. Hintermair, ACS Catal. 11 (21) (2021) 13649–13659; b) G.S. Caleffi, J. De, O.C. Brum, A.T. Costa, J.L.O. Domingos, P.R.R. Costa, J. Org. Chem. 86 (6) (2021) 4849–4858; c) T. Touge, M. Kuwana, Y. Komatsuki, S. Tanaka, H. Nara, K. Matsumura, N. Sayo, Y. Kashibuchi, T. Saito, Org. Process Res. Dev. 23 (4) (2019) 452–461.

[25] a) K. Gupta, D. Tyagi, A.D. Dwivedi, S.M. Mobina, S.K. Singh, Green Chem. 17 (9) (2015) 4618–4627;

b) M. Ruiz-Castañeda, L. Santos, B.R. Manzano, G. Espino, F.A. Jalón, Eur. J. Inorg. Chem. 2021 (14) (2021) 1358–1372.
[26] a) J. Shan, Q. Wang, H. Hao, H. Guo, Ind. Eng. Chem. Res. 62 (42) (2023) 17135–17147;
b) A. Démolis, N. Essayem, F. Rataboul, A.C.S. Sustain, Chem. Eng. 2 (6) (2014) 1338–1352;
c) L. Yan, Q. Yao, Y. Fu, Green Chem. 19 (23) (2017) 5527–5547;
d) G. Shrivastav, T.S. Khan, M. Agarwal, M.A. Haider, A.C.S. Sustain, Chem. Eng. 5 (8) (2017) 7118–7127;
e) A.M. Raspolli Galletti, D. Licursi, S. Ciorba, N. Di Fidio, V. Coccia, F. Cotana, C. Antonetti, Catalysts 11 (9) (2021) 1082;
f) A.M. Raspolli Galletti, C. Antonetti, S. Fulignati, D. Licursi, Catalysts 10 (10) (2020) 1221;
g) C. Antonetti, S. Gori, D. Licursi, G. Pasini, S. Frigo, M. López, J.C. Parajó, A. M. Raspolli Galletti, Catalysts 10 (5) (2020) 509.
[27] F.A. Freitas, D. Licursi, E.R. Lachter, A.M. Raspolli Galletti, C. Antonetti, T.C. Brito, R.S.V. Nascimento, Catal. Commun. 73 (2016) 84–87.
[28] A. Garcia-Ortiz, K.S. Arias, M.J. Climent, A. Corma, S. Iborra, ChemSusChem 13 (4) (2020) 707–714.
[29] D. Zhao, Y. Wang, F. Delbecq, C. Len, Mol. Catal. 475 (2019) 110456.
[30] a) A.S. Amarasekara, M.A. Animashaun, Catal. Lett. 146 (2016) 1819–1824;
b) G.B. Kasar, N.S. Date, P. Bhosale, C.V. Rode, Energy Fuels 32 (6) (2018) 6887–6900.
[31] a) S. Rivas, A.M. Raspolli Galletti, C. Antonetti, D. Licursi, V. Santos, J.C. Parajó, Catalysts 8 (4) (2018) 169;
b) K.G. Martínez Figueredo, F.A. Martínez, D.J. Segobia, N.M. Bertero, ChemPlusChem 88 (11) (2023) e202300381;
c) F. Valentini, G. Brufani, B. Di Erasmo, L. Vaccaro, Curr. Opin. Green Sustain. Chem. 36 (2022) 100634.
[32] a) B. Cai, R. Kang, J. Feng, T.L. Eberhardt, Z. Ma, Q. Zhu, H. Pan, Renew. Energy 222 (2024) 119833;
b) J. Qiu, B. Zhou, Q. Yang, Y. Liu, L. Zhang, B. Wang, S. Song, J. Zhang, S. Huang, J. Chen, L. Lin, X. Zeng, Fuel Process. Technol. 254 (2024) 108010;
c) Y. Xu, H. Zhang, H. Li, S. Yang, Curr. Green Chem. 7 (3) (2020) 304–313;
d) Z. Gao, G. Fan, L. Yang, F. Li, Mol. Catal. 442 (2017) 181–190.
[33] a) M.C. Fu, R. Shang, Z. Huang, Y. Fu, Synlett 25 (19) (2014) 2748–2752;
b) N. Dai, R. Shang, M. Fu, Y. Fu, Chin. J. Chem . 33 (4) (2015) 405–408;
c) A. Bruneau-Voisine, D. Wang, V. Dorcet, T. Roisnel, C. Darcel, J.B. Sortais, Org. Lett. 19 (13) (2017) 3656–3659;
d) F. Li, R. Yang, Z. Du, J. Dai, X. Wang, N. Li, J. Zhang, X. Zhang, Y. Liu, H. Gong, H. Yin, Z. Cai, Mol. Catal. 535 (2023) 112863;
e) K. Sung, M.H. Lee, Y.J. Cheong, H.Y. Jang, Appl. Organomet. Chem. 35 (2) (2021) e6105;
f) V.S. Shende, A.B. Raut, P. Raghav, A.A. Kelkar, B.M. Bhanage, ACS Omega 4 (21) (2019) 19491–19498;
g) R. Figliolia, P. Cavigli, C. Comuzzi, A. Del Zotto, D. Lovison, P. Strazzolini, S. Susmel, D. Zuccaccia, M. Ballico, W. Baratta, Dalton Trans. 49 (2) (2020) 453–465.
[34] a) C. Bao, A. Serrano-Lotina, M. Niu, R. Portela, Y. Li, K. Ho Lim, P. Liu, W. J. Wang, M.A. Banares, Q. Wang, Chem. Eng. J. 466 (2023) 142902;
b) A.M. Raspolli Galletti, L. Toniolo, C. Antonetti, C. Evangelisti, C. Forte, Appl. Cat. A: General 447–448 (2012) 49–59.
[35] a) L. Chen, Y. Liu, C. Gu, G. Feng, X. Zhang, J. Liu, Q. Zhang, C. Wang, L. Ma, A.C. S. Sustain, Chem. Eng. 9 (46) (2021) 15603–15611;
b) T. Arai, M. Tamura, Y. Nakagawa, K. Tomishige, ChemSusChem 9 (13) (2016) 1680–1688.
[36] D. Prat, A. Wells, J. Hayler, H. Sneddon, C.R. McElroy, S. Abou-Shehadad, P. J. Dunne, Green Chem. 18 (1) (2016) 288–296.
[37] a) K. Mashima, H. Kaneyoshi, S.I. Kaneko, A. Mikami, K. Tani, A. Nakamura, Organometallics 16 (5) (1997) 1016–1025;
b) E. Lindner, S. Pautz, R. Fawzi, M. Steimann, Organometallics 17 (14) (1998) 3006–3014;
c) J.H. Won, H.G. Lim, B.Y. Kim, J.D. Lee, C. Lee, Y.J. Lee, S. Cho, J. Ko, S.O. Kang, Organometallics 21 (26) (2002) 5703–5712;
d) T. Hayashida, H. Kondo, J.I. Terasawa, K. Kirchner, Y. Sunada, H. Nagashima, J. Organomet. Chem. 692 (1–3) (2007) 382–394;
e) M. Ito, H. Komatsu, Y. Endo, T. Ikariya, Chem. Lett. 38 (1) (2009) 98–99.
[38] Con-Quest 31/08/2023: 13 results. a) J. Cervinka, A. Gobbo, L. Biancalana, L. Markova, V. Novohradsky, M. Guelfi, S. Zacchini, J. Kasparkova, V. Brabec, F. Marchetti, J. Med. Chem. 65 (15) (2022) 10567–10587;
b) J. Li, H. Kang, K. Zhuo, Q. Zhuo, H. Zhang, Y.M. Lin, H. Xia, Chin. J. Chem. 36 (12) (2018) 1156–1160;
c) C. Tubaro, D. Bertinazzo, M. Monticelli, O. Saoncella, A. Volpe, M. Basato, D. Badocco, P. Pastore, C. Graiff, A. Venzo, Eur. J. Inorg. Chem. 2014 (9) (2014) 1524–1532;
d) D. Cuervo, E. Menèndez-Pedregal, J. Dìez, M. Pilar Gamasa, J. Organomet, Chemistry 696 (9) (2011) 1861–1867;
e) Y. Sunada, H. Ogushi, T. Yamamoto, S. Uto, M. Sawano, A. Tahara, H. Tanaka, Y. Shiota, K. Yoshizawa, H. Nagashima, J. Am. Chem. Soc. 140 (11) (2018) 4119–4134.
[39] a) W. Weber, P.C. Ford, Inorg. Chem. 25 (8) (1986) 1088–1092;
b) R.J. Lavallee, C.J. Kutal, J. Organomet. Chem. 562 (1) (1998) 97–104;
c) A.B. Chaplin, P.J. Dyson, J. Organomet. Chem. 696 (13) (2011) 2485–2490.
[40] a) J. Téllez, I. Méndez, F. Viguri, R. Rodríguez, F.J. Lahoz, P. García-Orduña, D. Carmona, Organometallics 37 (20) (2018) 3450–3464;
b) L. Feng, Y. Geisselbrecht, S. Blanck, A. Wilbuer, G.E. Atilla-Gokcumen, P. Filippakopoulos, K. Kräling, M. Ali Celik, K. Harms, J. Maksimoska, R. Marmorstein, G. Frenking, S. Knapp, L.O. Essen, E. Meggers, J. Am. Chem. Soc. 133 (15) (2011) 5976–5986;
c) V. Leigh, W. Ghattas, R. Lalrempuia, H. Müller-Bunz, M.T. Pryce, M. Albrecht, Inorg. Chem. 52 (9) (2013) 5395–5402.
[41] a) L. Biancalana, S. Zacchini, N. Ferri, M. Giovanna Lupo, G. Pampaloni, F. Marchetti, Dalton Trans. 46 (47) (2017) 16589–16604;
b) L. Biancalana, S. Zacchini, G. Pampaloni, F. Marchetti, J. Organomet. Chem. 848 (2017) 214–221;
c) L. Biancalana, A. Pratesi, F. Chiellini, S. Zacchini, T. Funaioli, C. Gabbiani, F. Marchetti, New J. Chem. 41 (23) (2017) 14574–14588;
d) A. Ashraf, M. Kubanik, F. Aman, H. Holtkamp, T. Söhnel, S.M.F. Jamieson, M. Hanif, W. Ahmad Siddiqui, C.G. Hartinger, Eur. J. Inorg. Chem. 2016 (9) (2016) 1376–1382;
e) M.V. Babak, S.M. Meier, K.V.M. Huber, J. Reynisson, A.A. Legin, M.A. Jakupec, A. Roller, A. Stukalov, M. Gridling, K.L. Bennett, J. Colinge, W. Berger, P.J. Dyson, G. Superti-Furga, B.K. Keppler, C.G. Hartinger, Chem. Sci. 6 (4) (2015) 2449–2456;
f) F. Aman, M. Hanif, W. Ahmad Siddiqui, A. Ashraf, L.K. Filak, J. Reynisson, T. Söhnel, S.M.F. Jamieson, C.G. Hartinger, Organometallics 33 (19) (2014) 5546–5553.
[42] S.L. Saraf, T.J. Fish, A.D. Benninghoff, A.A. Buelt, R.C. Smith, L.M. Berreau, Organometallics 33 (22) (2014) 6341–6351.
[43] Characterization limited to 1H/13C NMR:. a) V. Artero, D. Laurencin, R. Villanneau, R. Thouvenot, P. Herson, P. Gouzerh, A. Proust, Inorg. Chem. 44 (8) (2005) 2826–2835;
b) S. Rajkumar, S. Karthik, T. Gandhi, J. Org. Chem. 80 (11) (2015) 5532–5545;
c) S.E. Flowers, M.C. Johnson, B.Z. Pitre, B.M. Cossairt, Dalton Trans. 47 (4) (2018) 1276–1283.
[44] a) M. Lari, M. Martínez-Alonso, N. Busto, B.R. Manzano, A.M. Rodríguez, M. I. Acuña, F. Domínguez, J.L. Albasanz, J.M. Leal, G. Espino, B. García, Inorg. Chem. 57 (22) (2018) 14322–14336;
b) L. Suntrup, F. Stein, G. Hermann, M. Kleoff, M. Kuss-Petermann, J. Klein, O. S. Wenger, J.C. Tremblay, B. Sarkar, Inorg. Chem. 57 (21) (2018) 13973–13984.
[45] D. Schleicher, H. Leopold, T. Strassner, J. Organomet. Chem. 829 (2017) 101–107.
[46] a) T. Yamamura, H. Nakatsuka, S. Tanaka, M. Kitamura, Angew. Chem. Int. Ed. 52 (35) (2013) 9313–9315;
b) S. Nakane, T. Yamamura, S. Kumar Manna, S. Tanaka, M. Kitamura, ACS Catal. 8 (12) (2018) 11059–11075.
[47] E. Alessio, Chem. Rev. 104 (9) (2004) 4203–4242.
[48] M. Calligaris, Coord. Chem. Rev. 248 (3–4) (2004) 351–375.
[49] I. Bratsos, E. Alessio, M.E. Ringenberg, T.B. Rauchfuss, Inorg. Synt. 35 (2010) 148–152.
[50] a) J.A. Crayston, D.C. Cupertino, H.S. Forster, Synthesis, Synth. Metals 35 (3) (1990) 365–370;
b) J.A. Crayston, D.C. Cupertino, T.J. Dines, J. Chem. Soc. Dalton Trans. 6 (1991) 1603–1608.
[51] R.S. Srivastava, F.R. Fronczek, Inorg. Chim. Acta 355 (2003) 354–360.
[52] a) E. Alessio, B. Milani, M. Bolle, G. Mestroni, P. Faleschini, F. Todone, S. Geremia, M. Calligaris, Inorg. Chem. 34 (19) (1995) 4722–4734;
b) E. Alessio, E. Iengo, S. Geremia, M. Calligaris, Inorg. Chim. Acta 344 (2003) 183–189.
[53] M. Calligaris, N.S. Panina, J. Mol. Struct. 646 (1–3) (2003) 61–66.
[54] S. Geremia, S. Mestroni, M. Calligaris, E. Alessio, J. Chem. Soc. Dalton Trans. 15 (1998) 2447–2448.
[55] a) Q.A. De Paula, S. Dos Santos, J. Ellena, E.E. Castellano, A.A. Batista, J. Chem. Crystallogr. 39 (7) (2009) 519–524;
b) S. Neudeck, S. Maji, I. López, S. Dechert, J. Benet-Buchholz, A. Llobet, F. Meyer, Inorg. Chem. 55 (5) (2016) 2508–2511.
[56] R.L. Chowdhury, J.E. Bäckvall, J. Chem. Soc. Chem. Commun. 16 (1991) 1063–1064.
[57] a) S. Perdriau, S. Harder, H.J. Heeres, J.G. De Vries, ChemSusChem 5 (12) (2012) 2427–2434;
b) N. Sarki, V. Goyal, N.K. Tyagi, A. Puttaswamy, A.R. Narani, K. Natte, ChemCatChem 13 (7) (2021) 1722–1729;
c) P. Devi, M. Kannan, V. Kiran, A. Kumar, S. Muthaiah, J. Organomet. Chem. 980–981 (2022) 122515;
d) X. Chen, X.Y. Zhou, Synthesis 55 (09) (2023) 1460–1466.
[58] a) L. Chen, Y. Liu, C. Gu, G. Feng, X. Zhang, J. Liu, Q. Zhang, C. Wang, L. Ma, A.C. S. Sustain, Chem. Eng. 9 (46) (2021) 15603–15611;
b) T. Arai, M. Tamura, Y. Nakagawa, K. Tomishige, ChemSusChem 9 (13) (2016) 1680–1688;
c) D. Licursi, C. Antonetti, S. Fulignati, M. Giannoni, A.M. Raspolli Galletti, Catalysts 8 (7) (2018) 277.
[59] C.L. Kibby, W.K. Hall, J. Catal. 31 (1) (1973) 65–73.
[60] X. Tang, H. Chen, L. Hu, W. Hao, Y. Sun, X. Zeng, L. Lin, S. Liu, Appl. Cat. b. Environ. 147 (2014) 827–834.
[61] P. Panagiotopoulou, N. Martin, D.G. Vlachos, J. Mol. Catal. A Chem. 392 (2014) 223–228.
[62] Z. Yang, Y.B. Huang, Q.X. Guo, Y. Fu, Chem. Commun. 49 (46) (2013) 5328–5330.
[63] a) T. Razzaq, C.O. Kappe, ChemSusChem 1 (1–2) (2008) 123–132;
b) W. Wang, C. Zhao, J. Sun, X. Wang, X. Zhao, Y. Mao, X. Li, Z. Song, Energy 87 (2015) 678–685.
[64] T. Tabanelli, E. Paone, P.B. Vasquez, R. Pietropaolo, F. Cavani, F. Mauriello, A.C. S. Sustain, Chem. Eng. 7 (11) (2019) 9937–9947.
[65] J. Toubiana, Y. Sasson, Catal, Sci. Technol. 2 (8) (2012) 1644–1653.

[66] K.R. Hyde, E.W. Hooper, J. Waters, J.M. Fletcher, J. Less-Common Met. 8 (6) (1965) 428–434.
[67] A.H. Valekar, K.H. Cho, S.K. Chitale, D.Y. Hong, G.Y. Cha, U.H. Lee, D.W. Hwang, C. Serre, J.S. Chang, Y.K. Hwang, Green Chem. 18 (16) (2016) 4542–4552.
[68] C.A. Van Slagmaat, M.A. Delgove, J. Stouten, L. Morick, Y. Van Der Meer, K. V. Bernaerts, S.M. De Wildeman, Green Chem. 22 (8) (2020) 2443–2458.
[69] F. Menges, "Spectragryph - optical spectroscopy software", Version 1.2.16.1, @ 2016-2022, http://www.effemm2.de/spectragryph.
[70] G.R. Fulmer, A.J.M. Miller, N.H. Sherden, H.E. Gottlieb, A. Nudelman, B.M. Stoltz, J.E. Bercaw, K.I. Goldberg, Organometallics 29 (2010) 2176.
[71] G.M. Sheldrick, Acta Crystallogr. C 71 (2015) 3.

Supporting Information

New ruthenium(II) isocyanide catalysts for the transfer hydrogenation of ethyl levulinate to γ-valerolactone in C_2-C_6 alcohols

Lorenzo Biancalana,[a,b] Nicola Di Fidio,[a,b] Domenico Licursi,[a,b] Stefano Zacchini,[c] Alessia Cinci,[a] Anna Maria Raspolli Galletti,[a,b] Fabio Marchetti,[a,b] Claudia Antonetti*[a,b]

[a] *Università di Pisa, Dipartimento di Chimica e Chimica Industriale, Via Giuseppe Moruzzi 13, I-56124 Pisa, Italy.*

[b] *Consorzio Interuniversitario Reattività Chimica e Catalisi (CIRCC), Via Celso Ulpiani 27, 70126, Bari, Italy.*

[c] *Università di Bologna, Dipartimento di Chimica Industriale "Toso Montanari", Viale del Risorgimento 4, I-40136 Bologna, Italy.*

Table of contents — **Page(s)**

FT-IR and NMR spectra of isocyanide-arene complexes (**Figures S1-S24**)	S2-S13
Chart S1. Symmetry and isomerism for $[RuCl_2(CNXyl)(DMSO)_3]$	S14
FT-IR and NMR spectra of isocyanide-DMSO complexes (**Figures S25-S47**)	S15-S28
Stability of isocyanide-DMSO complexes in solution (**Figures S48-S49**)	S29-S31
Table S1. Comparison of selected IR/NMR data for isocyanide ligands	S32
Study of the *p*-cymene/DMSO exchange in toluene-d_8 (**Figures S50-S51**, **Tables S2-S3**)	S33-S36
FT-IR and NMR spectra of **4a** (**Figures S52-S53**)	S37
Table S4. Standard enthalpy dehydrogenation change of the investigated alcohols for transfer hydrogenation	S38
Investigation of the catalytic reaction mixture by GC-MS (**Figures S54-S58**)	S39-S41
Ruthenium speciation in the final reaction mixture (**Figure S59**)	S42-S43
Table S5. Crystal data and collection details	S44
References	S45

FT-IR and NMR spectra of isocyanide-arene complexes

Figure S1. Solid-state FT-IR spectrum (650-4000 cm^{-1}) of [$RuCl_2$(CNXyl)(η^6-*p*-cymene)], **1a**.

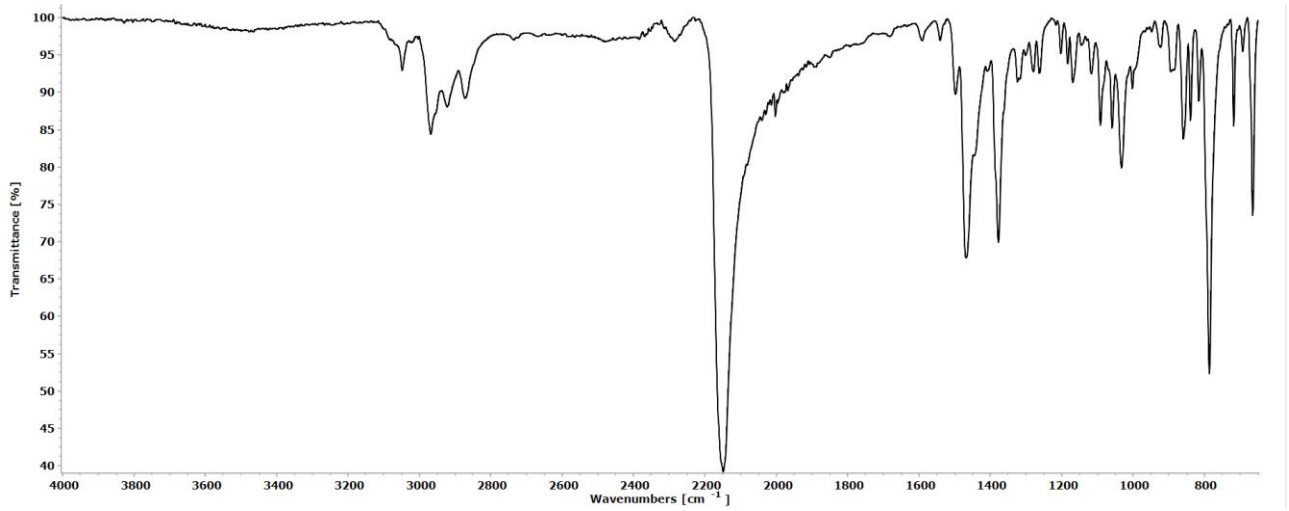

Figure S2. Solvent-subtracted FT-IR spectra (1300-2700 cm^{-1}) of **1a** (black line) and xylyl isocyanide (red dashed line) in CH_2Cl_2.

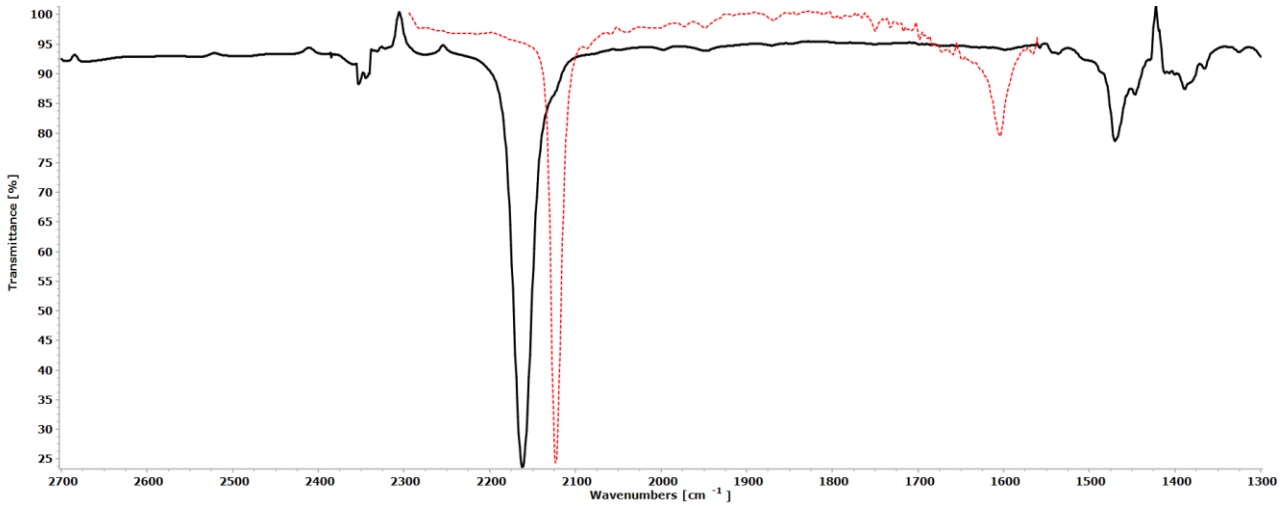

Figure S3. ^{1}H NMR spectrum (400 MHz, $CDCl_3$) of **1a**.

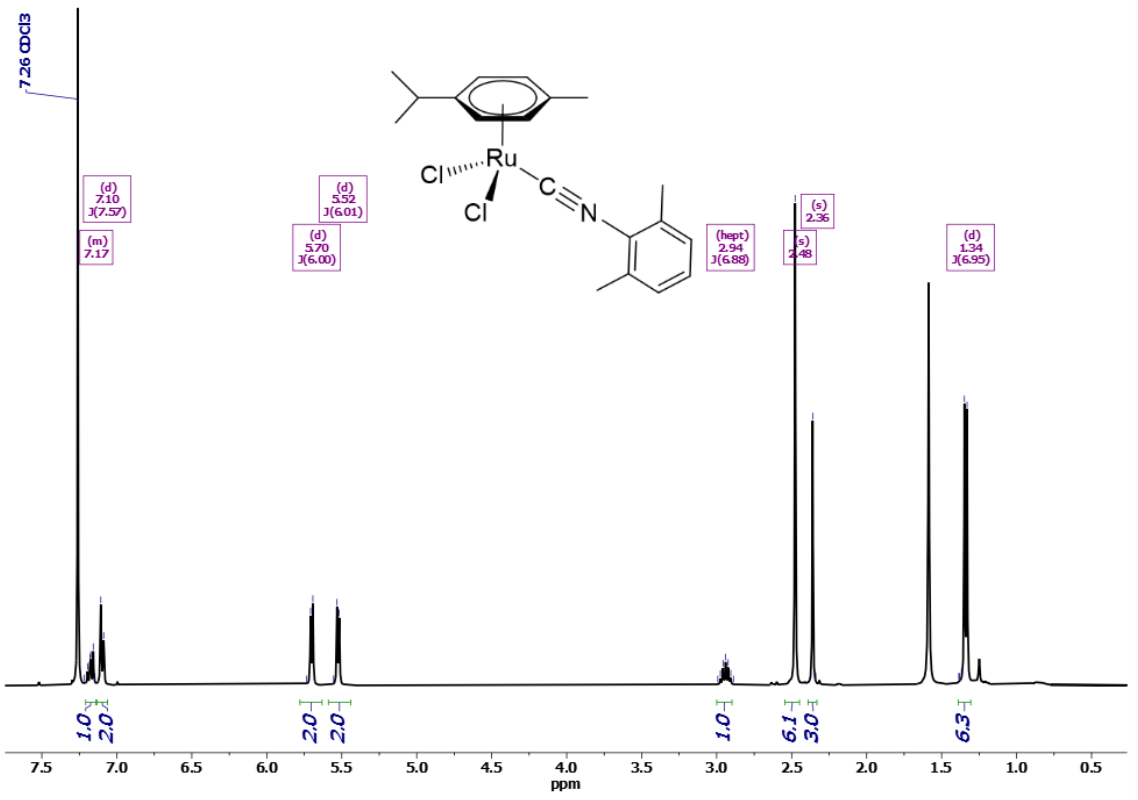

Figure S4. $^{13}C\{^{1}H\}$ NMR spectrum (100 MHz, $CDCl_3$) of **1a**.

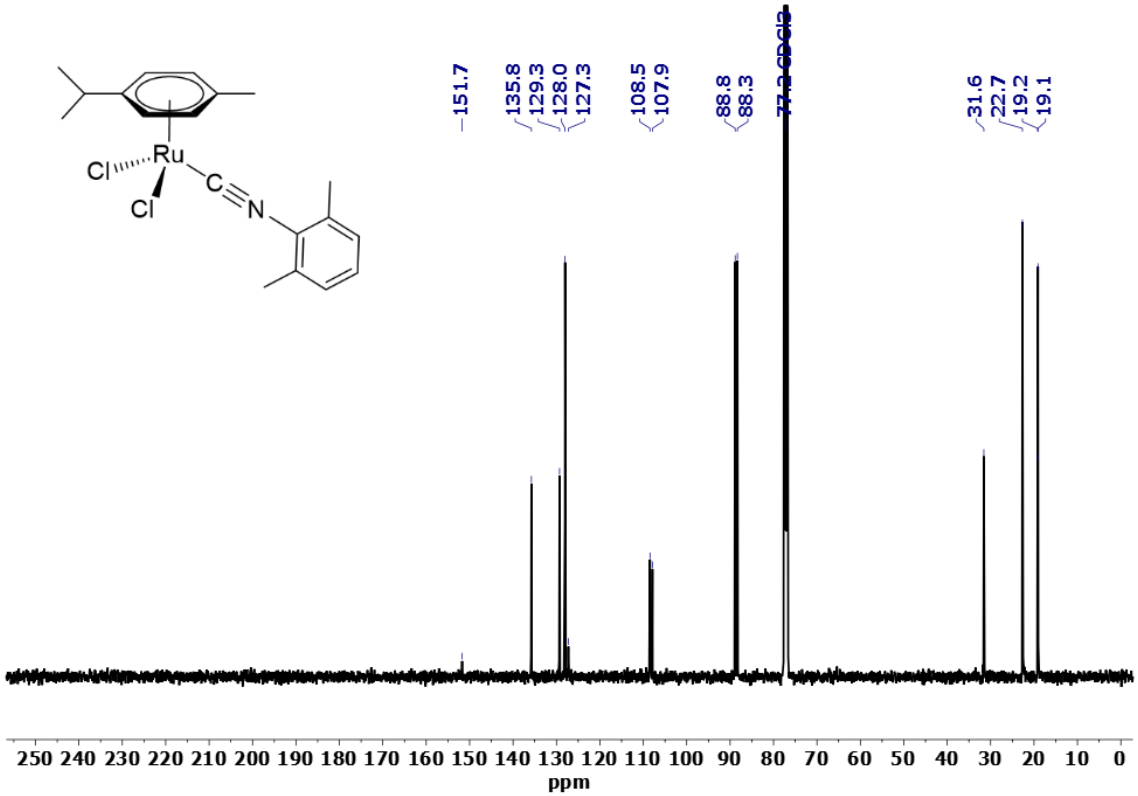

Figure S5. Solid-state FT-IR spectrum (650-4000 cm^{-1}) of [$RuCl_2${CN(2-naphthyl)}(η^6-*p*-cymene)], **1b**.

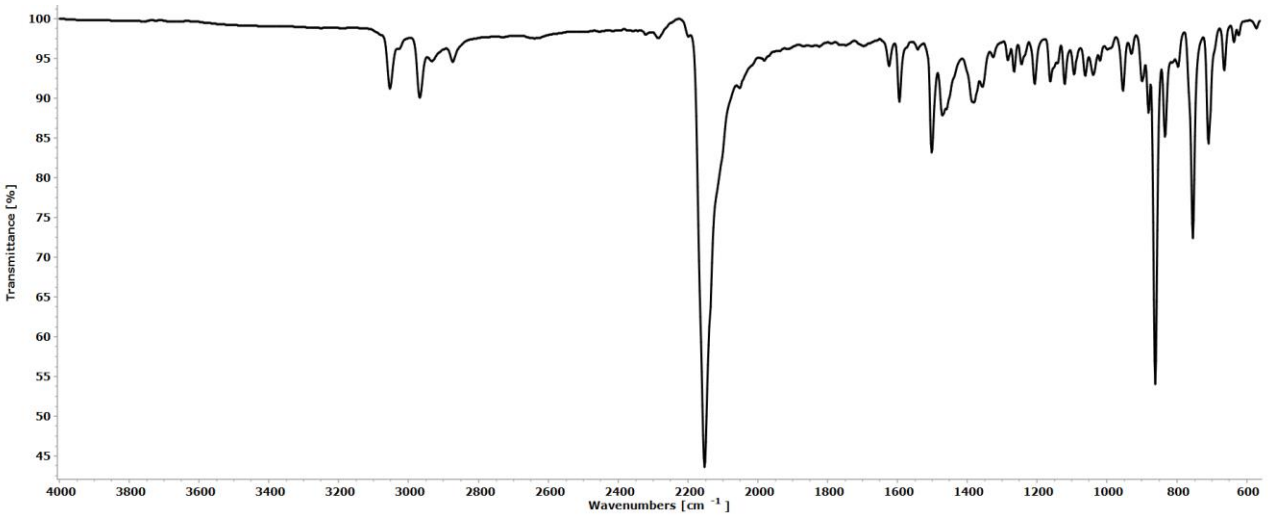

Figure S6. Solvent-subtracted FT-IR spectra (1400-2700 cm^{-1}) of **1b** (black line) and 2-naphthyl isocyanide (red dashed line) in CH_2Cl_2.

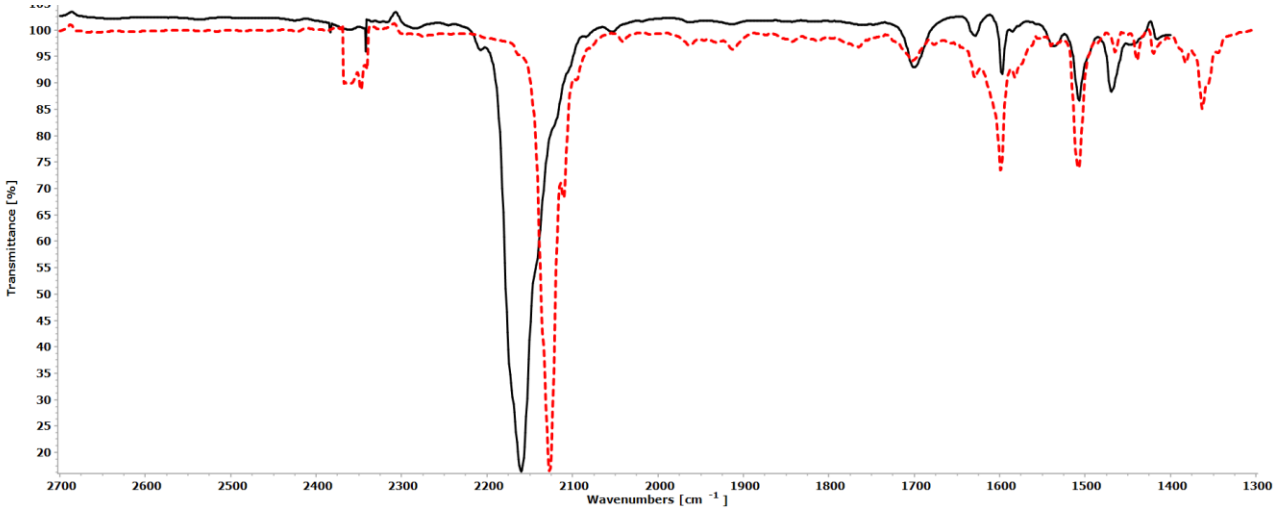

Figure S7. ^{1}H NMR spectrum (400 MHz, $CDCl_3$) of **1b**.

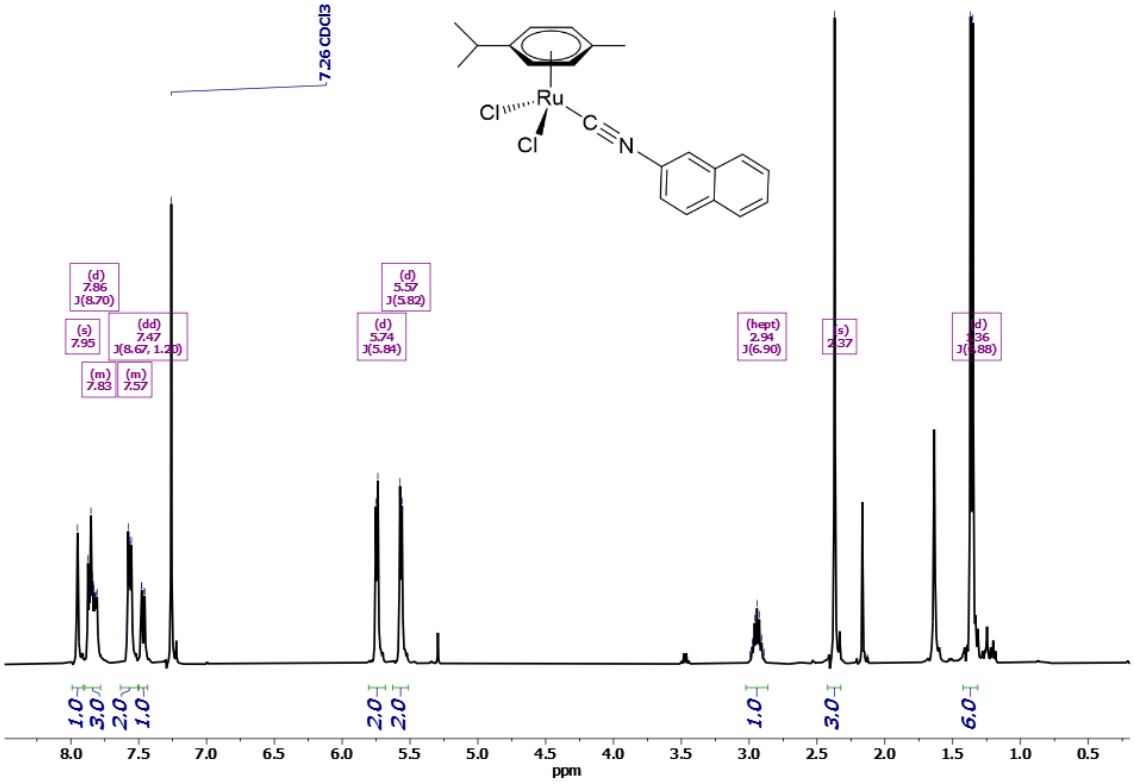

Figure S8. $^{13}C\{^{1}H\}$ NMR spectrum (100 MHz, $CDCl_3$) of **1b**.

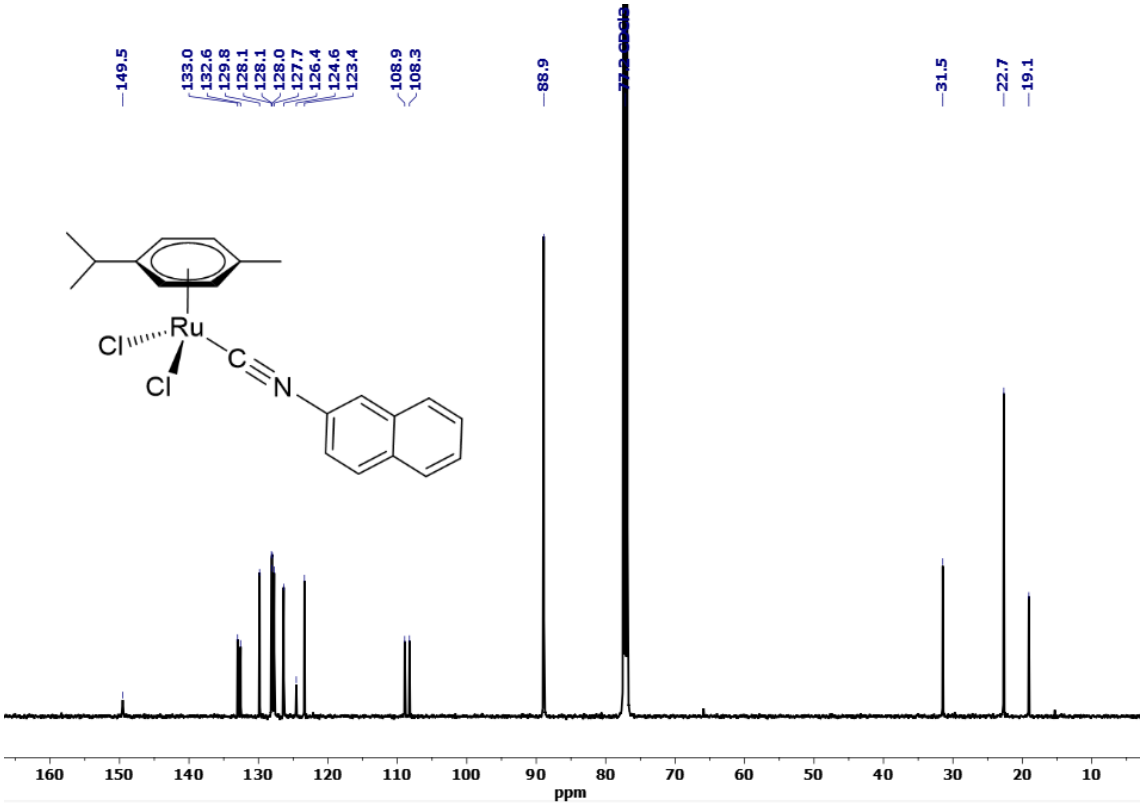

Figure S9. Solid-state FT-IR spectrum (650-4000 cm^{-1}) of [$RuCl_2$(CNBn)(η^6-*p*-cymene)], **1c**.

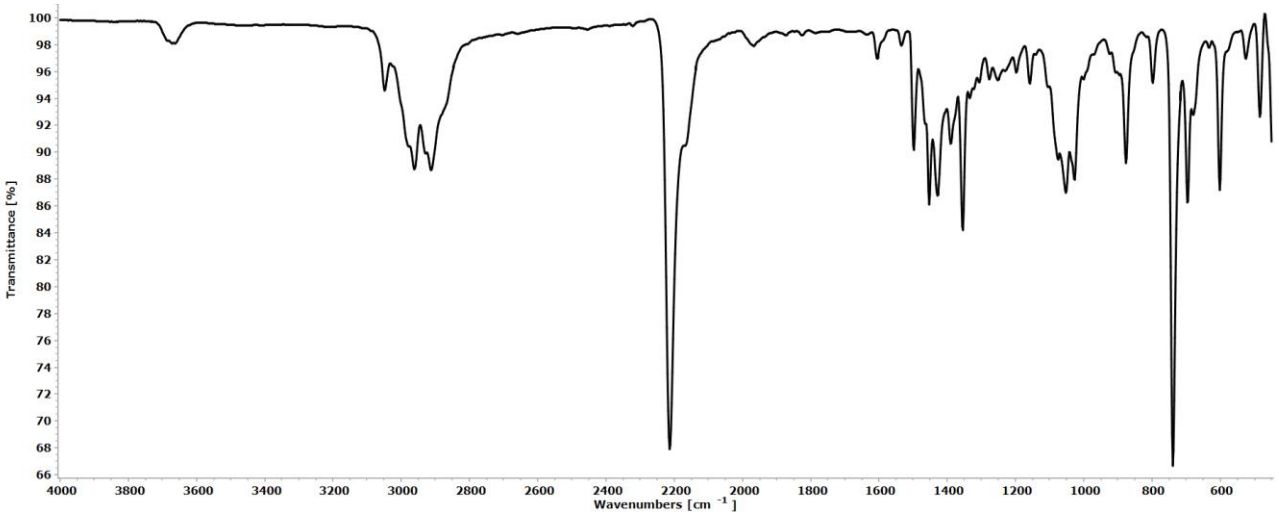

Figure S10. Solvent-subtracted FT-IR spectra (1300-2700 cm^{-1}) of **1c** (black line) and benzyl isocyanide (red dashed line) in CH_2Cl_2.

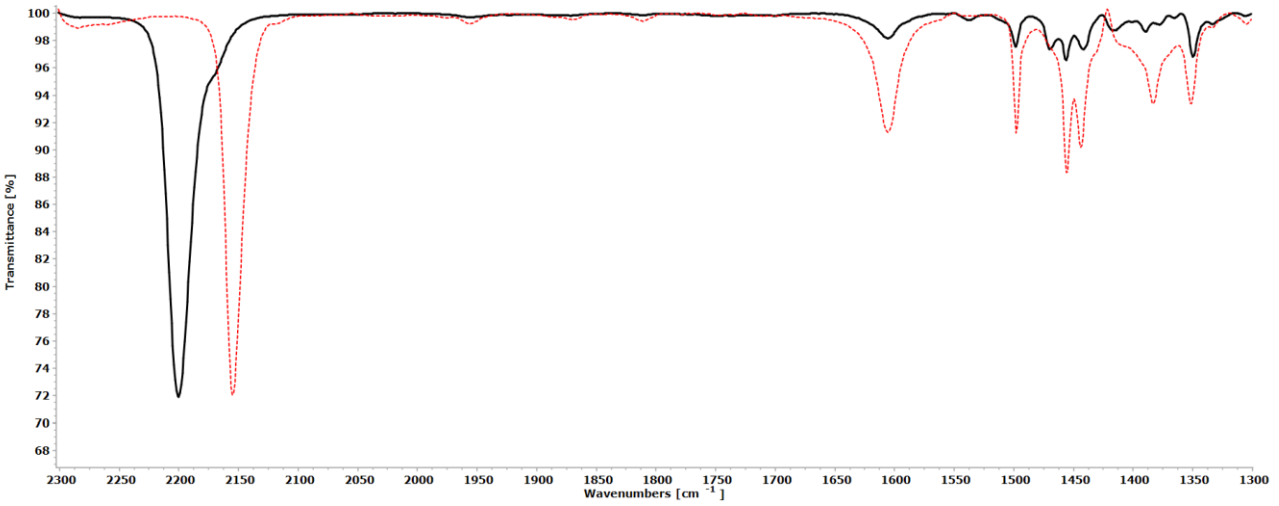

Figure S11. ^{1}H NMR spectrum (400 MHz, $CDCl_3$) of **1c**.

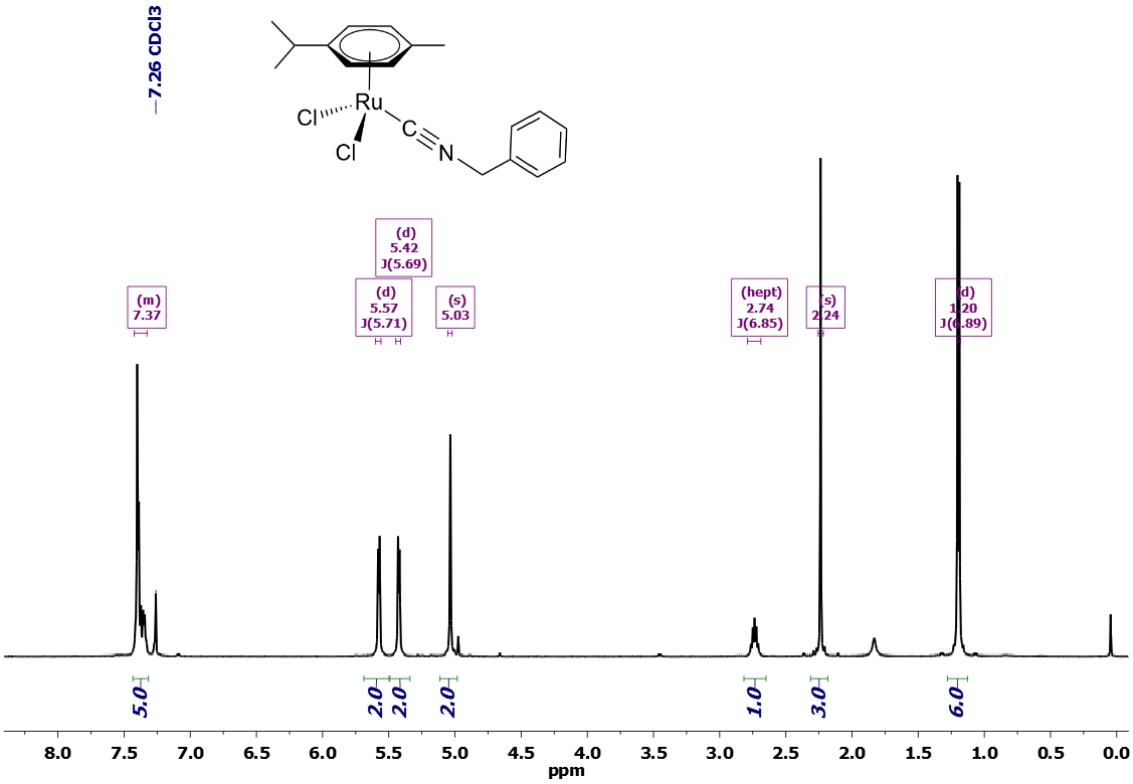

Figure S12. $^{13}C\{^{1}H\}$ NMR spectrum (100 MHz, $CDCl_3$) of **1c**.

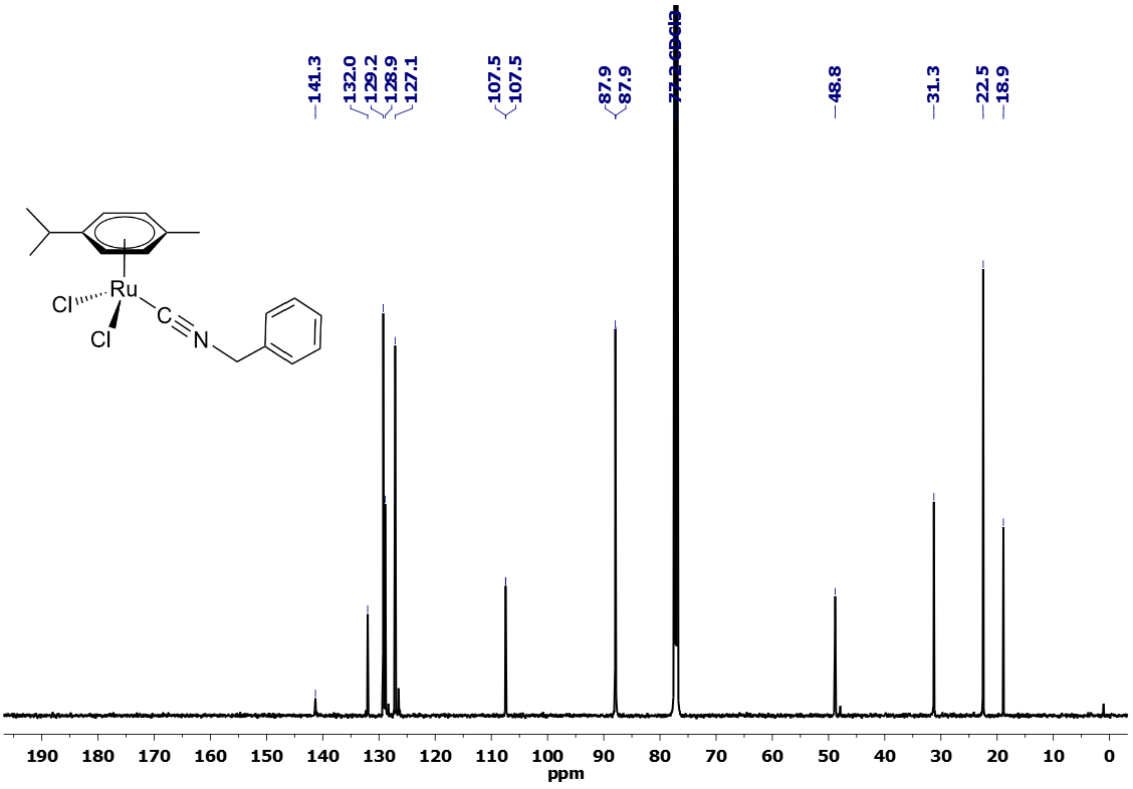

Figure S13. Solid-state FT-IR spectrum (650-4000 cm^{-1}) of [$RuCl_2$(CNCy)(η^6-*p*-cymene)], **1d**.

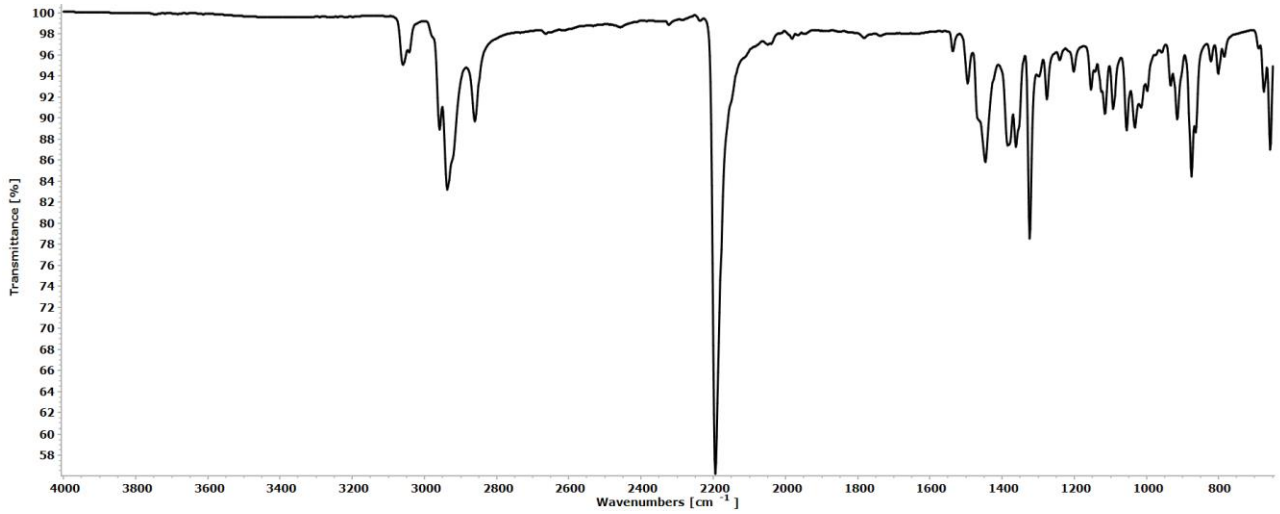

Figure S14. Solvent-subtracted FT-IR spectra (1300-2700 cm^{-1}) of **1d** (black line) and cyclohexyl isocyanide (red dashed line) in CH_2Cl_2.

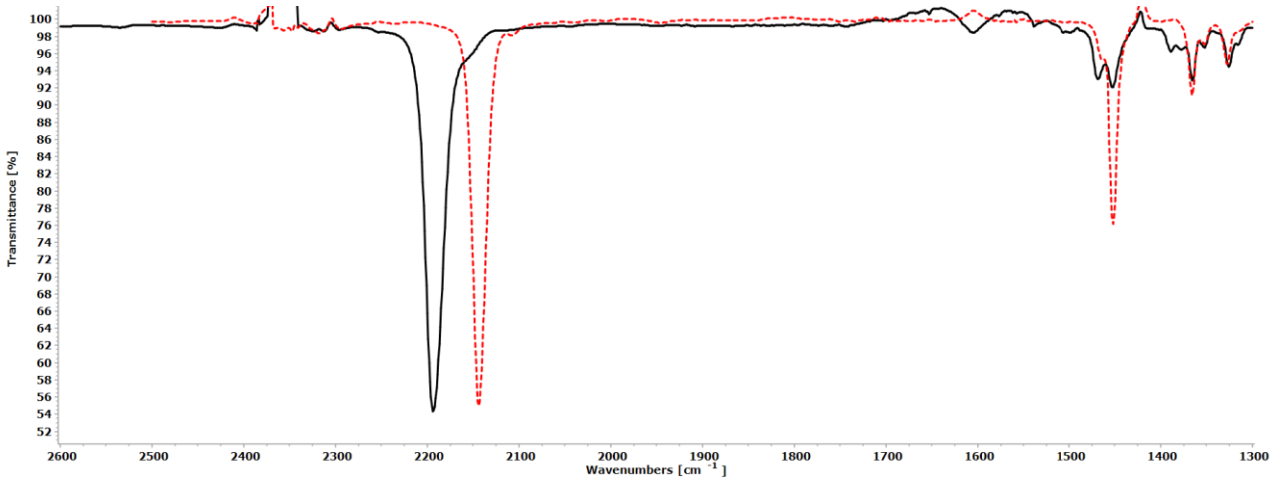

Figure S15. ^{1}H NMR spectrum (400 MHz, $CDCl_3$) of **1d**.

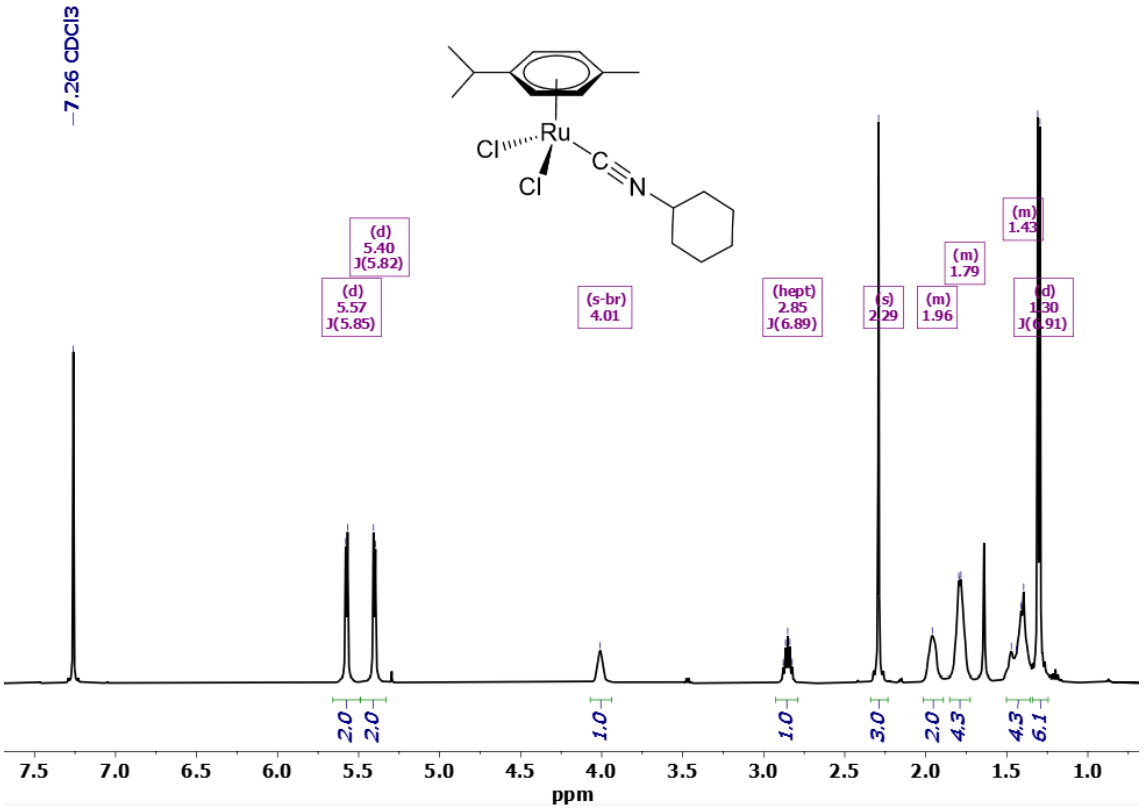

Figure S16. $^{13}C\{^{1}H\}$ NMR spectrum (100 MHz, $CDCl_3$) of **1d**.

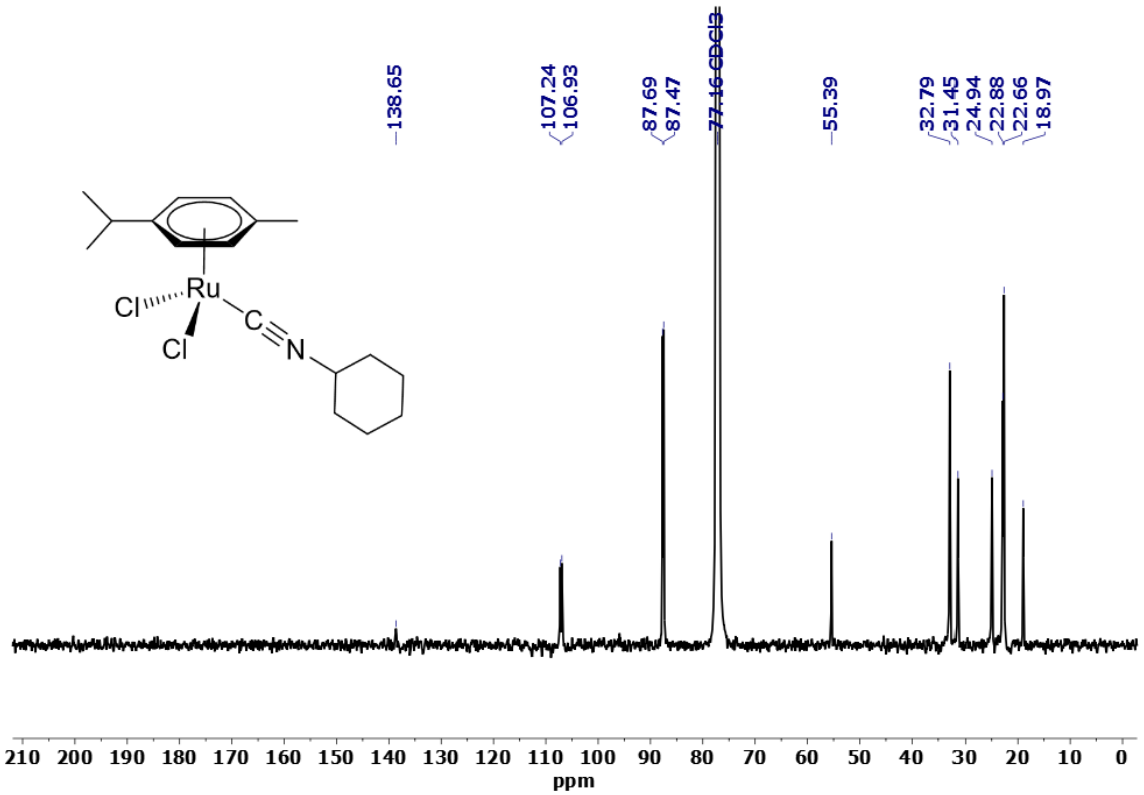

Figure S17. Solid-state FT-IR spectrum (650-4000 cm^{-1}) of $[RuCl_2(CN^tBu)(\eta^6\text{-}p\text{-cymene})]$, **1e**.

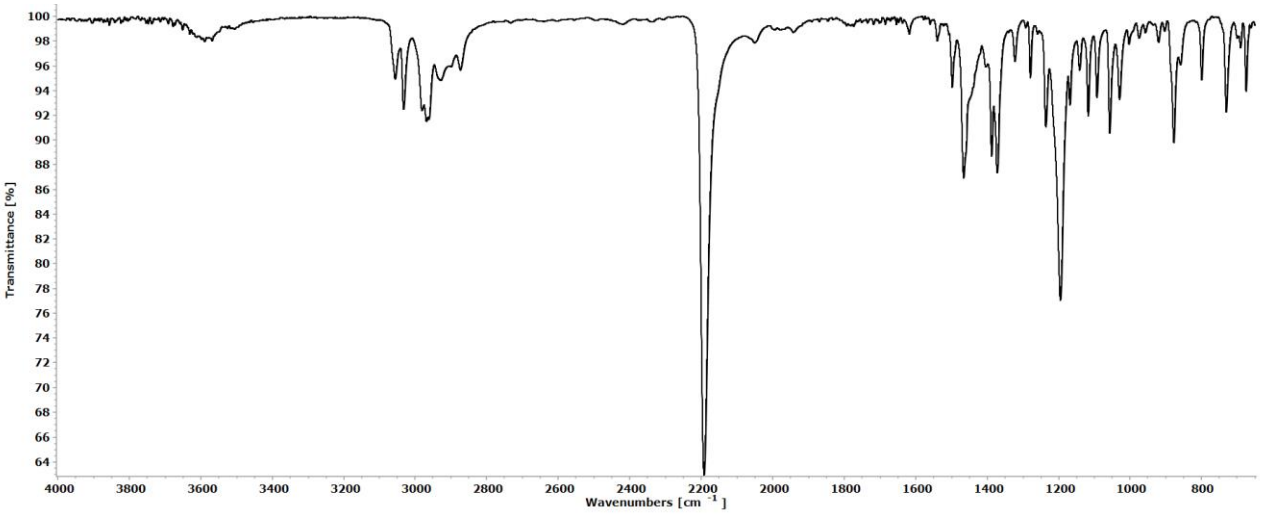

Figure S18. Solvent-subtracted FT-IR spectra (1300-2700 cm^{-1}) of **1e** (black line) and tert-butyl isocyanide (red dashed line) in CH_2Cl_2.

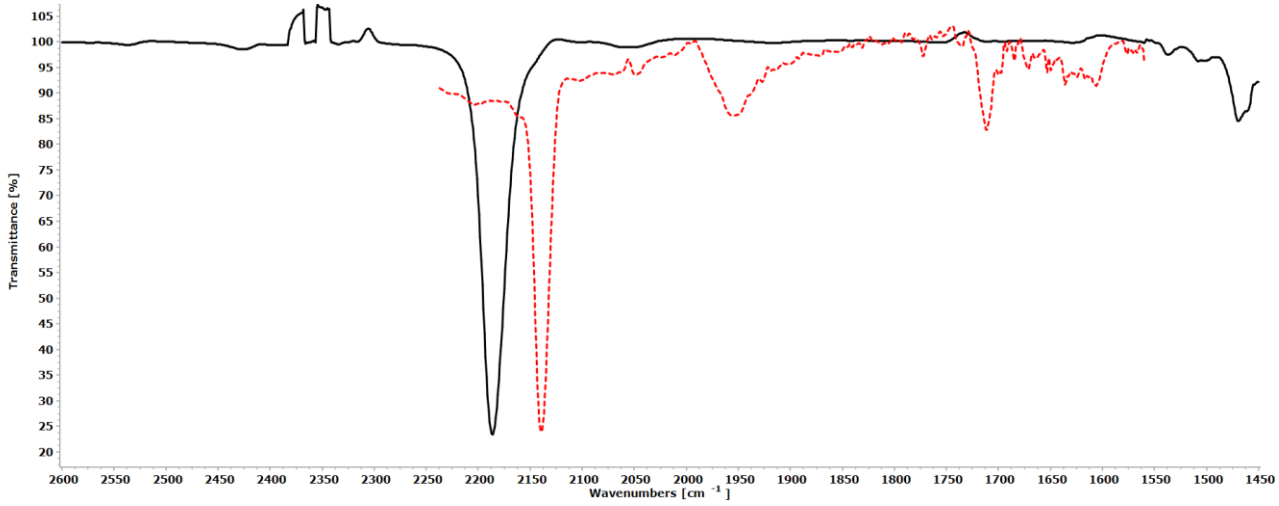

Figure S19. ^{1}H NMR spectrum (400 MHz, $CDCl_3$) of **1e**.

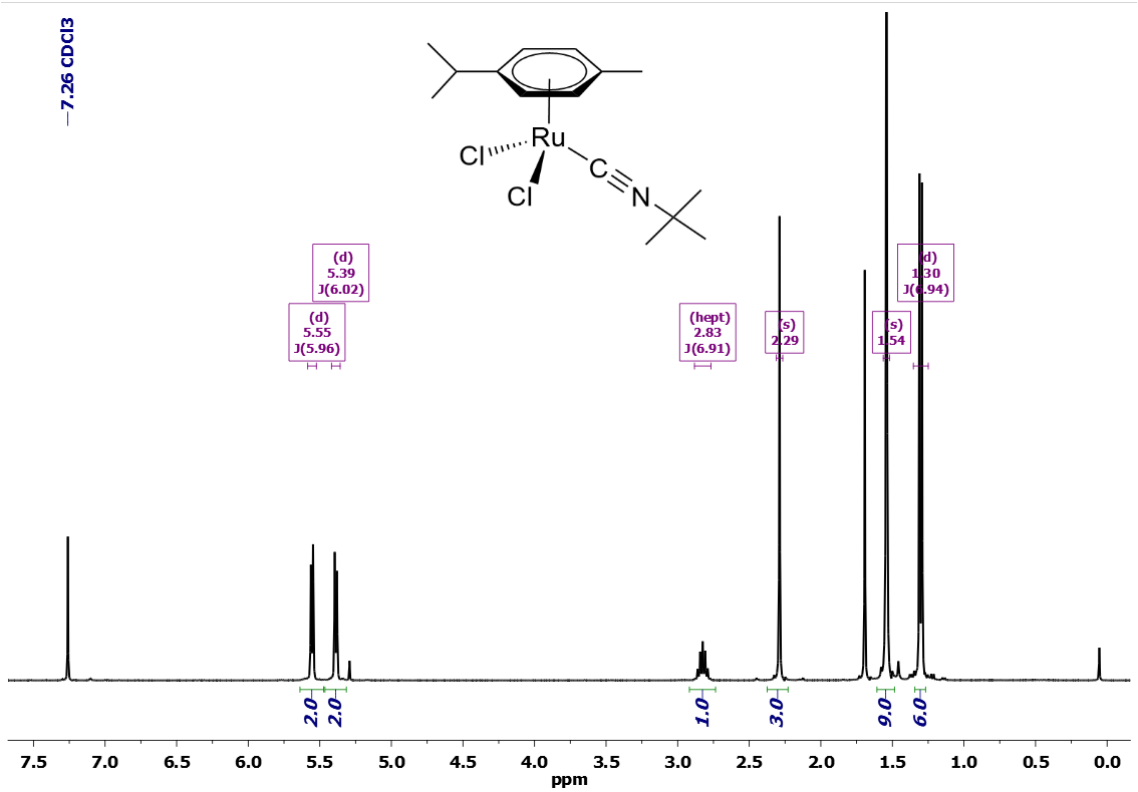

Figure S20. $^{13}C\{^{1}H\}$ NMR spectrum (100 MHz, $CDCl_3$) of **1e**.

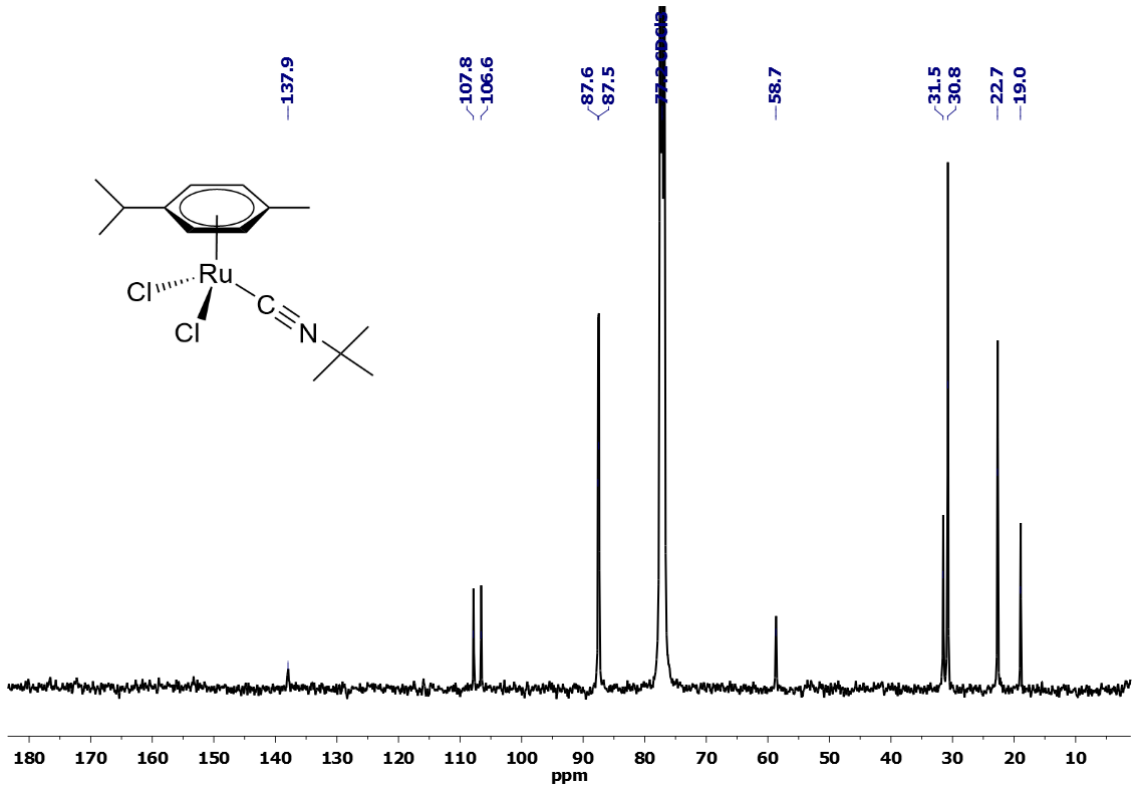

Figure S21. Solid-state FT-IR spectrum (650-4000 cm^{-1}) of [RuI_2(CN^tBu)(η^6-*p*-cymene)], **1f**.

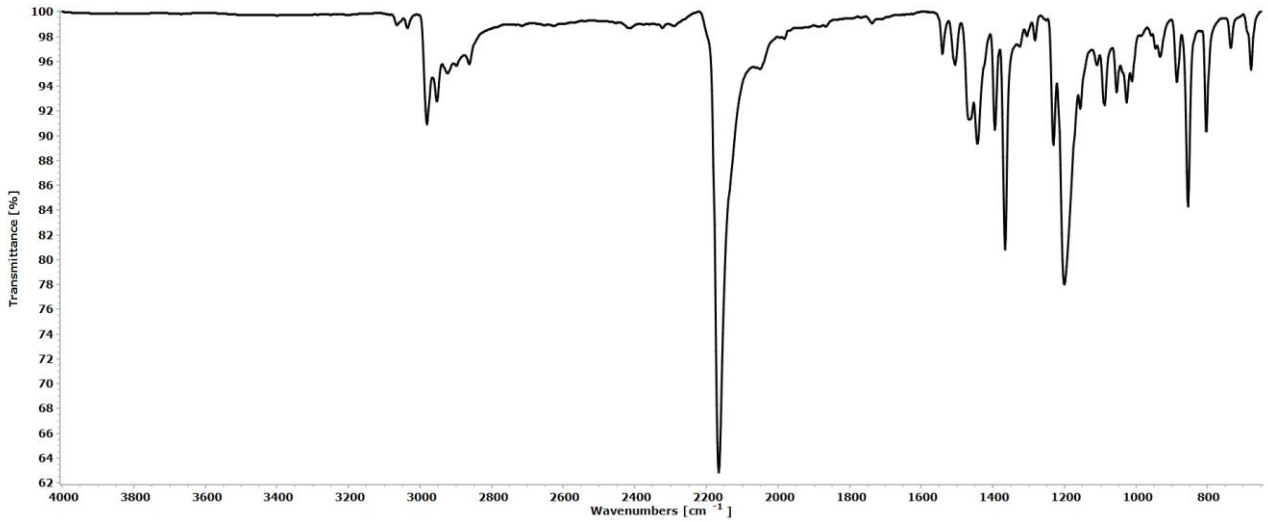

Figure S22. Solvent-subtracted FT-IR spectra (1300-2700 cm^{-1}) of **1f** in CH_2Cl_2.

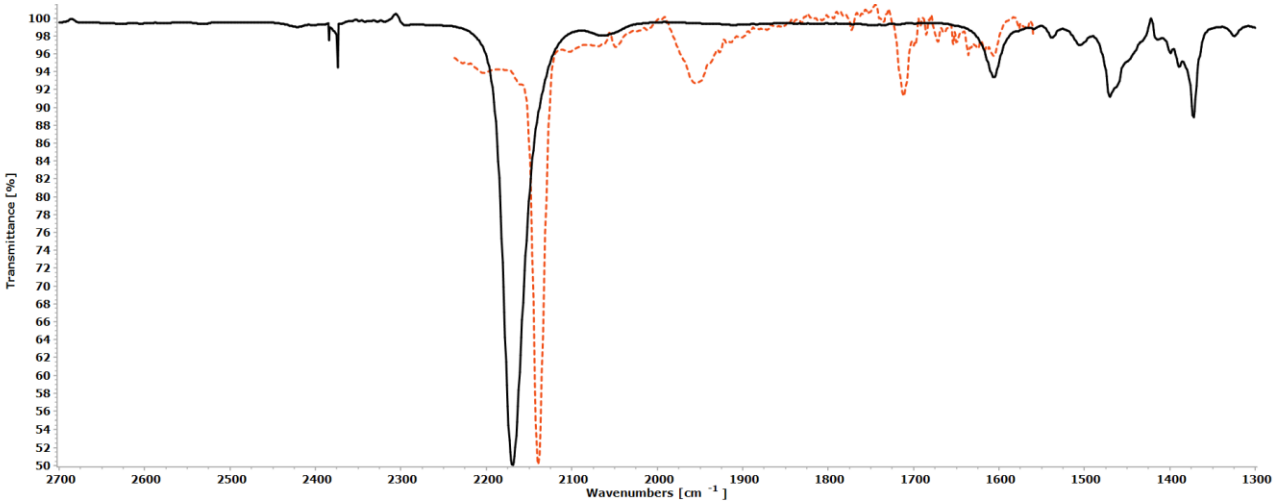

Figure S23. ^{1}H NMR spectrum (400 MHz, $CDCl_3$) of **1f**.

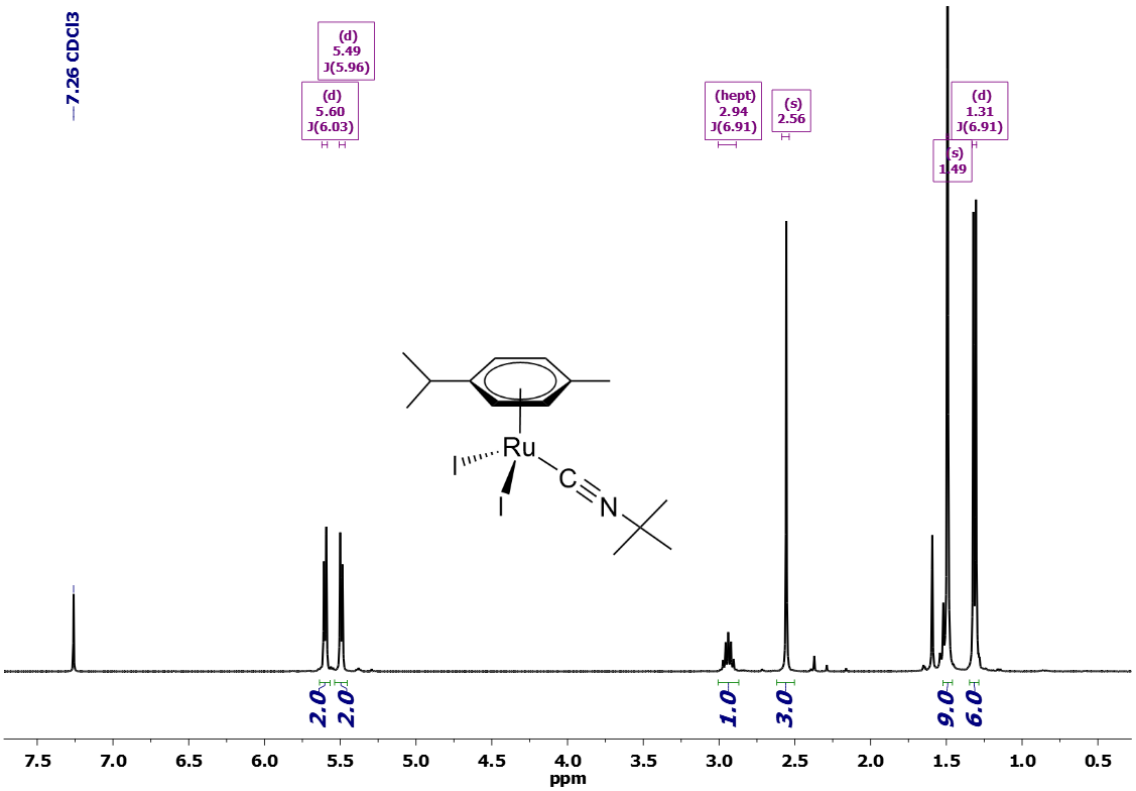

Figure S24. $^{13}C\{^{1}H\}$ NMR spectrum (100 MHz, $CDCl_3$) of **1f**.

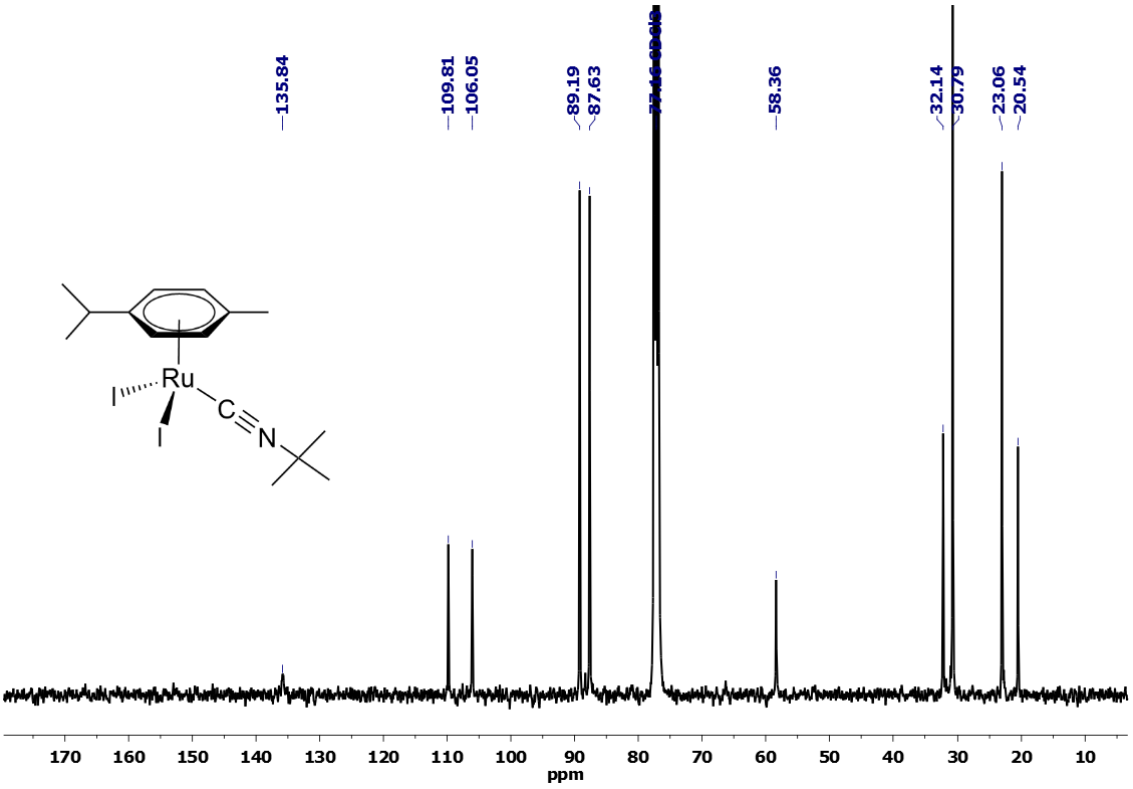

Symmetry and isomerism for [$RuCl_2$(CNXyl)$(DMSO)_3$]

Chart S1. Symmetry properties, inequivalent methyl groups (**a-d**) for *trans,mer*, *cis,mer* and *fac* isomers of [$RuCl_2$(CNXyl)$(DMSO)_3$], **2a**. Dashed red lines indicate NOEs expected from irradiation of the ^{1}H NMR CH_3 resonance of the xylyl group.

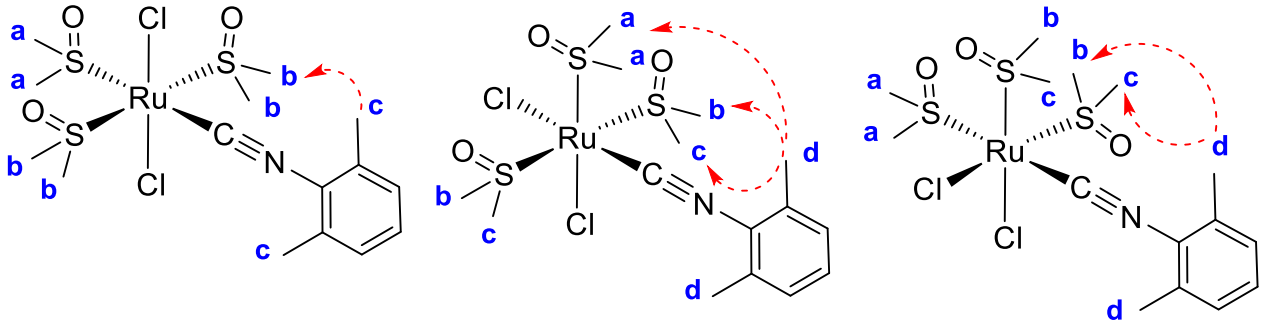

Trans,mer

C_{2v} symmetry

Cis,mer

C_s symmetry

fac

C_s symmetry

FT-IR and NMR spectra of isocyanide-DMSO complexes

Figure S25. Solid-state FT-IR spectrum (650-4000 cm^{-1}) *cis*,*mer*-[$RuCl_2$(CNXyl)(κS-DMSO)$_3$], **2a**.

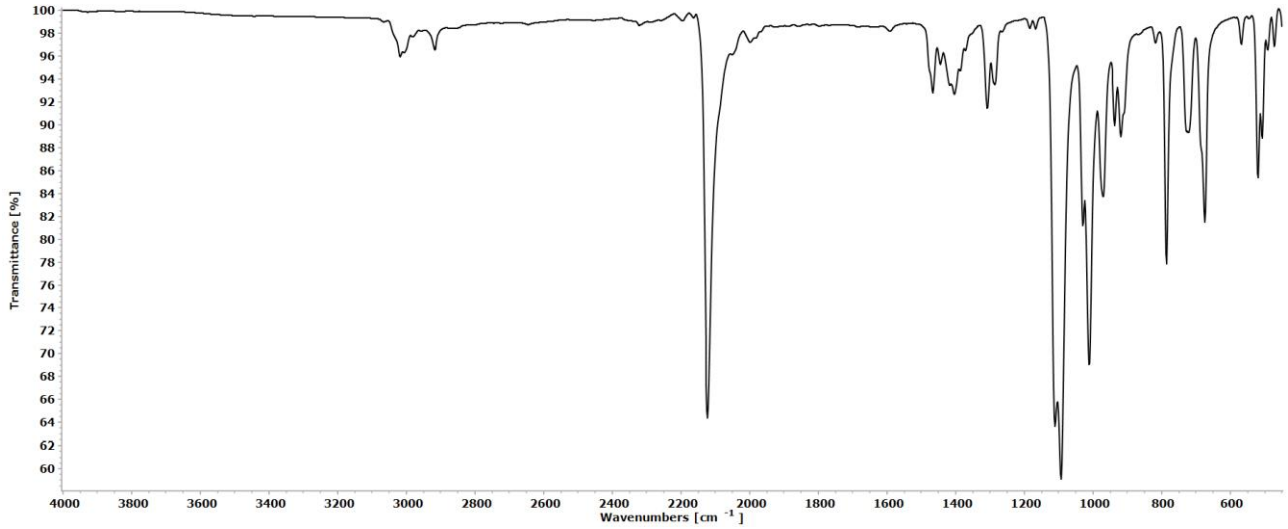

Figure S26. Solvent-subtracted FT-IR spectra (1300-2700 cm^{-1}) of **1a** (black line), **2a** (blue line) and xylyl isocyanide (red dashed line) in CH_2Cl_2.

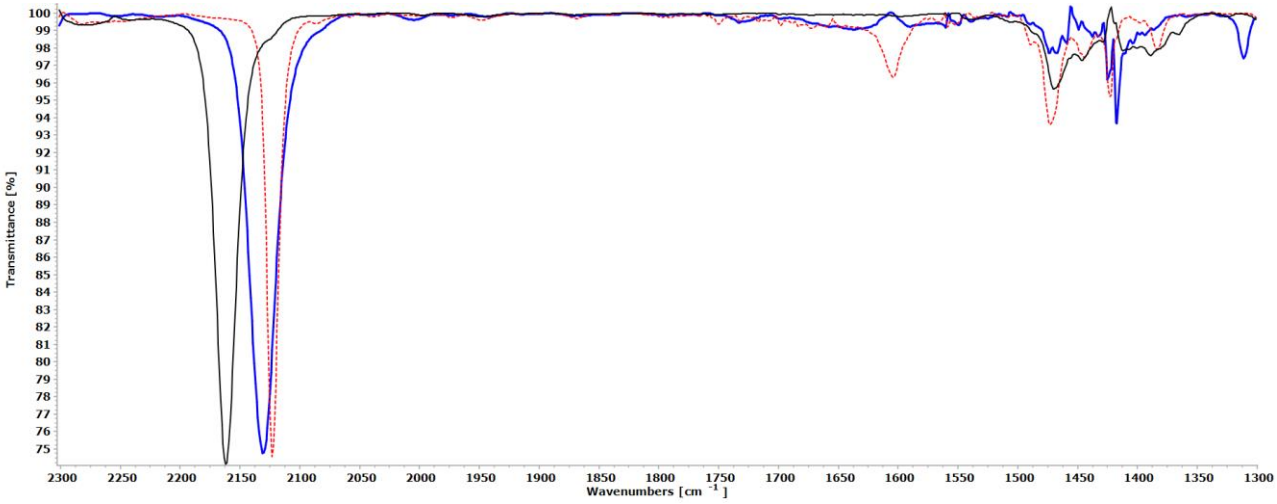

Figure S27. ^{1}H NMR spectrum (400 MHz, acetone-d_6) of **2a**.

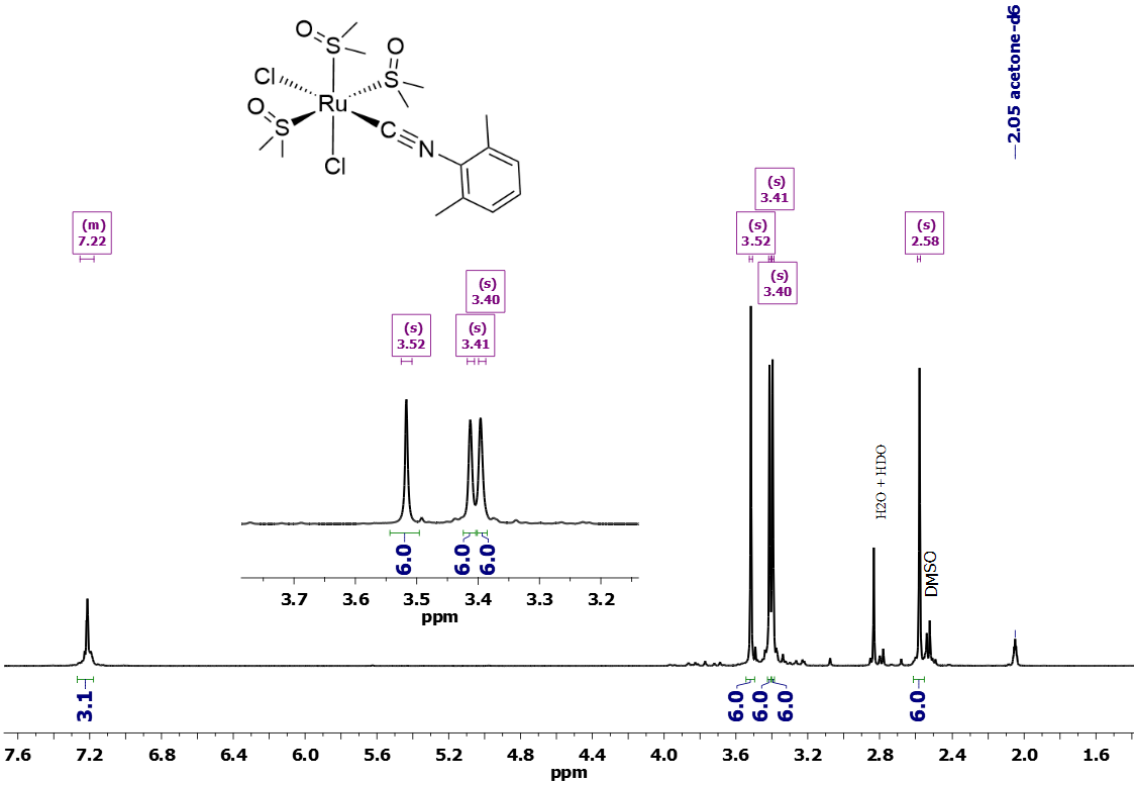

Figure S28. $^{13}C\{^{1}H\}$ NMR spectrum (100 MHz, acetone-d_6) of **2a**.

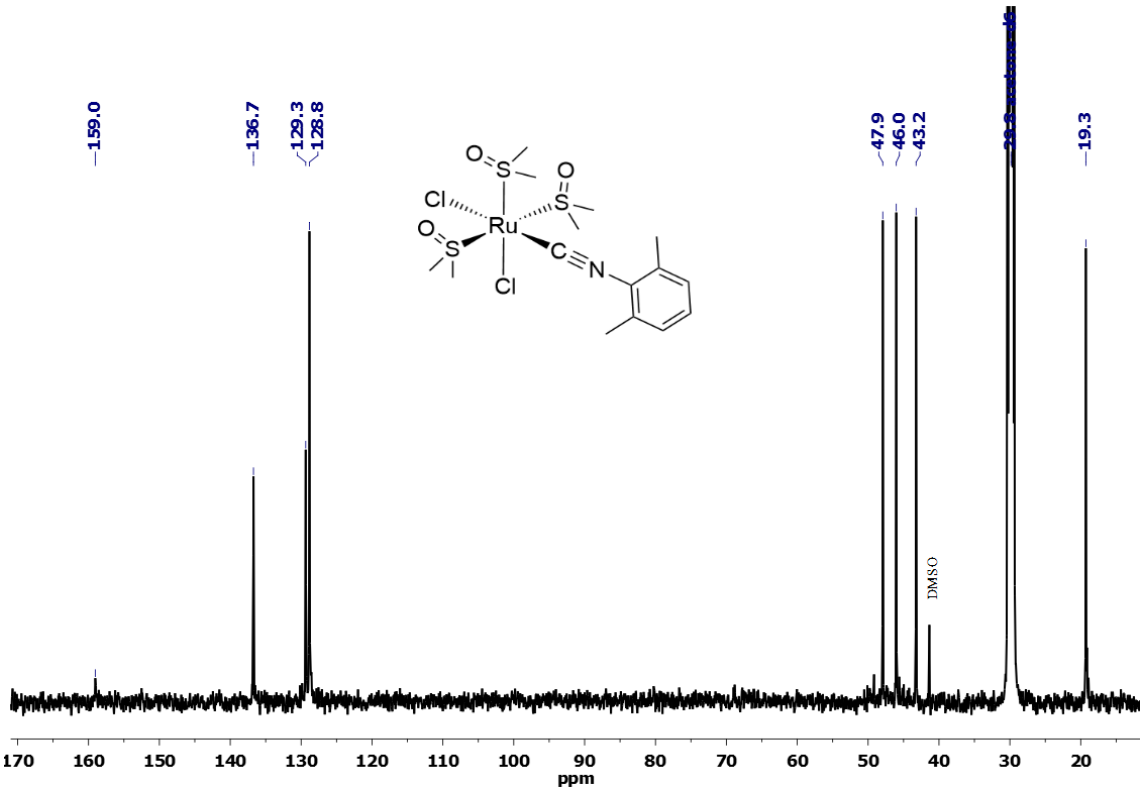

Figure S29. Black line: ^{1}H NMR spectrum (401 MHz, $CDCl_3$) of **2a**. Blue line: ^{1}H NOESY with irradiation at 3.53 ppm (SCH_3-**a**). Violet line: ^{1}H NOESY with irradiation at 3.45 ppm (SCH_3-**b**). Red line: ^{1}H NOESY with irradiation at 3.37 ppm (SCH_3-**c**). Green line: ^{1}H NOESY with irradiation at 2.56 ppm ($C\text{-}CH_3$). Observed NOEs are indicated by the arrows; dashed lines represent weaker NOE effects.

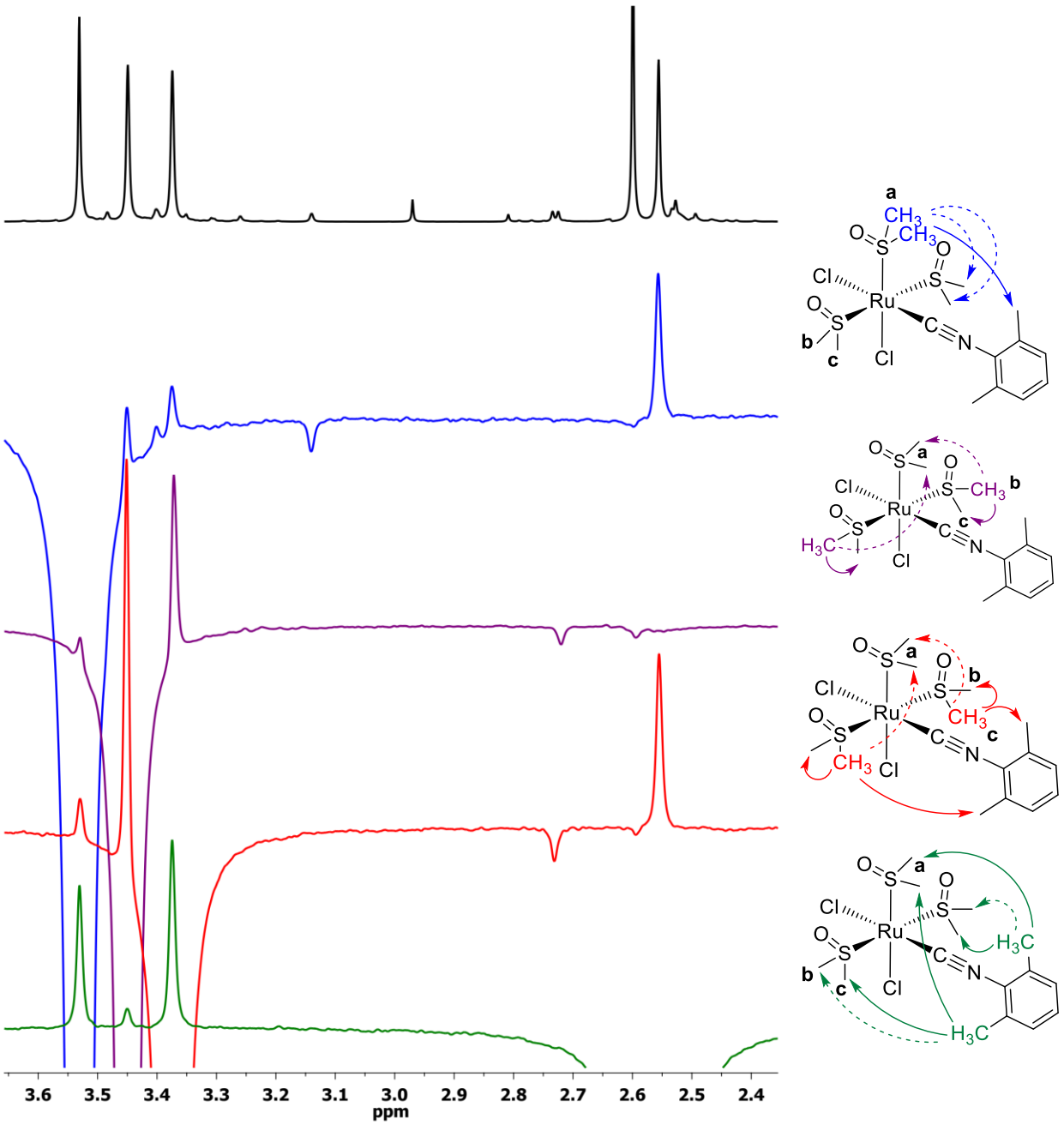

Figure S30. Solid-state FT-IR spectrum (650-4000 cm^{-1}) of *cis,mer*-[$RuCl_2${CN(2-naphthyl)}(κ*S*-DMSO)$_3$], **2b**.

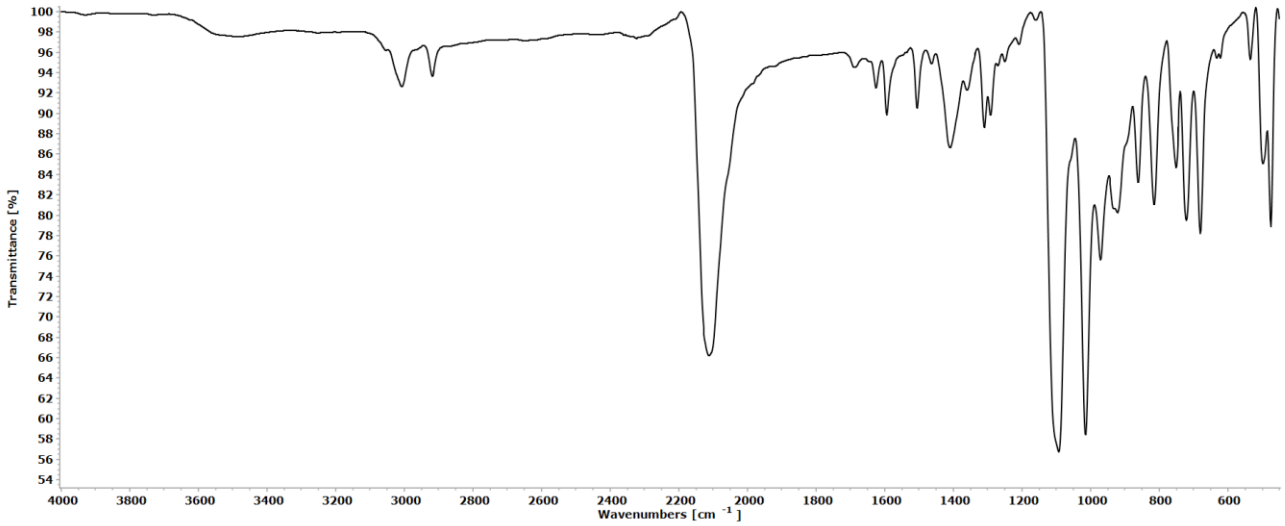

Figure S31. Solvent-subtracted FT-IR spectra (1300-2700 cm^{-1}) of **1b** (black line), **2b** (blue line) and 2-naphthyl isocyanide (red dashed line) in CH_2Cl_2.

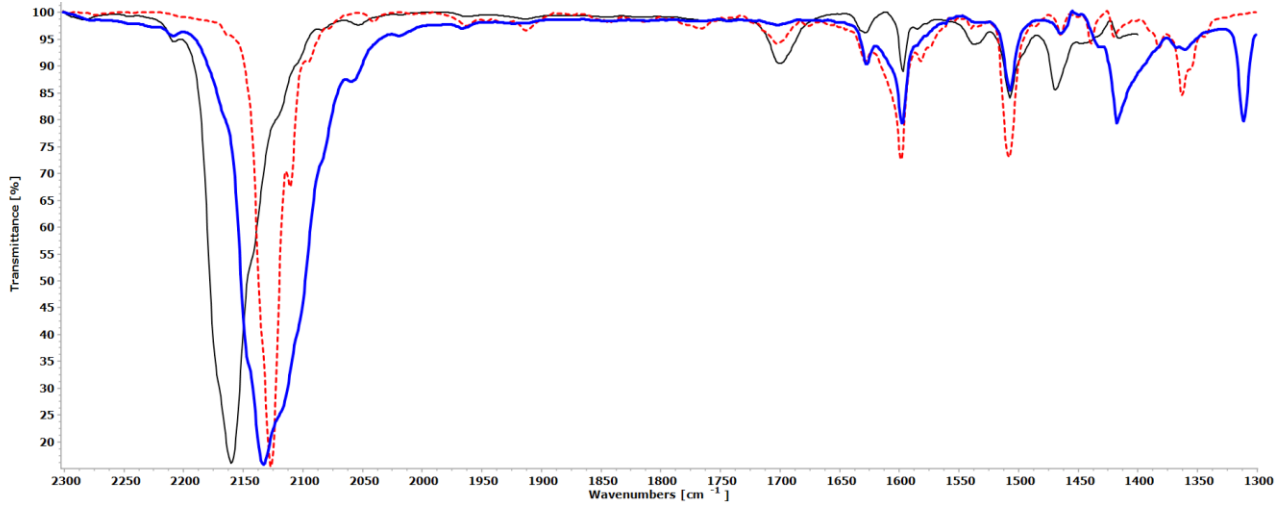

Figure S32. ^{1}H NMR spectrum (400 MHz, acetone-d_6) of **2b**.

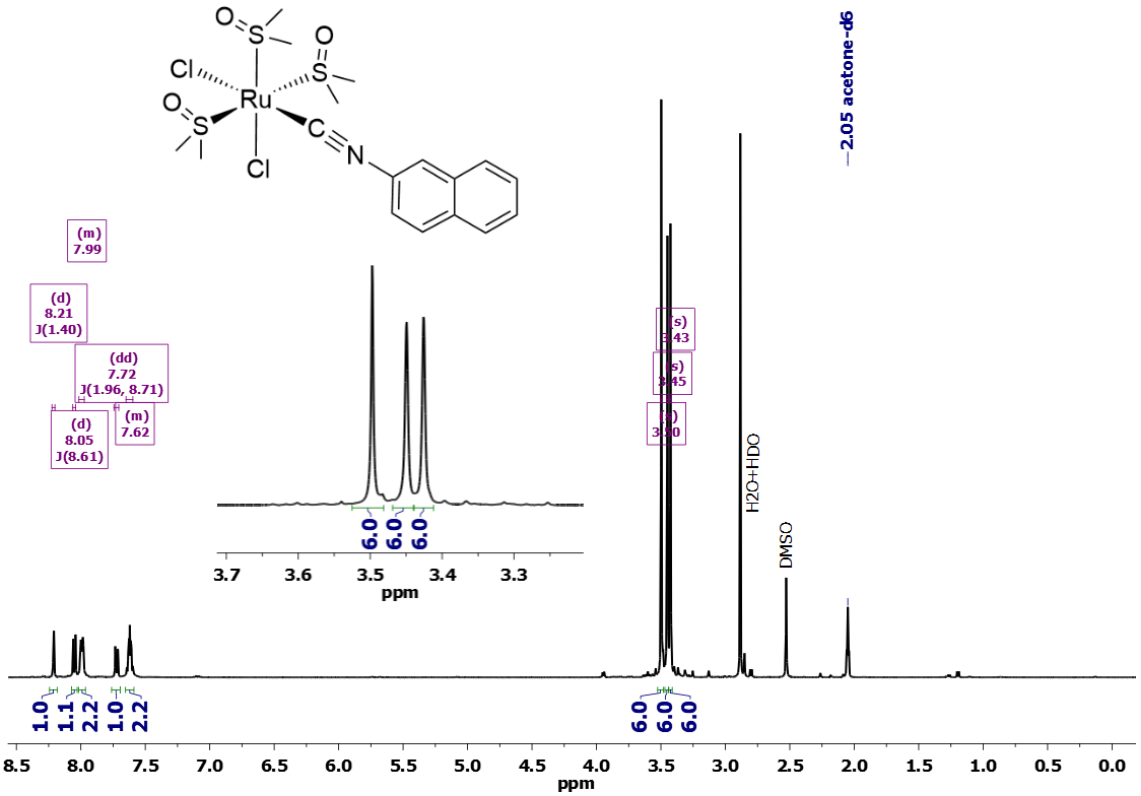

Figure S33. $^{13}C\{^{1}H\}$ NMR spectrum (100 MHz, acetone-d_6) of **2b**.

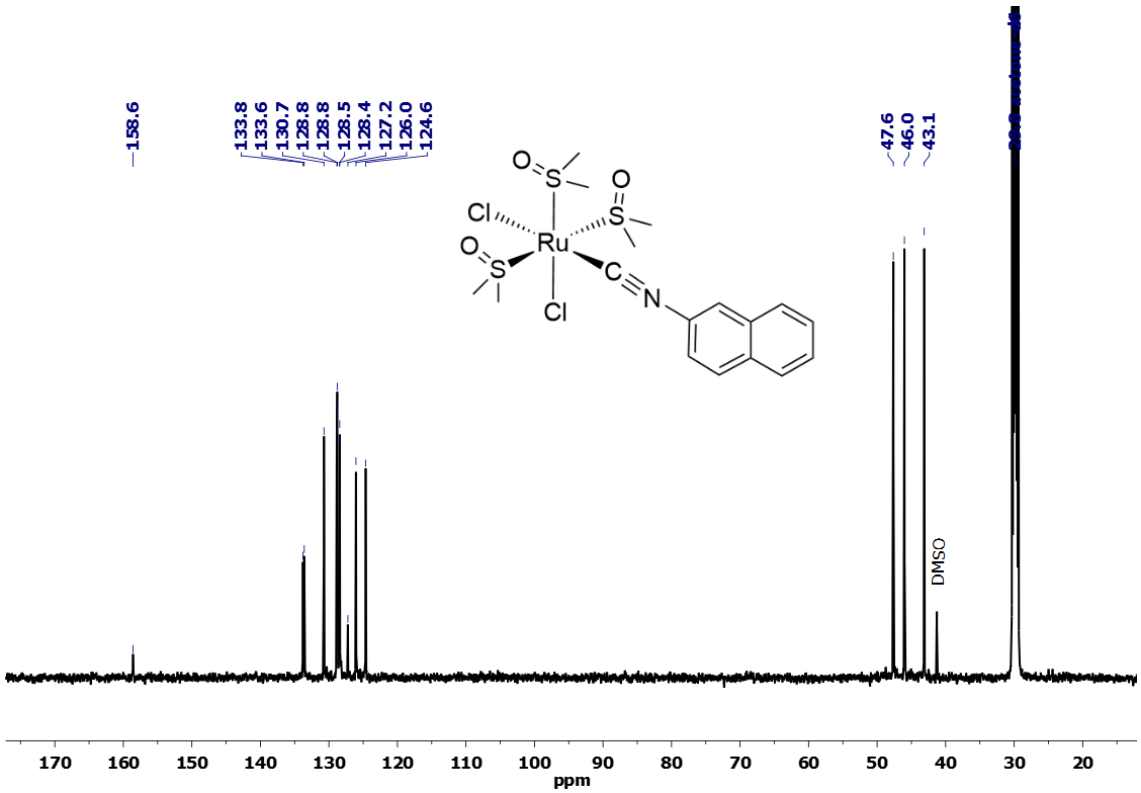

Figure S34. Black line: ^{1}H NMR spectrum (401 MHz, acetone-d_6) of **2b**. Blue line: ^{1}H NOESY with irradiation at 3.53 ppm (SCH_3-**a**). Red line: ^{1}H NOESY with irradiation at 3.37 ppm (SCH_3-**c**). Observed NOEs are indicated by the arrows; dashed lines represent weaker NOE effects. The NOE effect between SCH_3-**a** and SCH_3-**b** is probably weakened by co-irradiation.

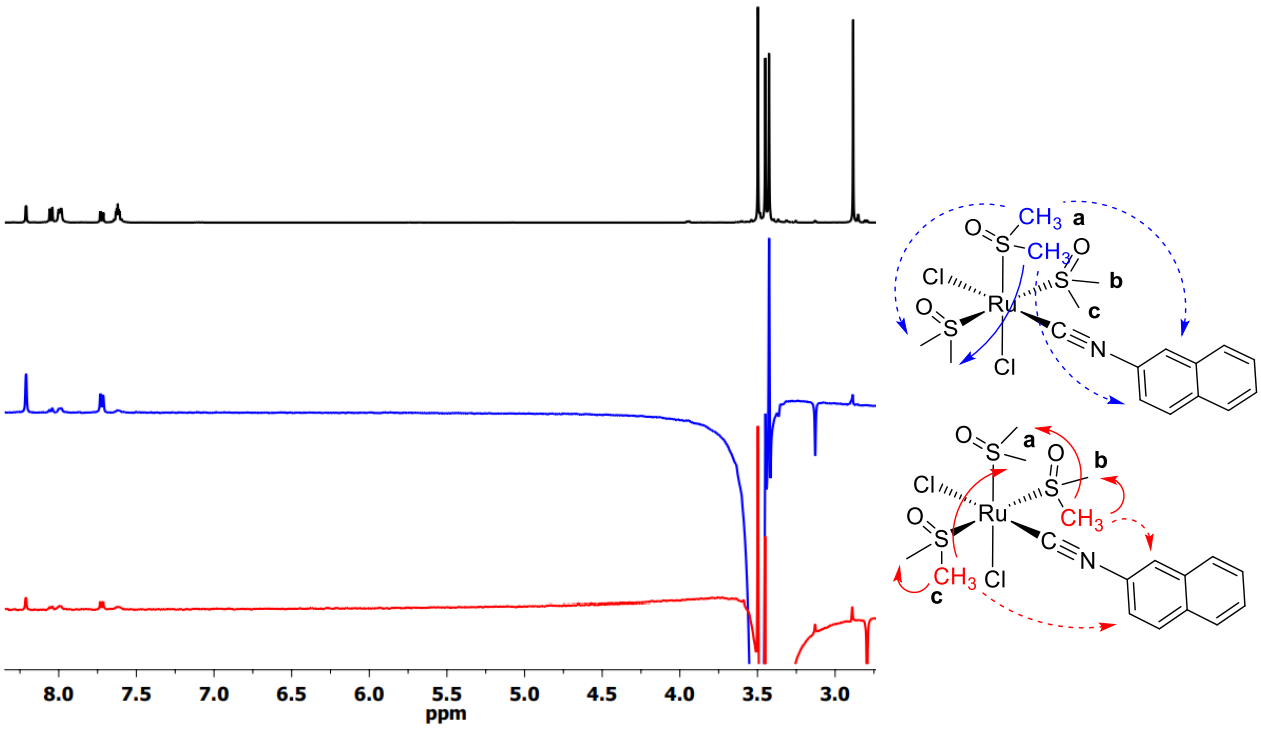

Figure S35. Solid-state FT-IR spectrum (650-4000 cm^{-1}) of *cis,mer*-[$RuCl_2$(CNBn)(κ*S*-DMSO)$_3$], **2c**.

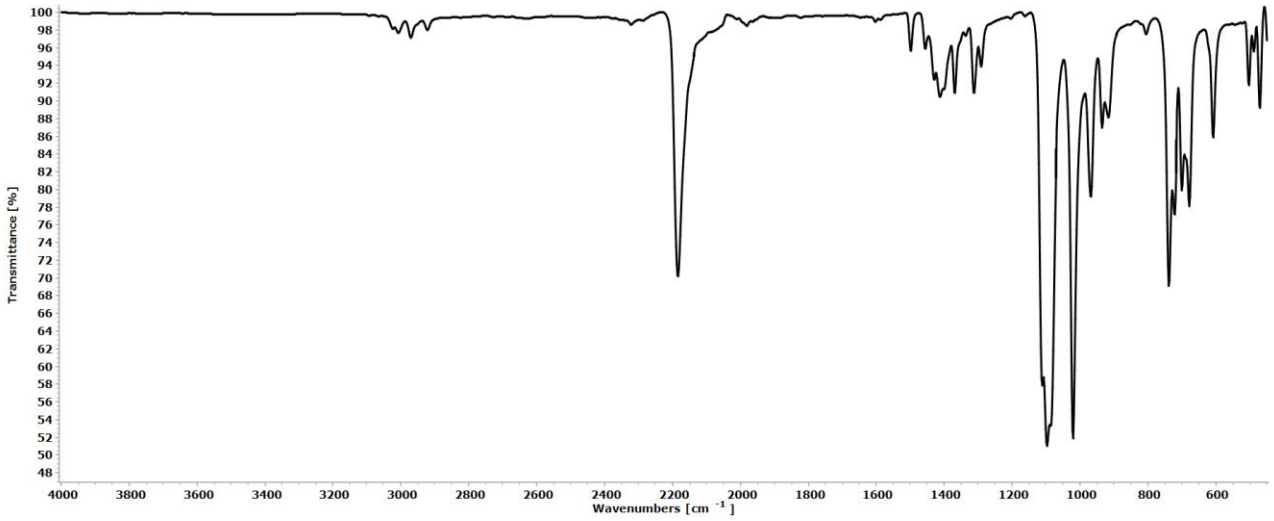

Figure S36. Solvent-subtracted FT-IR spectra (1300-2700 cm^{-1}) of **1c** (black line), **2c** (blue line) and benzyl isocyanide (red dashed line) in CH_2Cl_2.

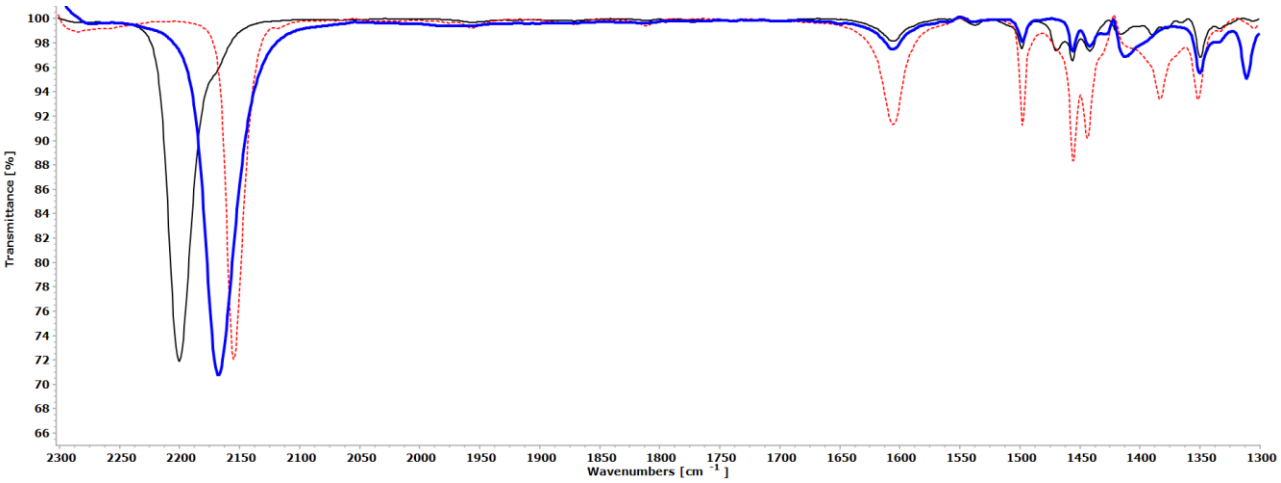

Figure S37. ^{1}H NMR spectrum (400 MHz, acetone-d_6) of **2c**.

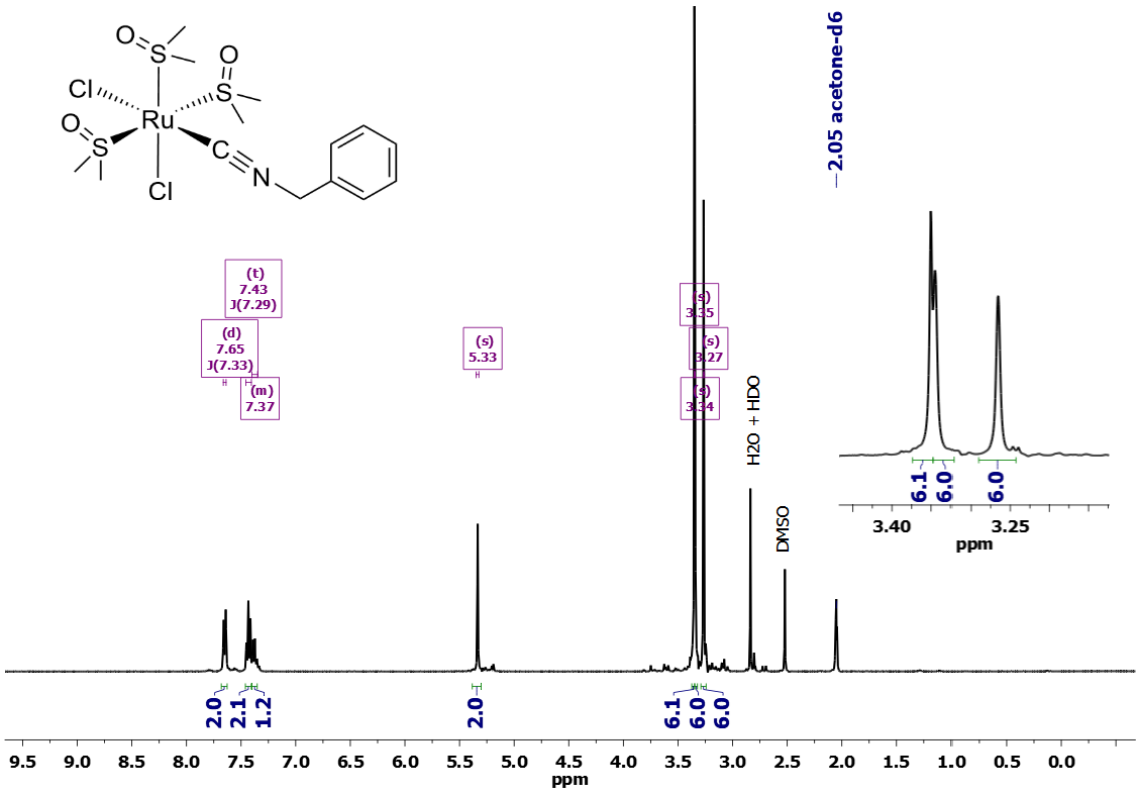

Figure S38. $^{13}C\{^{1}H\}$ NMR spectrum (100 MHz, acetone-d_6) of **2c**.

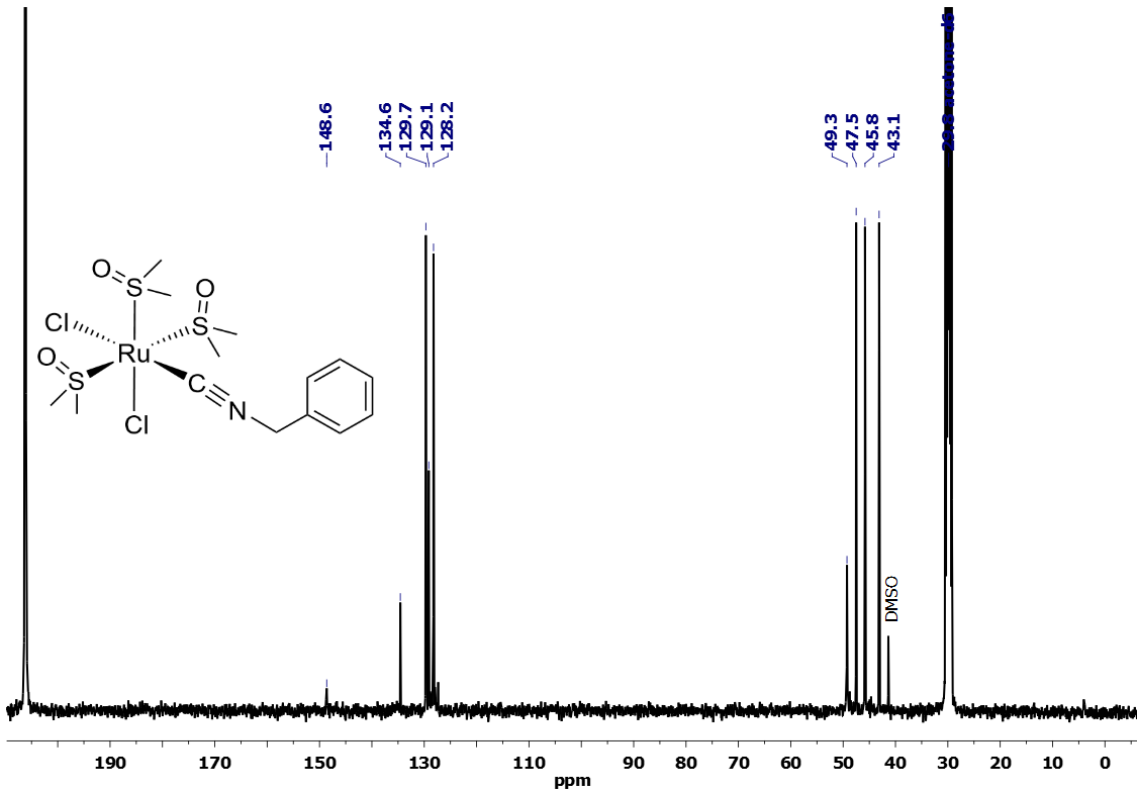

Figure S39. Black line: ^{1}H NMR spectrum (401 MHz, acetone-d_6) of **2c**. Green line: ^{1}H NOESY with irradiation at 5.33 ppm (CH_2). Red line: ^{1}H NOESY with irradiation at 3.27 ppm (SCH_3-**c**). Observed NOEs are indicated by the arrows; dashed lines indicate weaker NOE effects.

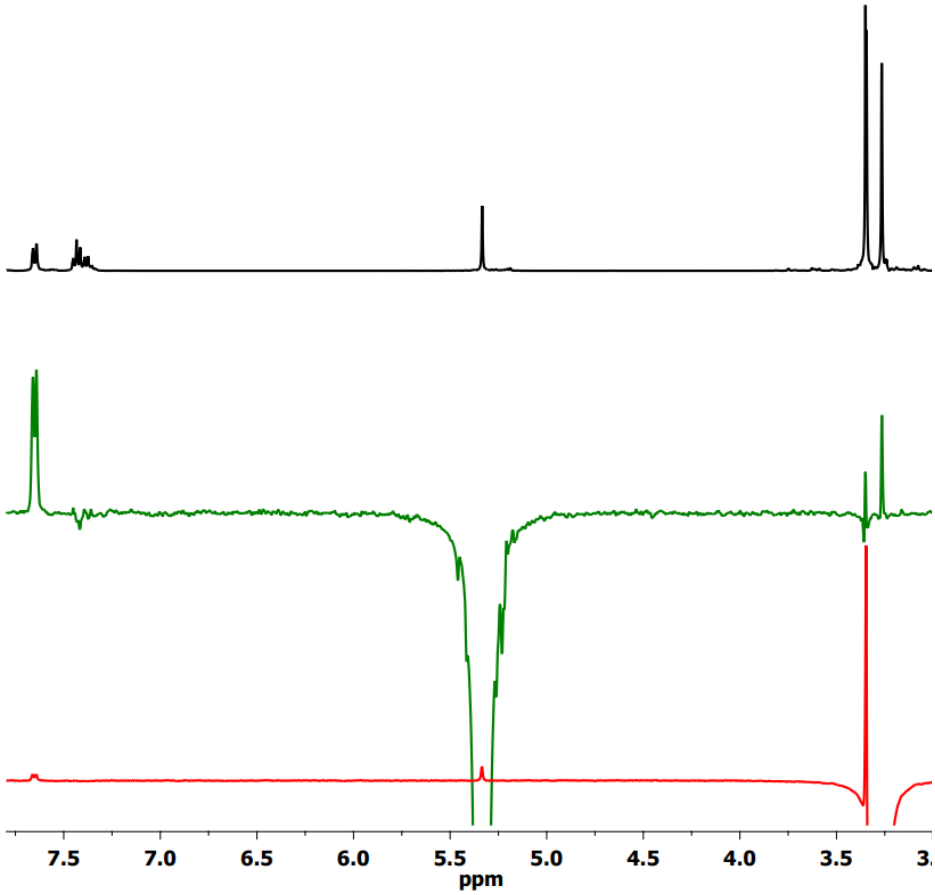

Figure S40. Solid-state FT-IR spectrum (650-4000 cm^{-1}) of *cis,mer*-[$RuCl_2$(CNCy)(κ*S*-DMSO)$_3$], **2d**.

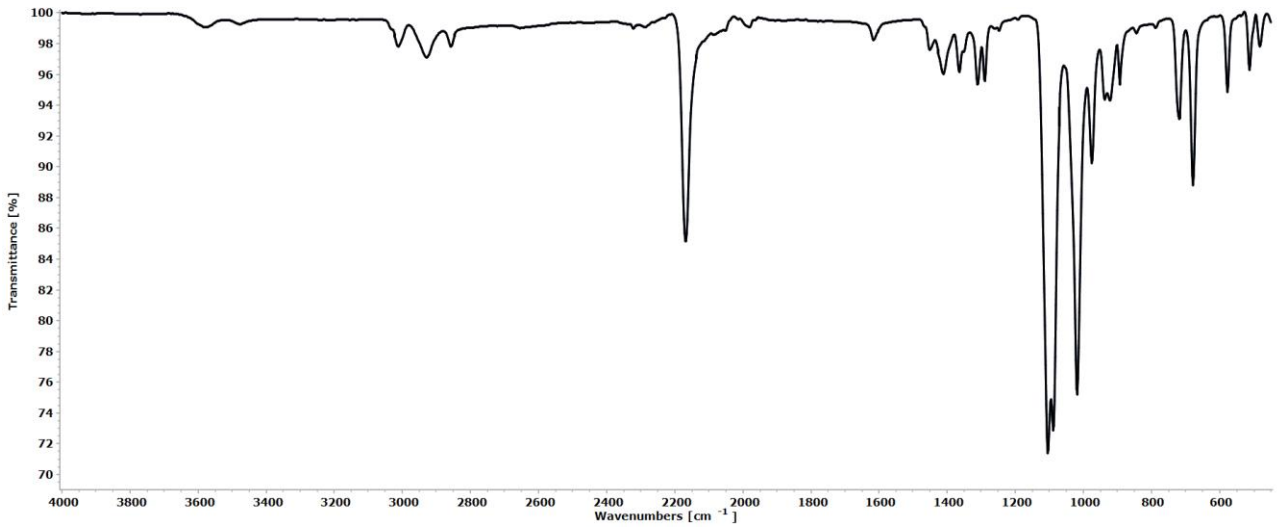

Figure S41. Solvent-subtracted FT-IR spectra (1300-2700 cm^{-1}) of **1d** (black line), **2d** (blue line) and cyclohexyl isocyanide (red dashed line) in CH_2Cl_2.

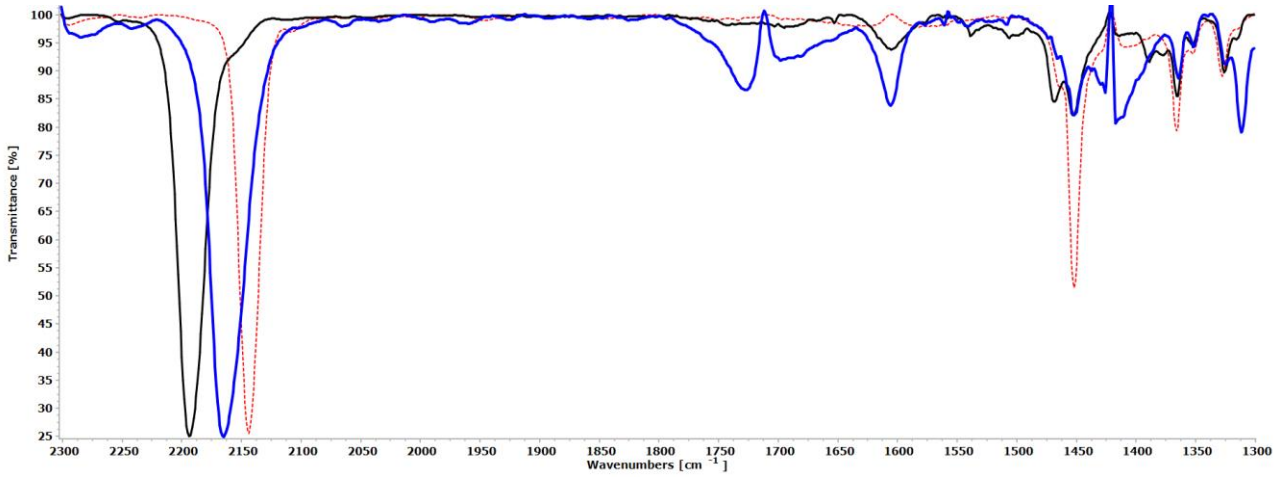

Figure S42. ^{1}H NMR spectrum (400 MHz, acetone-d_6) of **2d**.

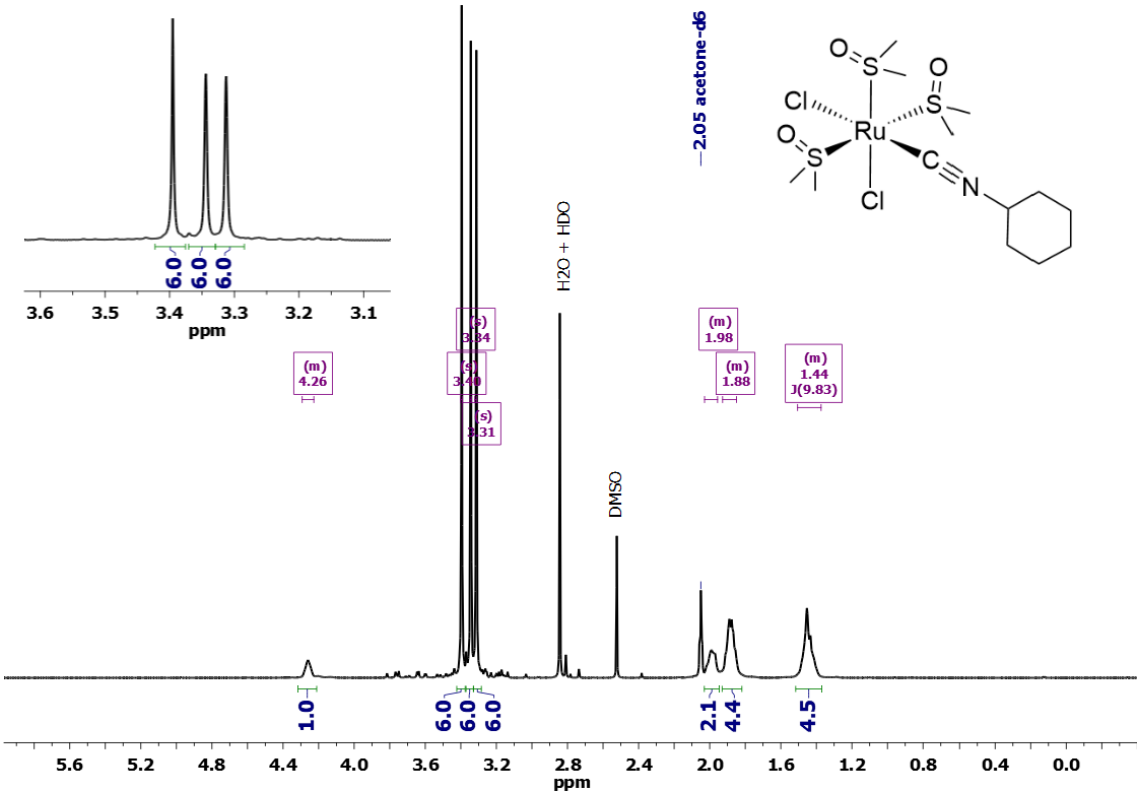

Figure S43. $^{13}C\{^{1}H\}$ NMR spectrum (100 MHz, acetone-d_6) of **2d**.

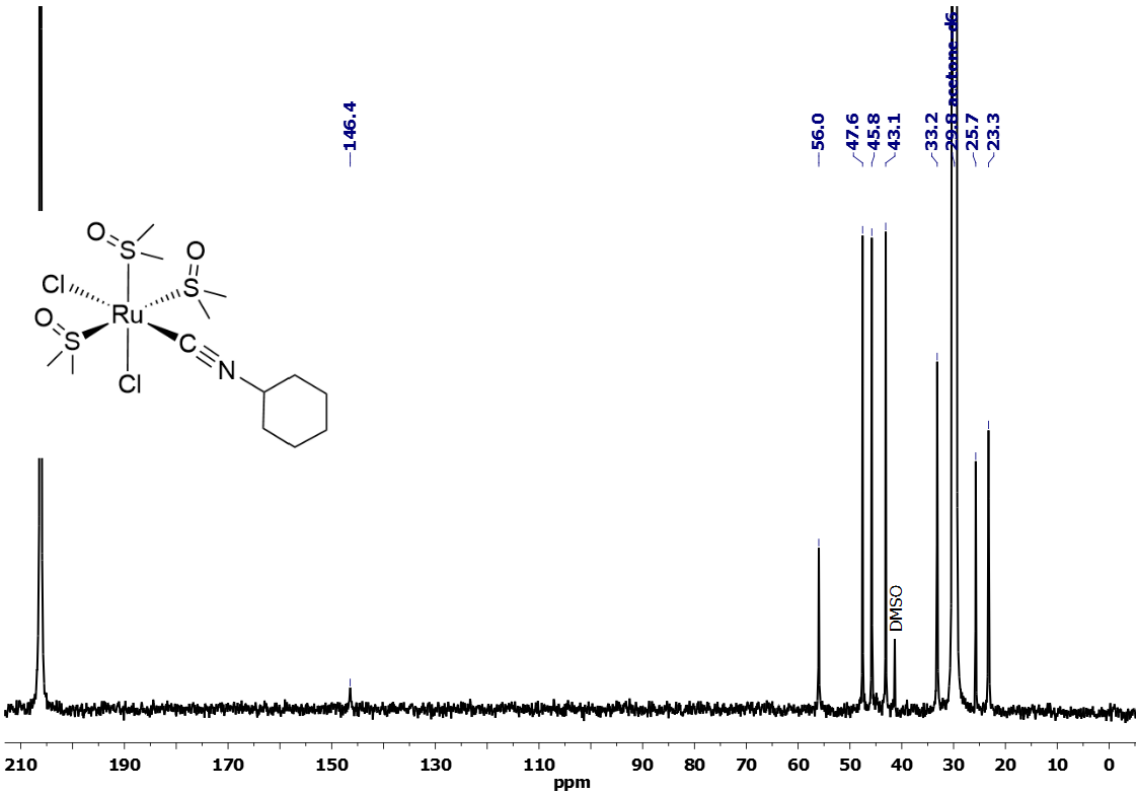

Figure S44. Black line: ^{1}H NMR spectrum (401 MHz, acetone-d_6) of **2d**. Blue line: ^{1}H NOESY with irradiation at 3.40 ppm (SCH_3-**a**). Red line: ^{1}H NOESY with irradiation at 3.31 ppm (SCH_3-**c**). Observed NOEs are indicated by the arrows; dashed lines reresent weaker NOE effects. The NOE effect between SCH_3-**b** and SCH_3-**c** is probably weakened by co-irradiation.

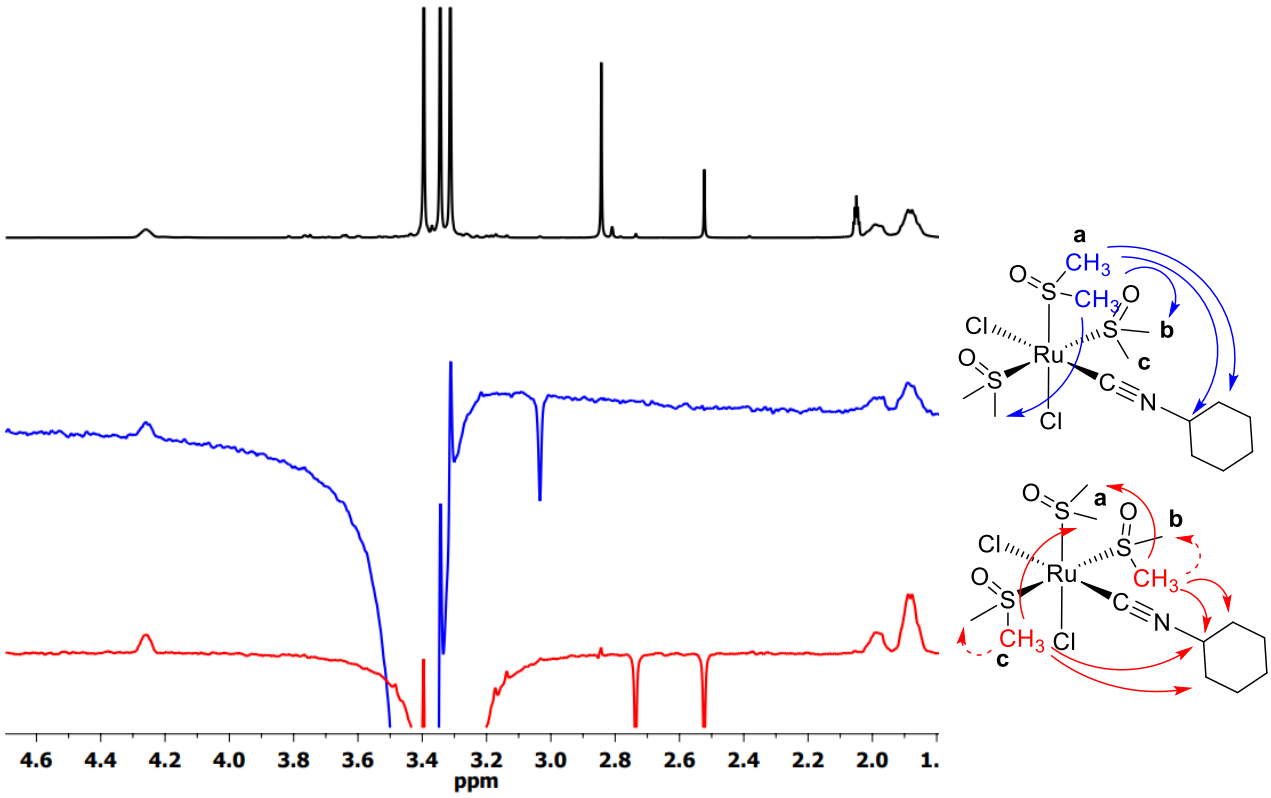

Figure S45. Solid-state FT-IR spectrum (650-4000 cm^{-1}) of *cis*,*mer*-[$RuCl_2(CN^tBu)(\kappa S\text{-}DMSO)_3$], **2e** in mixture with a byproduct of general formula {$Ru(CN^tBu)_n(DMSO)_n$}, **3e**.

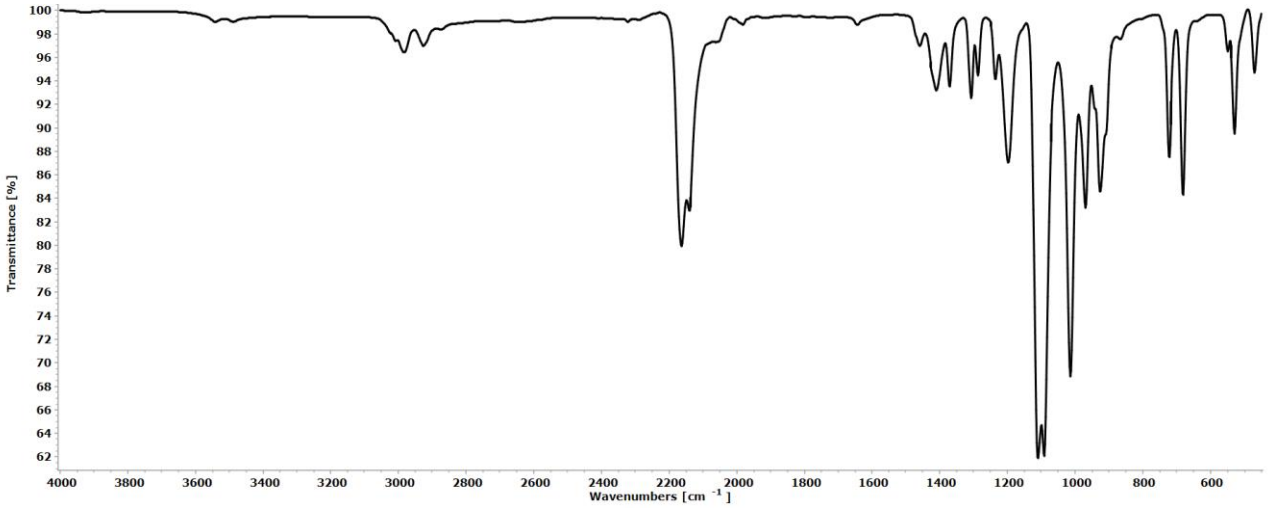

Figure S46. Solvent-subtracted FT-IR spectra (1300-2700 cm^{-1}) of **1e** (black line), **2e** (blue line; + **3e** by-product) and tert-butyl isocyanide (red dashed line) in CH_2Cl_2.

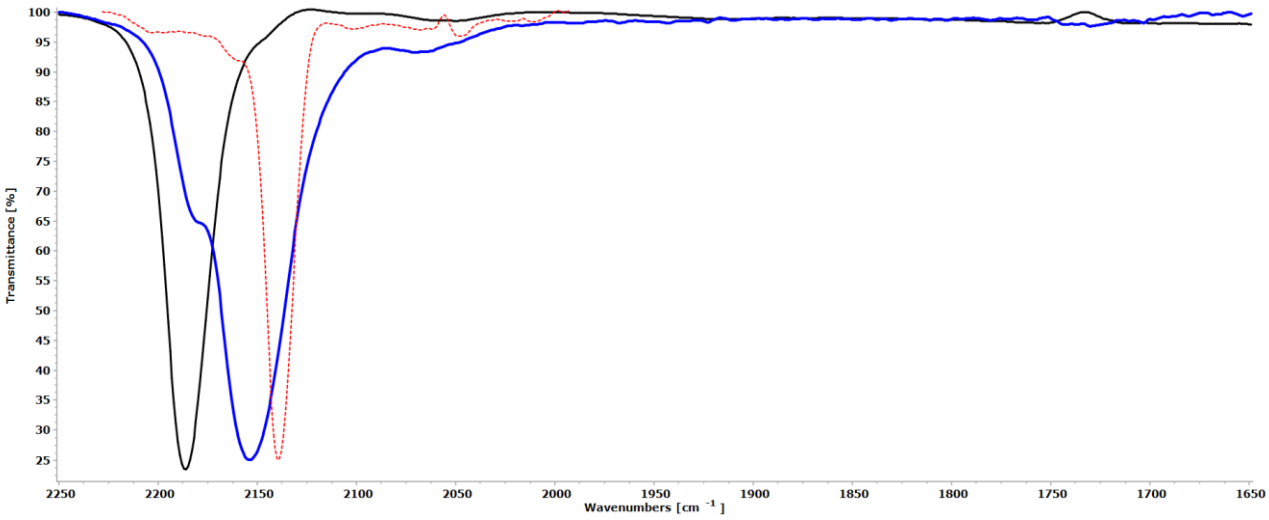

Figure S47. ^{1}H NMR spectrum (400 MHz, acetone-d_6) of **2e.** Signals due to the **3e** by-product are marked with asterisk (*).

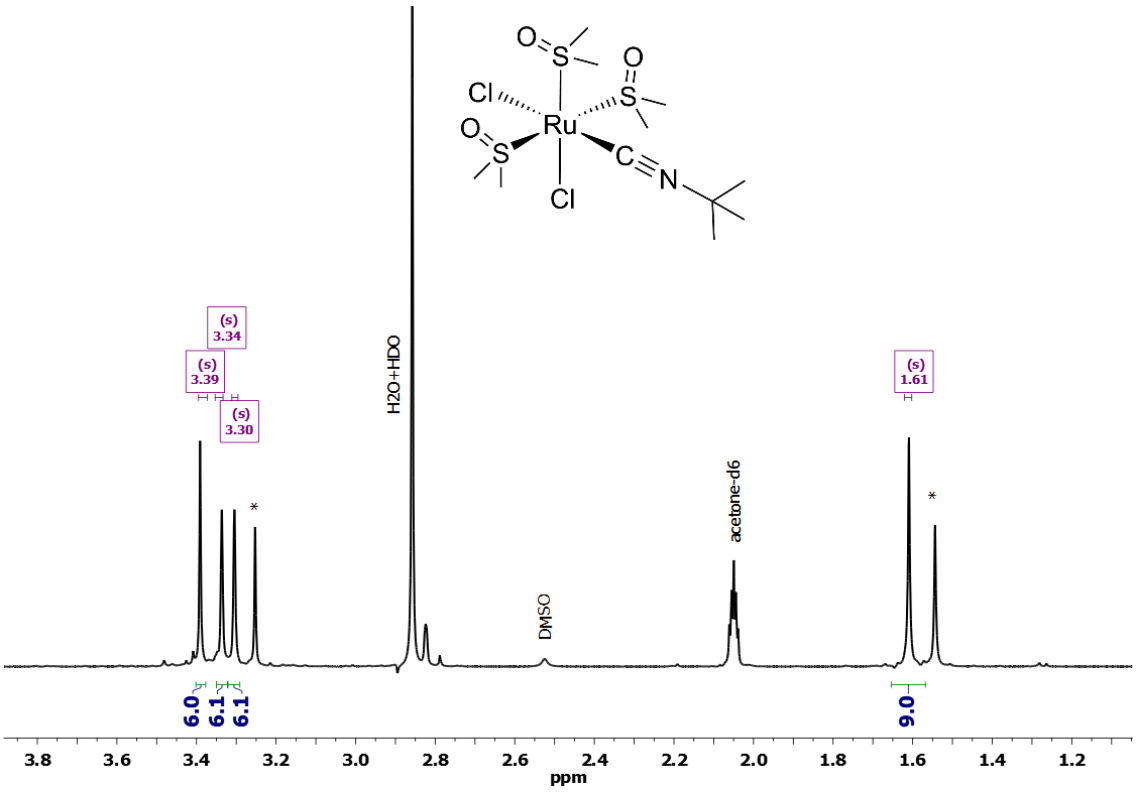

Stability of isocyanide-DMSO complexes in solution

Solutions of **2a-e** in acetone-d_6 or $CDCl_3$ were maintained at room temperature and analyzed by NMR (^1H and ^1H-^{13}C HMBC). A variable amount of DMSO ($CDCl_3$ >> acetone-d_6), presumably released from **2a-e**, and related signals ascribed to unidentified isocyanide-DMSO complexes, were detected in the freshly-prepared solutions. The % amount of the {Ru(CNR)$(DMSO)_n$} species was estimated by the relative integral of **2a-d** or **2e+3e** with respect to the total Ru-DMSO resonances and is given in the following. *$CDCl_3$*: **2a**, 18-20 %; **2b**, 21 %; **2c**, 28 %; **2d**, 22 %; **2e+3e**, 15 %. *Acetone-d_6*: **2a**, 8 %; **2b**, 5 %; **2c**, 4 %; **2d**, 5 %; **2e+3e**, 6 %. A modest increase in the amount of free DMSO was observed for **2a** and **2d** in the ^1H NMR spectra (acetone-d_6) after 24 h at room temperature, while minimal changes occurred for **2b** and **2d** in the same conditions. A comparative view of the ^1H NMR spectra of freshly-prepared solutions of **2a-d** in $CDCl_3$ or acetone-d_6 is given in Figures S48-S49.

DMSO. ^1H NMR: δ/ppm = 2.60 ($CDCl_3$); 2.54 (DMSO-d_6); 2.52 (acetone-d_6). $^{13}C\{1H\}$ NMR: δ/ppm = 41.1 ($CDCl_3$); 41.3 (acetone-d_6).

Figure S48. Comparative ^{1}H NMR spectra (400 MHz) of freshly-prepared solutions of **2a** (top) or **2b** (bottom) in acetone-d_6 (blue line) or in $CDCl_3$ (red line).

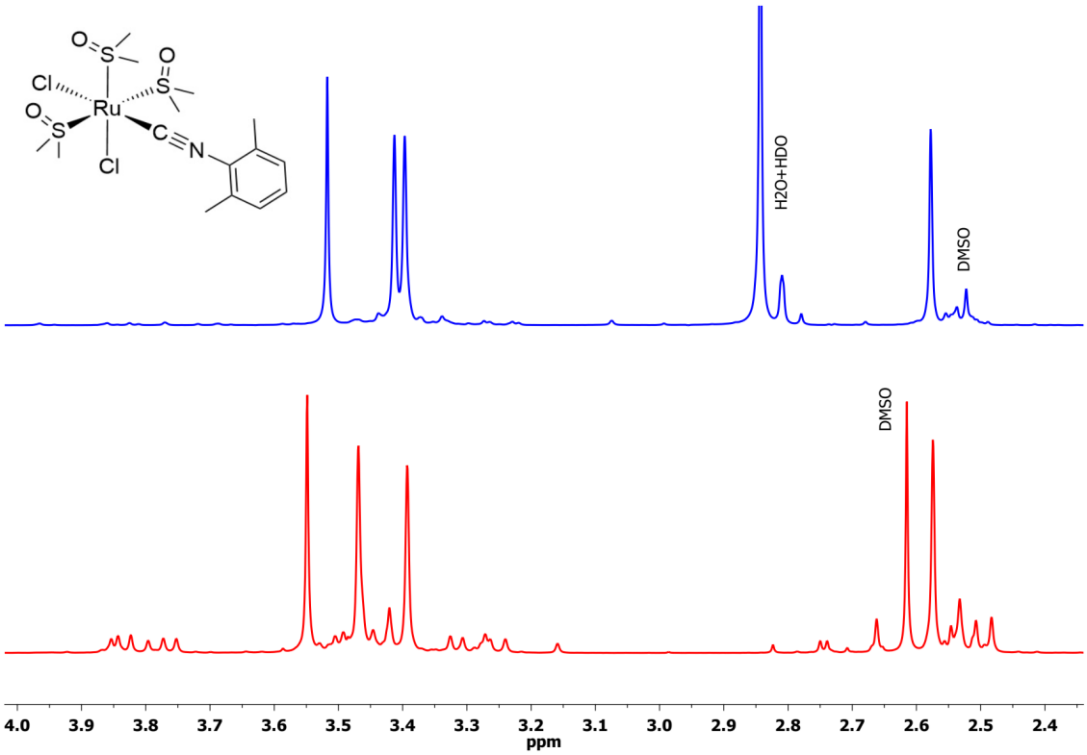

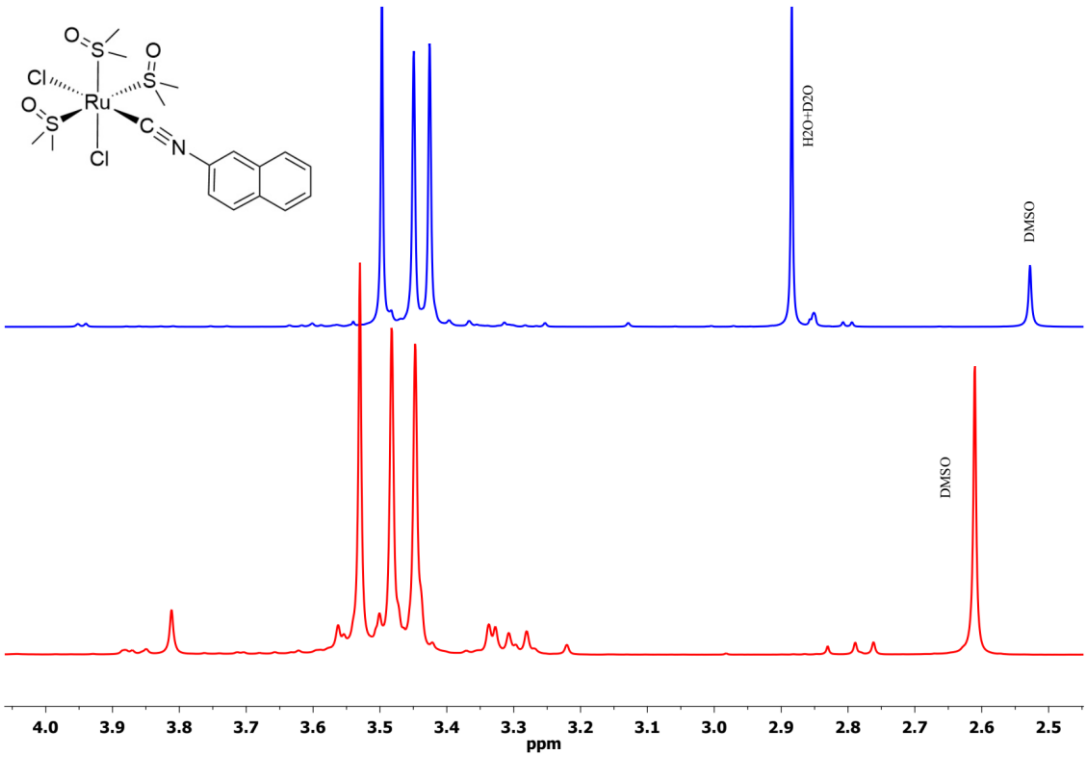

Figure S49. Comparative ^{1}H NMR spectra (400 MHz) of freshly-prepared solutions of **2c** (top) or **2d** (bottom) in acetone-d_6 (blue line) or in $CDCl_3$ (red line).

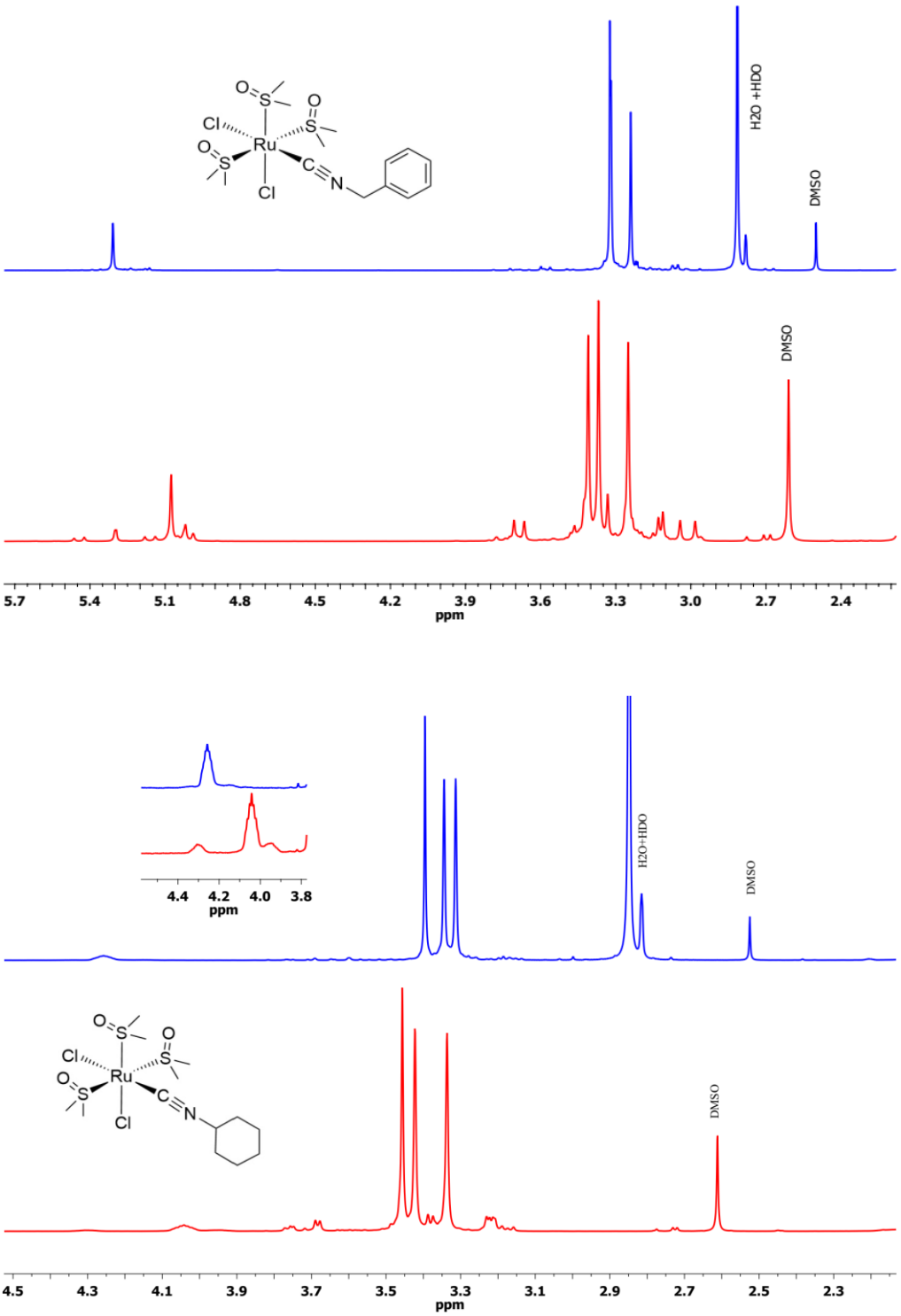

Table S1. Comparison of selected FT-IR and NMR data for $[RuCl_2(CNR)(\eta^6\text{-}p\text{-cymene})]$ (**1a-e**), $[RuI_2(CN^tBu)(\eta^6\text{-}p\text{-cymene})]$ (**1f**), *cis,mer*-$[RuCl_2(CNR)(\kappa S\text{-DMSO})_3]$ (**2a-d**) and the respective isocyanide ligand (CNR).

Isocyanide substituent R		**IR (CH_2Cl_2) ν(CN) / cm^{-1} (*Δν / cm^{-1}*)[a]**			**^{13}C NMR δ(CN) / ppm (*Δδ / ppm*)[a][b]**		
Compound		**CNR**	**1**	**2**	**CNR**	**1**	**2**
Xylyl	a	2123	2162 (*+39*)	2131 (*+8*)	167.6	151.7 (*−15.9*)	159.0 (*−8.6*)
2-naphthyl	b	2127 [c]	2160 [c] (*+33*)	2133 [c] (*+6*)	164.3 [d]	149.5 (*−14.8*)	158.6 (*−5.7*)
benzyl	c	2155	2200 (*+45*)	2168 (*+13*)	157.7 [d]	141.3 (*−16.4*)	148.6 (*−9.1*)
cyclohexyl	d	2144	2194 (*+50*)	2165 (*+21*)	154.0	138.7 (*−15.3*)	146.4 (*−7.6*)
tert-butyl	e	2139	2186 (*+47*)	2154 (*+15*)	152.6 [d]	137.9 (*−14.7*)	
	f		2169 (*+30*)			135.8 (*−16.8*)	

[a] Coordination-induced shift (Ru-CNR vs CNR). [b] In $CDCl_3$ for isocyanides and **1a-f**; in acetone-d_6 for **2a-e**. [c] Only the main IR band is reported. [d] Taken from the literature.[1,2,3]

Study of the *p*-cymene/DMSO exchange in toluene-d_8.

Table S2. Monitoring of the reaction of $[RuCl_2(CNXyl)(\eta^6\text{-}p\text{-cymene})]$ (**1a**) and DMSO in toluene-d_6.

Temperature, time	Reaction mixture	Compounds detected in solution (^{1}H NMR)
room T, 21 h	*Orange solid* (**1a**) + pale yellow solution	**1a** (traces), **2a**, **2a^X**, *p*-cymene **2a** / **2a^X** ratio = 0.61 (**2a**+**2a^X**) / *p*-cymene ratio = 0.96
+ 60 °C, 1 h	Yellow-orange solution	**1a, 1a^X, 2a**, **2a^X**, **3a**, *p*-cymene **1a / 1a^X** / **2a** / **2a^X / 3a** ratio = 6:7:**62**:18:7 (**2a**+**2a^X**+**3a**) / *p*-cymene ratio = 0.97
+ 60 °C, 15 h	Yellow solution	**1a^X**, **2a**, **3a** *p*-cymene **1a^X** / **2a** / **3a** ratio = 5:**82**:13 (**2a**+**3a**) / *p*-cymene ratio = 1.0

DMSO. ^{1}H NMR (toluene-d_8): δ/ppm = 1.74 (s). $^{13}C\{^1H\}$ NMR (toluene-d_8): δ/ppm = 40.2.

***p*-cymene**. ^{1}H NMR (toluene-d_8): δ/ppm = 6.99 (s-br), 6.97* (s-br) (C_6H_4); 2.70 (hept, $^3J_{HH}$ = 6.9 Hz, 1H, C<u>H</u>Me$_2$), 2.14 (s, 3H, C<u>Me</u>), 1.14 (d, $^3J_{HH}$ = 6.9 Hz, 6H, CH<u>Me</u>$_2$); *hidden by toluene-d_7.

1a. ^{1}H NMR (toluene-d_8): δ/ppm = 5.17 (d, $^3J_{HH}$ = 5.8 Hz, 2H), 4.96 (d, $^3J_{HH}$ = 5.8 Hz, 2H) (C_6H_4); 2.30 (s, 6H, $C^{Xyl}CH_3$); 2.04 (s, 3H, C_6H_4<u>CH_3</u>); 1.04 (d, $^3J_{HH}$ = 6.8 Hz, 6H, CH<u>Me</u>$_2$).

1a^X (unknown η^6-cymene complex). ^{1}H NMR (toluene-d_8): δ/ppm = 5.07 (d, $^3J_{HH}$ = 5.8 Hz, 2H), 4.88 (d, $^3J_{HH}$ = 5.8 Hz, 2H) (C_6H_4); 1.05 (d, $^3J_{HH}$ = 6.9 Hz, 3H, CH<u>Me</u>$_2$).

2a. ^{1}H NMR (toluene-d_8): δ/ppm = 6.79–6.74 (m, 1H), 6.67 (d, $^3J_{HH}$ = 7.6 Hz, 2H) (C_6H_3); 3.20 (s, 12H, DMSO), 2.98 (s, 6H) (SCH_3); 2.38 (s, 6H, CCH_3). $^{13}C\{^1H\}$ NMR (toluene-d_8): δ/ppm = 47.3, 45.6, 42.9 (SCH_3).

2a^X (unknown DMSO complex). ^{1}H NMR (toluene-d_8): δ/ppm = 3.07 (s, 6H), 3.05 (s, 12H) (SCH_3); 2.36 (s, 6H, CCH_3). ^{13}C NMR (toluene-d_8): δ/ppm = 42.8 (DMSO).

3a (unknown DMSO:CNXyl 1:1 complex). ^{1}H NMR (toluene-d_8): δ/ppm = 3.09 (s, 6H, SCH_3), 2.41 (s, 6H, CCH_3). ^{13}C NMR (toluene-d_8): δ/ppm = 44.6 (DMSO).

Figure S50. ^{1}H NMR spectra (400 MHz) of the **1a**+DMSO reaction mixture in toluene-d_8 after 21 h at room temperature (top, blue line) and after a subsequent heating at 60 °C for 1 h (middle, green line) or 15 h (bottom, red line).

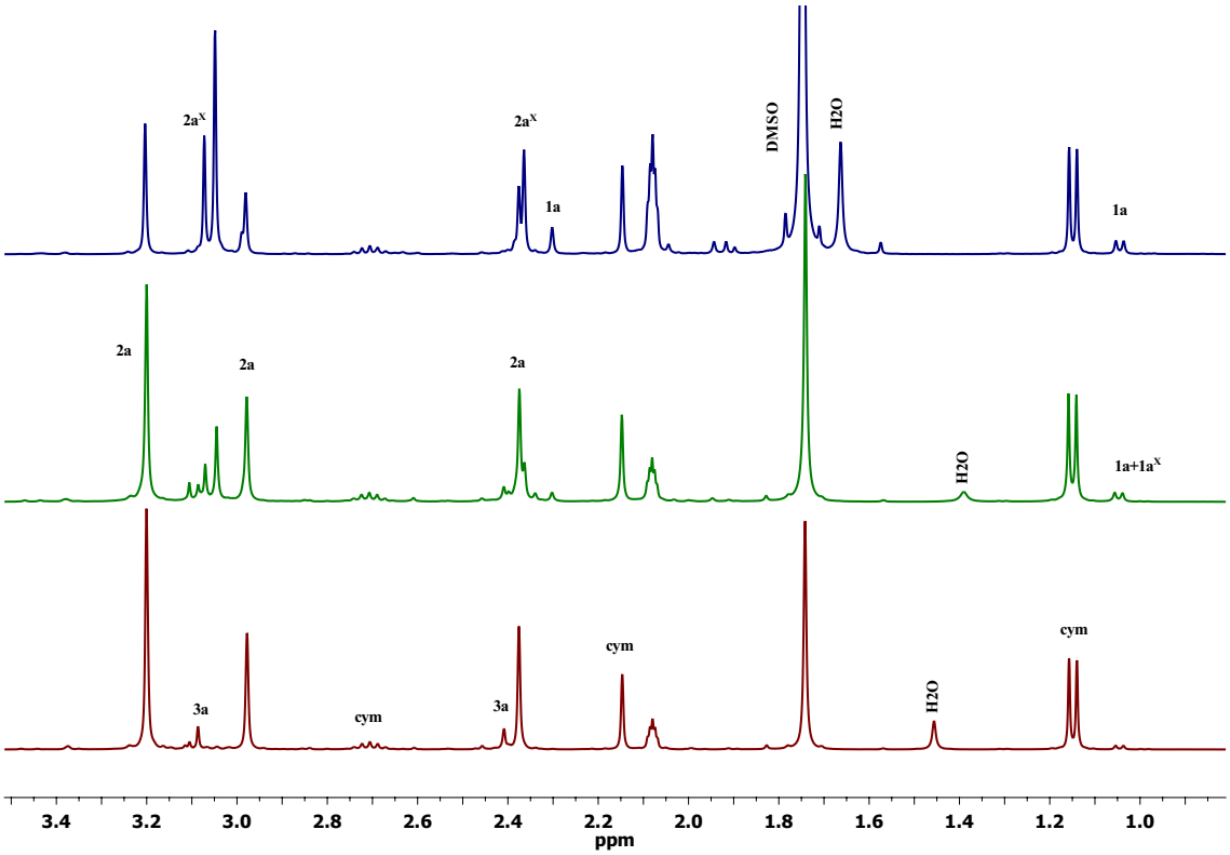

Table S3. Monitoring of the reaction of [$RuCl_2$(CNCy)(η^6-*p*-cymene)] (**1d**) and DMSO in toluene-d_6.

Temperature, time	Reaction mixture	Compounds detected in solution (^{1}H NMR)
room T, 16 h	Orange solid (**1d**) + orange solution	**1d**, **2d**, **2d^X**, *p*-cymene **1d** / **2d** / **2d^X** ratio = **67**:9:24 (**2d**+**2d^X**) / *p*-cymene ratio = 0.91
+ 65 °C, 3 h	Yellow-orange solution	**1d^{X1}**, **1d^{X2}**, **2d**, **3d**, *p*-cymene **1d^{X1}** / **1d^{X2}** / **2d** / **3d** ratio = 5:10:**53**:32 (**2d**+**3d**) / *p*-cymene ratio = 0.91
+ 65 °C, 18 h	Golden yellow solution	**1d^{X2}**, **2d**, **3d**, *p*-cymene **1d^{X2}** / **2d** / **3d** ratio = 17:**51**:32 (**2d**+**3d**) / *p*-cymene ratio = 0.91

1d. ^{1}H NMR (toluene-d_8): δ/ppm = 5.12 (d, $^3J_{HH}$ = 6.0 Hz, 2H), 4.91 (d, $^3J_{HH}$ = 5.9 Hz, 2H) (C_6H_4); 3.37–3.27 (m, 1H, NCH^{Cy}); 2.66 (hept, $^3J_{HH}$ = 5.9 Hz, 1H, $\underline{CH}Me_2$); 1.95 (s, 3H, $C\underline{CH_3}$); 1.69–1.58 (m), 1.51–1.32 (m), 1.04–0.93 (m, 10H, CH_2^{Cy}); 1.07 (d, $^3J_{HH}$ = 6.9 Hz, 6H, $CH\underline{Me_2}$).

1d^{X1} (unknown η^6-*p*-cymene complex). ^{1}H NMR (toluene-d_8): δ/ppm = 5.08 (d, $^3J_{HH}$ = 5.9 Hz, 2H), 4.86 (d, $^3J_{HH}$ = 5.9 Hz, 2H) (C_6H_4); 1.93 (s, 3H, $C\underline{CH_3}$); 1.06 (d, $^3J_{HH}$ = 6.9 Hz, 6H, $CH\underline{Me_2}$).

1d^{X2} (unknown η^6-*p*-cymene complex). ^{1}H NMR (toluene-d_8): δ/ppm = 5.04 (d, $^3J_{HH}$ = 6.1 Hz, 2H), 4.84 (d, $^3J_{HH}$ = 6.1 Hz, 2H) (C_6H_4); 1.82 (s, 3H, $C\underline{CH_3}$); 1.05 (d, $^3J_{HH}$ = 7.0 Hz, 6H, $CH\underline{Me_2}$). $^{13}C\{^1H\}$ NMR (toluene-d_8): δ/ppm = 100.0 87.0 (C_6H_4).

2d. ^{1}H NMR (toluene-d_8): δ/ppm = 3.22 (s, 6H), 3.20 (s, 6H), 3.03 (s, 6H) (SCH_3). $^{13}C\{^1H\}$ NMR (toluene-d_8): δ/ppm = 47.1, 45.5, 42.9 (SCH_3); 2.71? (m, NCH^{Cy}).

2d^X (unknown DMSO complex). ^{1}H NMR (toluene-d_8): δ/ppm = 3.10 (s, 12H), 3.08 (s, 6H) (SCH_3).

3d. (unknown DMSO complex). ^{1}H NMR (toluene-d_8): δ/ppm = 3.15 (s, 6H, SCH_3). $^{13}C\{^1H\}$ NMR (toluene-d_8): δ/ppm = 44.6 (SCH_3).

Figure S51. ^{1}H NMR spectra (400 MHz) of the **1d**+DMSO reaction mixture in toluene-d_8 after 16 h at room temperature (top, blue line) and after a subsequent heating at 65 °C for 3 h (middle, green line) or 21 h (bottom, red line).

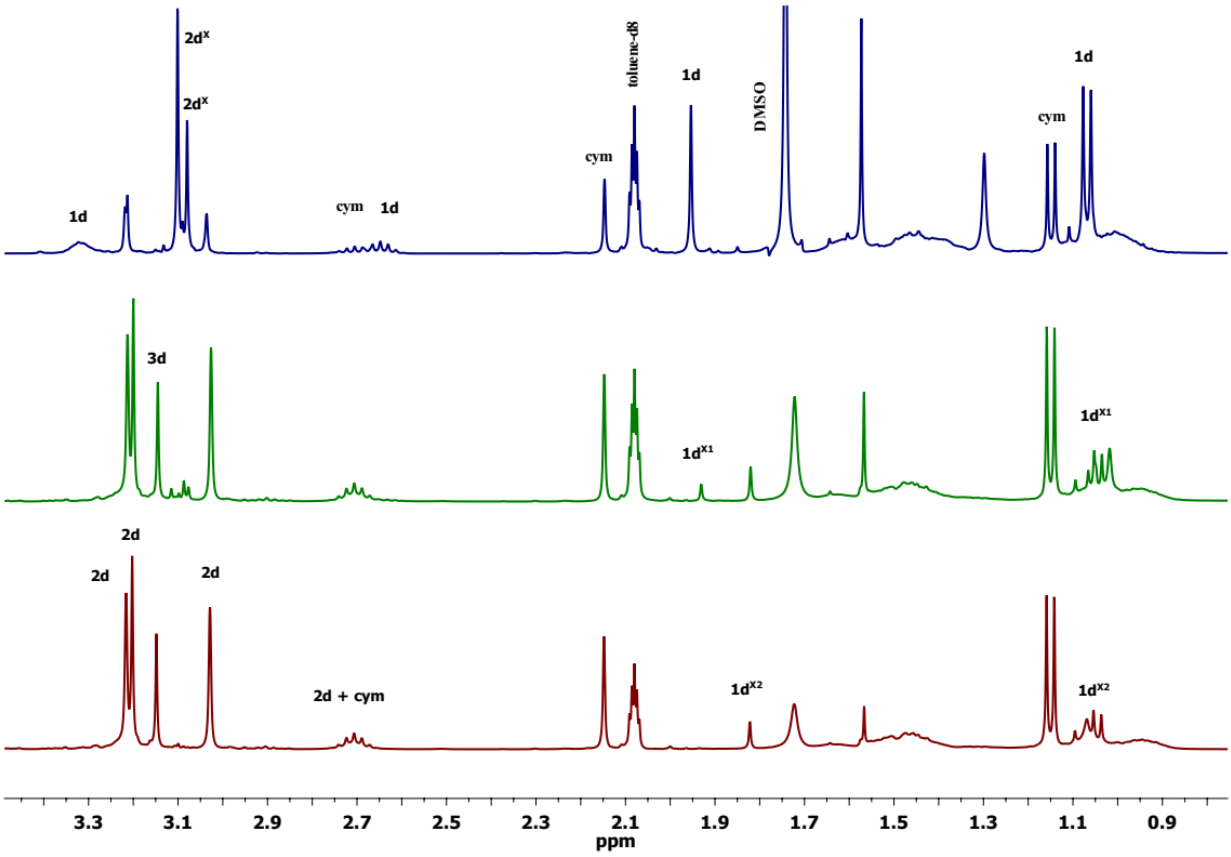

FT-IR and NMR spectra of 4a

Figure S52. Solid-state FT-IR spectrum (650-4000 cm^{-1}) of $[RuCl_2(CNXyl)(\kappa S\text{-}DMSO)(\mu\text{-}DMSO)_2]_2$, **4a**.

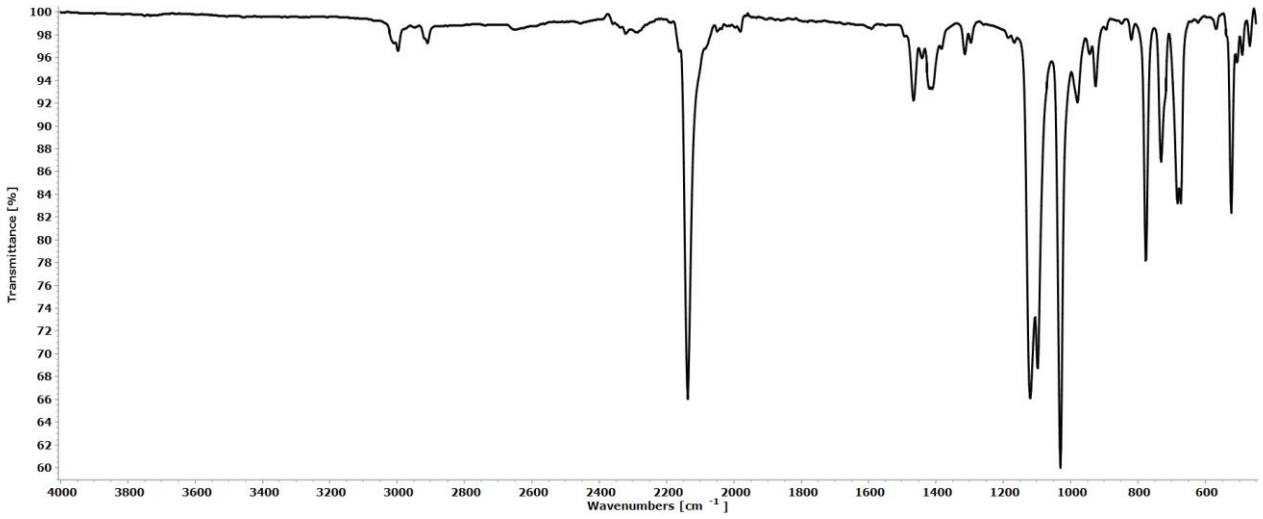

Figure S53. ^1H NMR spectrum (400 MHz, $CDCl_3$) of **4a**. Only the major set of signals is highlighted; minor signals are ascribed to different isomers.

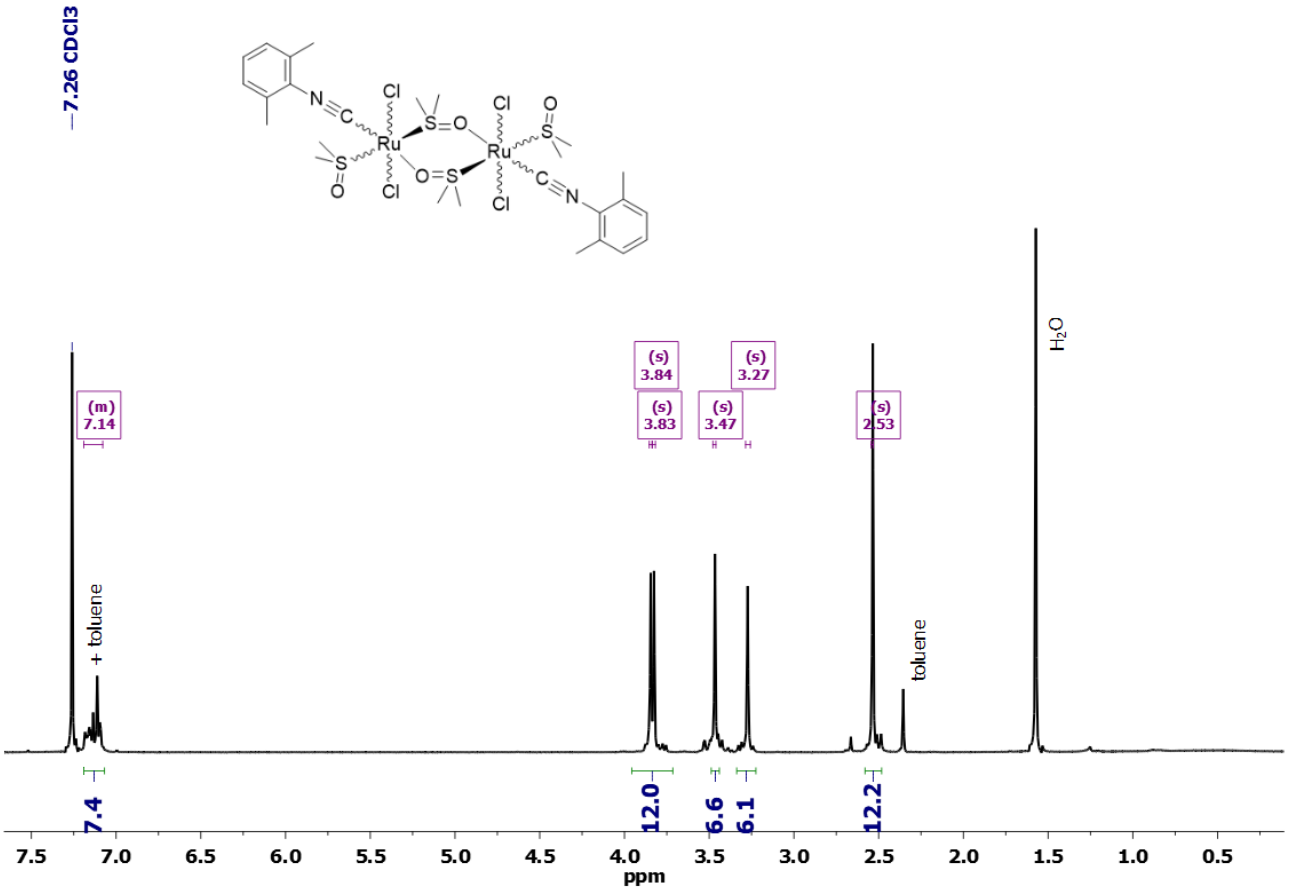

Table S4. The standard enthalpy change of dehydrogenation of different alcohols used as hydrogen donors in CTH.

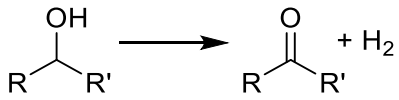

Alcohol	ΔH° (kJ/mol)
Methanol	+ 130.1
Ethanol	+ 85.4
1-Propanol	+ 87.3
2-Propanol	+ 70.0
1-Butanol	+ 79.7
2-Butanol	+ 69.3
1-Pentanol	+ 84.3
2-Pentanol	+ 67.9
1-Hexanol	+ 68.2
2-Hexanol	+ 70.0

Investigation of the catalytic reaction mixture by GC-MS

Figure S54. Chromatogram of the post-reaction mixture obtained under the optimized reaction conditions: compound *1* is γ-valerolactone; compound *2* is ethyl levulinate; compound *3* is 2-butyl levulinate and compound *4* is 2-butyl-4-hydroxypentanoate (MW heating, 150 °C, 60 min, complex **1a** 0.56 mol% with respect to EL 5 mmol, 2-butanol 10 mL, KOH 1 mol% with respect to EL).

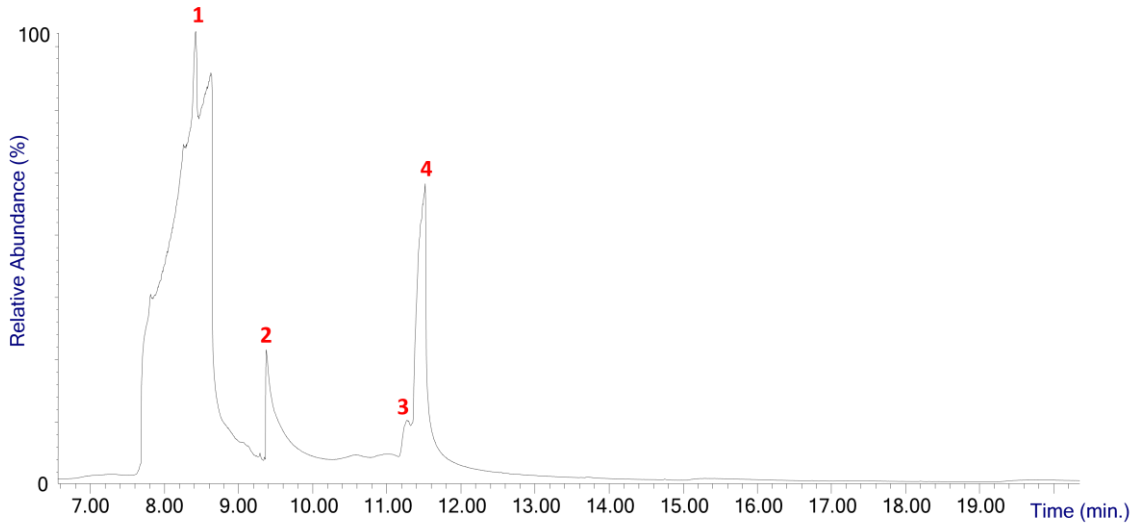

Figure S55. Mass spectrum of compound 1 reported in Figure S52.

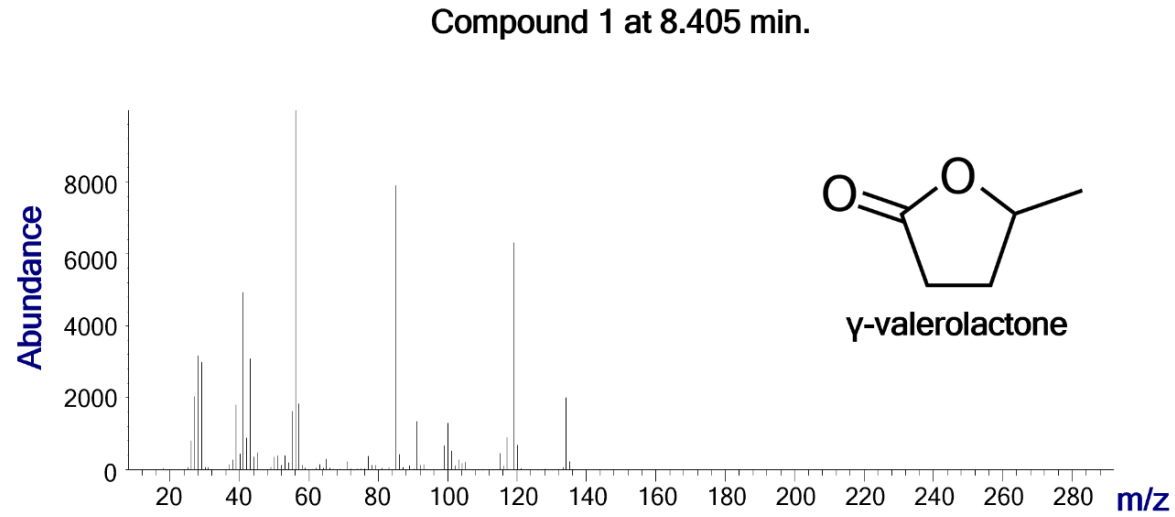

Figure S56. Mass spectrum of compound 2 reported in Figure S52.

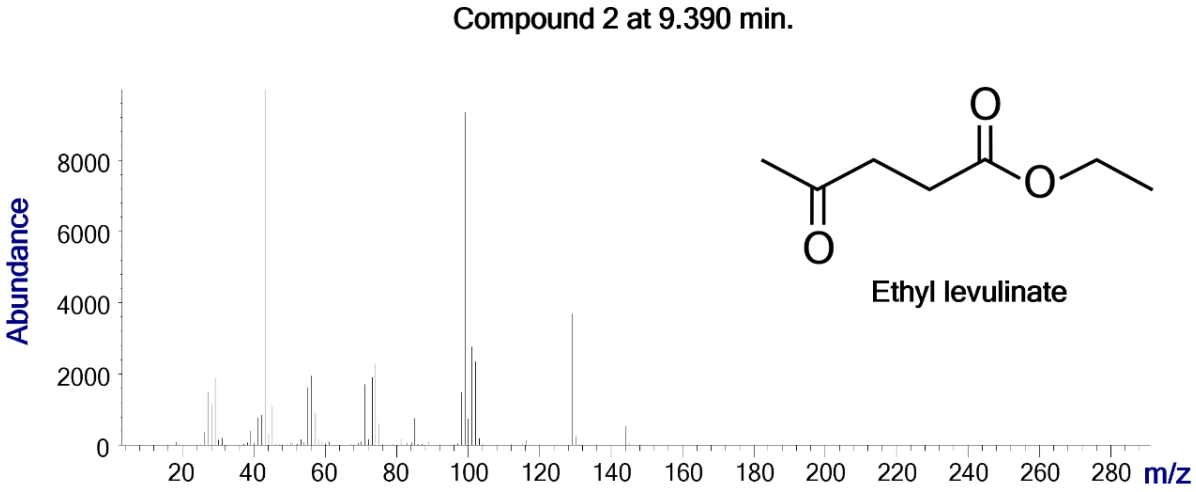

Figure S57. Mass spectrum of compound 3.

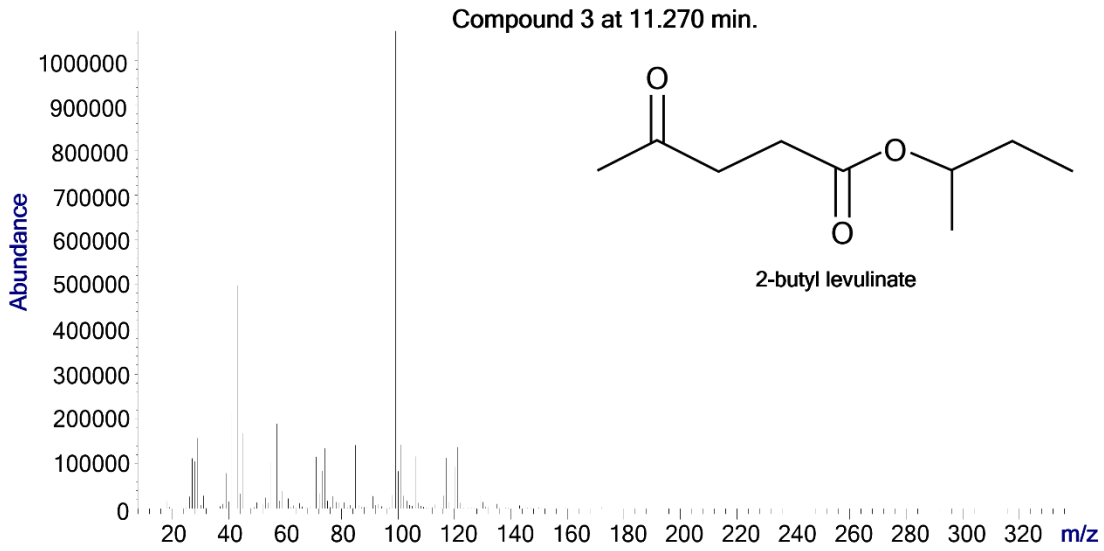

Figure S58. Mass spectrum of compound 4.

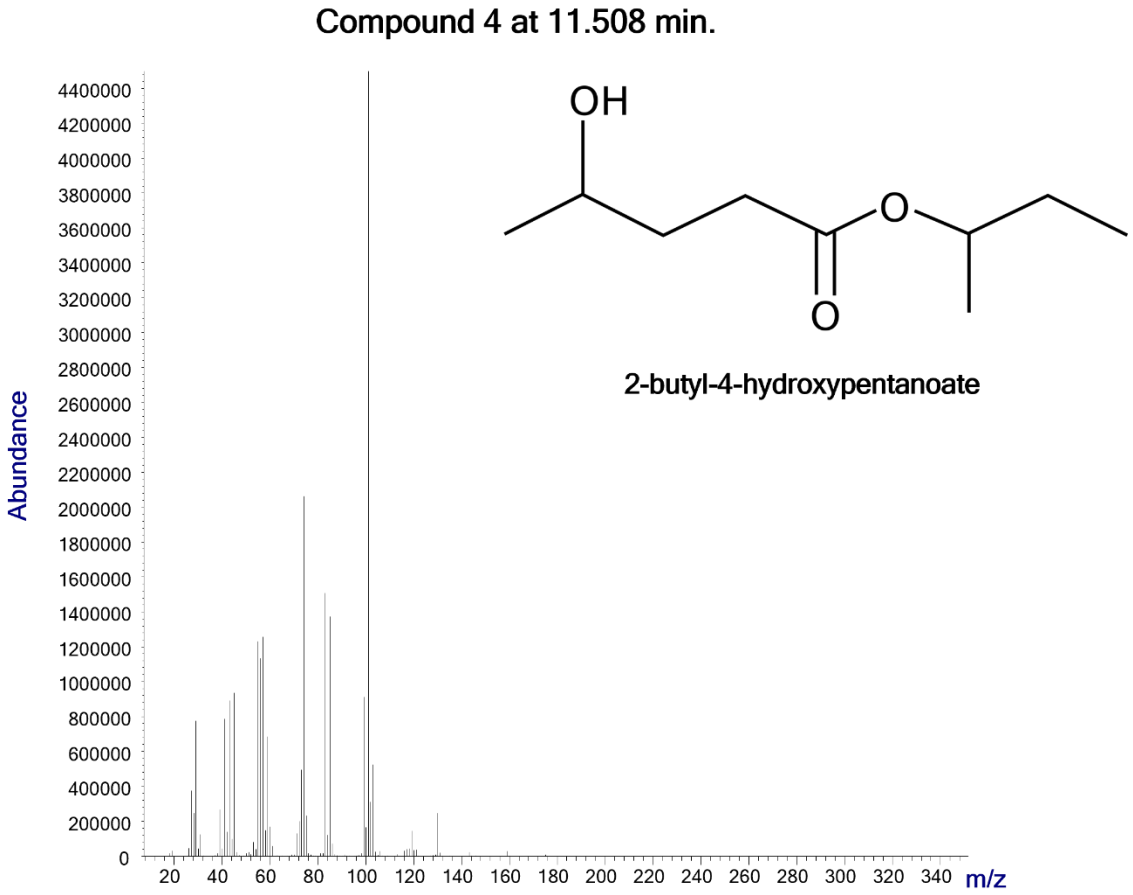

Ruthenium speciation in the final reaction mixture

A freshly-prepared solution of ethyl levulinate + 2-butanol/KOH and **1a** was sampled for ICP-OES analyses (soluble Ru: 0.362 ± 0.001 mg/mL). Next, the transfer hydrogenation reaction was carried out under the optimized conditions, affording a black solid and pale brown-green solution. The final solution was sampled for ICP-OES analyses (soluble Ru: 0.212 ± 0.001 mg/mL; corresponding to about 59 % of the initial level). Therefore, the mixture was filtered twice on a G4 sintered glass filter and the resulting black solid was washed with Et_2O, petroleum ether and dried under vacuum (40 °C). The solid-state FT-IR spectrum showed no isocyanide or carbonyl stretching band. The ^{1}H NMR (DMSO-d_6) spectrum showed no resonances in the typical range of η^6-*p*-cymene ligands (5-6 ppm). Anal. Found: C, 7.30; H, 1.12; N, 0.07.

The filtrate was taken to dryness under vacuum. The residue was analyzed by ^{1}H NMR and FT-IR, which allowed us to identify γ-valerolactone as the predominant component. IR (CH_2Cl_2): $\tilde{\upsilon}$/cm^{-1} = 1772s (C=O). ^{1}H NMR (DMSO-d_6): δ/ppm = 3.60–3.53 (m, 1H, $\underline{CH}CH_3$); 2.46 (t, J = 7.0 Hz), 2.12–2.06 (m), 2.03–1.95 (m) (2H, $\underline{CH_2}CO$); 1.46 (dd, J = 12.3, 6.3 Hz, 2H, $\underline{CH_2}CH$); 0.98 (d, $^3J_{HH}$ = 6.2 Hz, CH_3).

Ru analyses (ICP-OES). Samples were 1:100 diluted in 2% HNO_3 and analyzed by Inductively Coupled Plasma – Optical Emission Spectroscopy (ICP-OES). Analyses were carried out with Optima 8000 ICP-OES (Perkin Elmer) operating at 1500W and equipped with autosampler S10, MiraMist® Nebulizer (Perkin Elmer) and cyclonic chamber. Argon (420.069 nm) was used as the internal standard. Ru was examined at 240.272 nm wavelength. Metal content was determined by comparison with calibration curves obtained by commercial standard solutions (Fluka TraceCERT©) properly diluted in 2% HNO_3 to a final concentration of 0.5-1-2-5 mg/L. The results are expressed as the average of three independent measurements. A blank solution was analyzed after each sample to check for memory effects of the system.

SEM measurements. Scanning electron microscopy associated with energy-dispersion spectrometry (SEM/EDS) analysis was performed with a JEOL-6010/LA microscope. The EDS spectra were obtained using a working distance of 10 mm and a voltage of 20 KV.

Figure S59. SEM-EDS of the black Ru-based solid recovered at the end of the catalytic reaction under optimized conditions (MW heating, 150 °C, 60 min, **1a** 0.56 mol% with respect to EL 5 mmol, 2-butanol 10 mL, KOH 1 mol% with respect to EL).

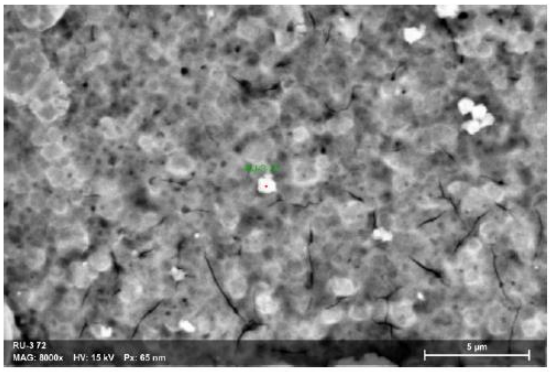

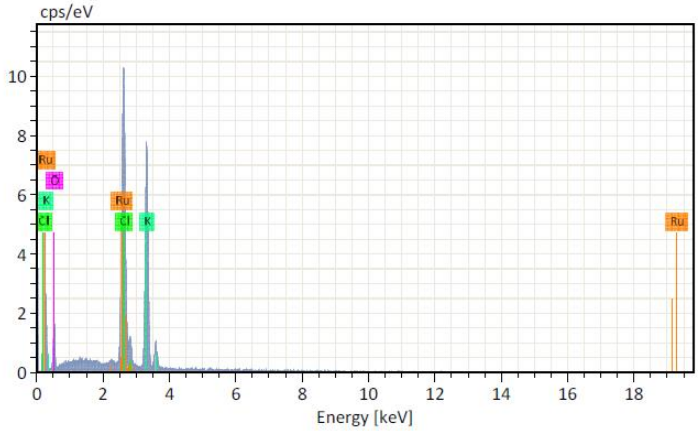

RU-3 78

Element	At. No.	Netto	Mass [%]	Mass Norm. [%]	Atom [%]	abs. error [%] (1 sigma)
Oxygen	8	1893	20.41	20.44	41.17	3.94
Chlorine	17	18695	27.09	27.13	24.66	0.96
Potassium	19	16799	34.45	34.50	28.44	1.12
Ruthenium	44	7971	17.91	17.94	5.72	0.67
		Sum	**99.86**	**100.00**	**100.00**	

A transfer hydrogenation reaction was carried out with **1a** in 2-propanol at 110 °C for 2 h, as described in the main text. An aliquot of the final mixture was filtered over celite and transferred into an NMR tube, together with a sealed glass capillary filled with C_6D_6. The ^{1}H NMR spectrum was recorded with 500 scans. Low-intensity resonances that do not correspond to those of organic species are listed in the following. ^{1}H NMR: δ/ppm = 10.9 (s), 10.0 (s), 7.36 (m, 2H, Xyl), 7.10 (m, 1H, Xyl), − 21.1 (s, Ru-H), − 23.5 (s, Ru-H).

Table S5. Crystal data and measurement details for **1d**, **1e** and **2a**.

Compound	**1d**	**1e**	**2a**
Formula	$C_{17}H_{25}Cl_2NRu$	$C_{15}H_{23}Cl_2NRu$	$C_{15}H_{27}Cl_2NO_3RuS_3$
FW	415.35	398.31	537.52
T, K	100(2)	293(2)	100(2)
λ, Å	0.71073	0.71073	0.71073
Crystal system	Monoclinic	Tetragonal	Monoclinic
Space group	$P2_1/c$	$P4_32_12$	$P2_1/c$
a, Å	10.1271(7)	14.9514(7)	10.5216(4)
b, Å	14.7241(10)	14.9154(7)	16.1879(5)
c, Å	12.3019(8)	16.0020(9)	12.8394(4)
β,°	97.854(2)	90	91.9860(10)
Cell Volume, Å^3	1817.2(2)	3577.2(4)	2185.53(13)
Z	4	8	4
D_c, g·cm^{-3}	1.518	1.446	1.634
μ, mm^{-1}	1.151	1.163	1.263
F(000)	848	1584	1096
Crystal size, mm	0.24×0.21×0.18	0.15×0.12×0.09	0.19×0.16×0.13
θ limits,°	2.457-27.136	1.864-25.497	1.937-25.997
Reflections collected	25665	43491	30193
Independent reflections	4002 [R_{int} = 0.0288]	3341 [R_{int} = 0.0659]	4284 [R_{int} = 0.0382]
Data / restraints /parameters	4002 / 0 / 193	3341 / 72 / 191	4284 / 0 / 234
Goodness on fit on F^2 [a]	1.111	1.160	1.205
R_1 ($I > 2\sigma(I)$) [b]	0.0179	0.0356	0.0205
wR_2 (all data) [c]	0.0439	0.0854	0.0465
Largest diff. peak and hole, e Å^{-3}	0.407 / –0.417	0.824 / –0.363	0.368 / –0.332

[a] Goodness on fit on $F^2 = [\Sigma w(F_O^2 - F_C^2)^2/(N_{ref} - N_{param})]^{1/2}$, where $w = 1/[\sigma^2(F_O^2) + (aP)^2 + bP]$, where $P = (F_O^2 + 2F_C^2)/3$; N_{ref} = number of reflections used in the refinement; N_{param} = number of refined parameters. [b] $R_1 = \Sigma||F_O| - |F_C||/\Sigma|F_O|$. [c] $wR_2 = [\Sigma w(F_O^2 - F_C^2)^2/\Sigma w(F_O^2)^2]^{1/2}$, where $w = 1/[\sigma^2(F_O^2) + (aP)^2 + bP]$, where $P = (F_O^2 + 2F_C^2)/3$.

References

1 **2-Naphthyl isocyanide**: X. Yan, S. Zhang, P. Zhang, X. Wu, A. Liu, G. Guo, Y. Dong, X. Li, Angew. Chem. Int. Ed. 57 (2018) 8947;

2 **Benzyl isocyanide**: T.M. El Dine, D. Evans, J. Rouden, J. Blanchet, Chem. Eur. J. 22 (2016) 5894;

3 **Tert-butyl isocyanide**: N. Liu, F. Chao, M.G. Liu, N.Y. Huang, K. Zou, L. Wang, J. Org. Chem. 84 (2019) 2366.